Doctoral Dissertation

Design and Performance of Hybrid Control Rod

For Passive IN-core Cooling System

Kyung Mo Kim

Department of Nuclear Engineering
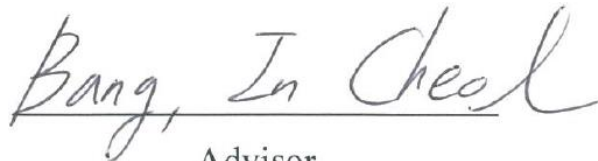
Graduate School of UNIST

2017. 06. 07

Design and Performance of Hybrid Control Rod

For Passive IN-core Cooling System

A dissertation

submitted to the Graduate School of UNIST

in partial fulfillment of the

requirements for the degree of

Doctor of Philosophy

Kyung Mo Kim

2017. 06. 07

Approved by

Bang, In Cheol
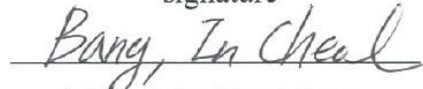
Advisor

Prof. In Cheol Bang

Design and Performance of Hybrid Control Rod

For Passive IN-core Cooling System

Kyung Mo Kim

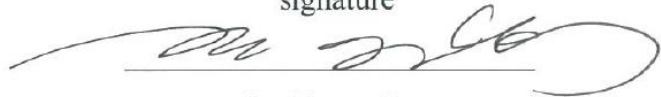This certifies that the dissertation of Kyung Mo Kim is approved.

06. 07. 2017

signature

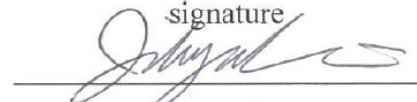*Bang, In Cheol*

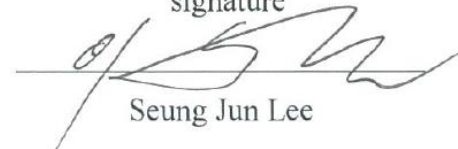Advisor: In Cheol Bang

signature

Jae Young Lee

signature

Ki-Yong Choi

signature

Ji Hyun Kim

signature

Seung Jun Lee

Abstract

Protection of the public and the environment from undue radiation hazards is a definition of nuclear safety. Although there are various safety systems in nuclear power plants to achieve the nuclear safety, Fukushima-Daiichi accident showed the vulnerabilities of the installed safety systems. After the Fukushima accident, various passive safety systems and strategies are under development to cope with the postulated accidents. The majority of passive safety systems concentrated to inject emergency core coolant (ECC) or feedwater with the circuits comprise many pipelines and valves. In station blackout condition, the pressure of reactor vessel would be higher than the ECC injection pressure resulting in failure of ECC supply and eventually causing core damage. The reliability issues about the performance of passive safety systems have been discussed owing to their high uncertainties, low performance, and lack of experience in operation compared to active safety systems. In aspect of probabilistic safety, complex circuits which comprise many valves and pipelines have possibilities of single failure and common cause failure. Development of innovative passive safety system having differentiated working principle, significant performance, and low possibility of failure can enhance reactor safety providing solutions for the aforementioned problems. Based on these requirements, hybrid control rod which combines the functions of control rod and heat pipe was proposed for the development of passive in-core cooling system (PINCs). The control rods drop to the core using gravity and shutdown the reactor by neutron absorption. The thermosyphon heat pipe is a passive heat transfer device using phase change and convection of working fluid in a closed metal container having two different temperature interfaces (evaporator and condenser). The combination of thermosyphon and control rod, hybrid control rod can achieve reactor shutdown and decay heat removal simultaneously at accident conditions.

Hybrid control rod was designed considering the aspects of neutronics (reactivity worth) and mechanical integrity. Most of the nuclear reactors operate at high temperature and high pressure environment with high power density. Thus, pressure control strategies of the hybrid control rod using non-condensable gas and expansion of the working fluid were established to achieve high decay heat removal capacity and operating conditions. The designed hybrid control rods were equipped on the experimental facility and their thermal performances were studied under various amount of working fluid, amount of non-condensable gas, and operating pressures of the test section. The experimental results showed relations between heat transfer characteristics and controlled parameters. Controlling operating condition of hybrid control rod in high pressure worked successfully, and the proportionality between maximum heat removal capacity and operating pressure of hybrid control rod design has been proven. Measured maximum heat transfer rate of single hybrid control rod was 6 kW at 20 bar.

Simulations of multi-dimensional analysis for reactor safety (MARS) code were also performed to

validate the experimental results and evaluate the prediction capability of the code on the hybrid control rod. The simulation results showed the limits of heat transfer models in the code analyzing the hybrid control rod in which the boiling and condensation heat transfer occurs simultaneously in a manner of countercurrent flow. The experimental results were compared with several models associated with boiling heat transfer, condensation heat transfer, and critical heat flux (CHF) of thermosyphon for the development or the selection of optimal models. The selected models could be implemented to system analysis codes in the purpose of deterministic safety assessment of PINCs against design basis accidents. Imura's correlation, which was developed in two-phase natural convection condition and validated with experiments in wide range, was selected as boiling heat transfer model of pressurized hybrid control rod. The existing condensation models were based on Nusselt's film condensation theory. Hence, the effect of non-condensable gas and perturbation between upward vapor flow and downward liquid film flow were not considered at the same time. The change of effective heat transfer length due to presence of non-condensable gas and effect of fluid inertia were considered for the derivation of new condensation model. The main thermal-hydraulic phenomenon which induces CHF of thermosyphon is flooding. The flooding-based CHF models for thermosyphon were derived with theories on instability of the liquid film or maximum liquid film flow rate in countercurrent flow condition. The limited prediction capabilities of the models were attributed to difference between hydraulic diameter and heated diameter as well as high operating pressure. Consequently, new model regarding the CHF of hybrid control rod was suggested to explain its unique characteristics.

The hybrid control rod could be equipped on spent fuel dry storage casks for the extension of their thermal margins. The mock-up was designed to be scaled-down to 1/10 of metal dry storage cask developed by NAC. The effect of hybrid control rod on thermal margins of the cask was experimentally studied. The equipment of hybrid control rod with installation of heat sink lid reduced the temperature distributions inside the cask at equal power density condition. Application of hybrid control rod could extend the thermal margin up to 30 %. Feasibility of PINCs based on experimentally and analytically studied hybrid control rods were discussed according to commercial reactors.

A number of nuclear facilities has been built to supply and manage energy. The nuclear fuels generate decay heat even in shutdown condition by fission products. Management of the decay heat is important to satisfy demand for nuclear safety. Therefore, new conceptual safety system is required to supplement the issues on existing safety systems. Passive in-core cooling system based on hybrid control rod is the effective way to be applied on extensive nuclear facilities containing nuclear fuels. Pressurized hybrid control rod could meet the operating conditions of application objects with significant decay heat removal capacity.

Contents

List of figures

List of table

Nomenclature

A	heat transfer area	[m^2]
Bo	Bond number	
c	specific heat	[Jkg^{-1}K^{-1}]
C	constant	
D	diameter	[m^2]
E	entrainment rate	[kgm^{-2}s^{-1}]
f	constant	
g	acceleration due to gravity	[ms^{-2}]
h	latent heat	[Jkg^{-1}]
h	heat transfer coefficient	[Wm^{-2}K^{-1}]
I	current	[A]
j	superficial velocity	[ms^{-1}]
k	thermal conductivity	[Wm^{-1}K^{-1}]
K	Kutateladze number	
L	length	[m]
m	constant	
M	Molar mass	[gmol^{-1}]
n	number of moles	[mol]
Nu	Nusselt number	
q"	heat flux	[kWm^{-2}]
p	pressure	[bar]
Pr	Prandtl number	
Q	Heat	[W]
r	radius	[m]
Ra	Rayleigh number	
Re	Reynolds number	
t	time	[s]
T	Temperature	[K]
V	voltage	[V]
We	Weber number	

Greek symbols

α	void fraction	
η	wave amplitude	[m]
ρ	density	[kgm^{-3}]
θ	angle	[degree]
σ	surface tension	[Nm^{-1}]
σ	Stefan-Boltzmann constant	[Wm^{-2}K^{-4}]
ε	emissivity	[Nm^{-1}]
δ	thickness	[m]
ν	kinematic viscosity	[m^{2}s^{-1}]
μ	dynamic viscosity	[kgm^{-1}s^{-1}]

Subscripts

adia	adiabatic
atm	atmospheric
b	bubble
con	condensation
cs	cross-sectional
eva	evaporation
f	fluid
fg	vaporization
g	gas
j	junction
k	Kutateladze
l	liquid
max	maximum
rad	radiation
s	system
v	vapor
w	Wallis

Chapter 1. Introduction

1.1 Research Background and Motivation

There are various types of safety systems on nuclear power plants to protect human and environment from radiative hazards, while nuclear accidents occurred at Chernobyl, Three-Mile Island, and Fukushima nuclear power plants. Although the accidents were caused by complex reasons such as human error, failure of safety systems, unpredictable natural disaster, and so on. Current decay heat removal systems installed on commercial nuclear power plants supply additional coolant to the reactor pressure vessel or feeding water to the steam generators using the pump or pressure difference between the coolant reservoir and target system. However, working principles of the systems could be failed during station blackout (SBO) conditions due to the potential inability of depressurization of the reactor coolant system. Station blackout is one of key contributor to core damage frequency (CDF) of reactors. Therefore, various passive safety systems including auto-depressurization system have been under development for the purpose of risk reduction. The developed passive safety systems consist of many valves and pipelines because they must be operated at the accident conditions without backflow. The complex composition of the system has possibilities of single failure and common cause failure contributing malfunction of the systems. Size of the passive safety systems are larger than active safety systems due to lower driving force in equal scale. Reliability issues on passive safety systems are consistently discussed because they have high uncertainties and lack of operating experience. Thus, new conceptual passive decay heat removal system which is differentiated with the existing passive safety systems is required. The newly proposed system has to be simply designed in terms of system composition to operate with different working principle reducing failure risk. In this study, passive in-core cooling system (PINCs) integrated with hybrid control rods is proposed. The hybrid control rod is a new type of thermosyphon heat pipe having unique characteristics in aspects of operating condition and geometry compared to conventional gravity-assisted wickless heat pipes. To clarify the heat transfer characteristics and hydrodynamic phenomena of the hybrid control rod, experimental works were conducted with designs such as operating strategies and composition. The thermal-hydraulic phenomena inside the designed hybrid control rod was modeled based on theories and experimental data.

1.2 Review on Passive Safety Systems

Active safety systems depend on pumping power which requires the external power sources and operation signals. Owing to requirements for the operation, the possibility of failure under accident conditions. Representative examples are accidents occurred at TMI and Fukushima nuclear power plants. In TMI accident, the integrated active safety systems were not in operation because operator misjudged the condition of reactor in small break loss of coolant accident. As a result, the core was damaged although the corium was retained in reactor pressure vessel. Vulnerabilities of the active safety systems were also revealed by Fukushima accident. External power sources failed to supply electricity due to earthquake. The diesel generator and batteries which are internal power sources of the plants could not be operated because the building was flooded by tsunami. The integrated passive safety systems could not secure the coolability of reactor due to high operating pressure of the reactor pressure vessel. Eventually, the fuel-coolant interaction generated hydrogen and hydrogen explosion was occurred destroying the containment building. It can be concluded that the existing safety systems have limitation of impact on reactor safety under station blackout condition.

Passive safety systems which are equipped on nuclear power plants to supplement the weakness of active safety systems are summarized in Fig. 1-1. Most of them utilize the buoyant force which makes natural convection of the reactor coolant. Safety features drawn by blue lines are emergency core coolant injection systems; safety injection tank (SIT), core make-up tank (CMT), elevated gravity-driven drain tank (EGDT)[1]. They focus on injection of additional coolant to reactor pressure vessel to mitigate the dramatic increase of cladding temperature results from shortage of reactor coolant. However, they have insufficient driving force to overcome the high operating pressure inside the reactor pressure vessel in the condition of SBO. To enhance operability of the systems, hybrid-SIT which uses operating pressure of the reactor pressure vessel as a driving force of coolant injection by connection between primary system and storage tank was developed by Korea atomic energy research institute (KAERI).

The systems depicted by red lines are core cooling systems. Isolation condenser (IC) is a system condensing the generated steam from the reactor vessel and return the condensate to the core. Passive residual heat removal system (PRHRS) cools the reactor coolant by natural circulation with inclusion of pipelines connected to reactor pressure vessel inside the heat sink. The several PRHRS or IC are harmonized with suppression pool in boiling water reactors.

Third one is steam generator cooling system expressed by green lines. Passive auxiliary feedwater system (PAFS) could comprises pipelines connecting the main steam line and feedwater line. The steam generated by steam generator would be condensed passing the piping inside the heat sink, and the condensed coolant would be returned to the steam generator as a feedwater. The heat sink could be water storage tank or air tower using air convection. In this system, the decay heat generated by core is

removed by heat exchange between primary and secondary systems[2].

Various designs for passive containment cooling systems (PCCS) were suggested and they are under development to condense the leaked reactor coolant in the form of steam because the discharged reactor coolant as a vapor will increase the containment pressure and threaten the integrity[3]. By condensing the steam at the inner wall of containment, the containment pressure is expected to be reduced and the condensate can be recirculated to the reactor pressure vessel by recirculation system with sump.

Except the passive safety systems related with decay heat removal or cooling of power plant, there is a passive auto-catalytic recombiner (PAR) which reduces the hydrogen concentration inside the containment by recombining the produced hydrogen from fuel-cladding interaction with oxygen[4]. The PAR concentrates on the mitigation of hydrogen explosion which was occurred at Fukushima-Daiich accident.

Passive safety systems on nuclear power plants were studied for the enhanced safety with recognition about danger of active safety systems. However, there are inherent issues originates from system composition; i) the pipelines have possibility of break, ii) there are possibility of common cause failure or single failure of the valves, iii) low driving force which requires the relatively large system volume in comparison with the active safety systems, iv) reliability issues due to high uncertainties caused by sensitivity of natural circulation according to variables. The arranged problems make the application of the passive safety systems difficult. For the reduction of the suggested issues on previous safety systems, various system designs utilizing the heat pipe concept have been proposed owing to advantages of the heat pipes. Heat pipe has following advantages as a heat transfer device; i) simple working principle, ii) easy fabricability, iii) high heat transfer rate in small volume, iv) wide range of applicability. The proposed concepts applying heat pipes to nuclear power plants are summarized in Table 1-1. Nam et al.[5] used a multipod heat pipe (MPHP) design in a passive containment cooling system for the APR-1400, representative commercial pressurized water reactor in Korea. The multipod heat pipe was designed in aspect of thermal performances according to geometric parameters. In the analysis, thermal resistance model was used to design the MPHP meeting the required heat removal capacity. The volume of MPHP sink was determined to satisfy the accident managing time. Their numerical calculation results showed the PCCS based on MPHP can mitigate the sharp increase of containment pressure including long-term cooling phase. A concept of spent fuel pool cooling system with thermosyphon heat pipes was proposed by Mochizuki et al.[6]. They constituted the thermal resistance circuit across the heat transfer path, and the heat removal capacity of the thermosyphon was calculated using the constructed thermal resistance circuit. The analysis secured the prevention of boiling of coolant in the spent fuel pool due to sufficient decay heat removal capacity of the heat pipes. Sviridenko[7] designed various passive decay heat removal systems which equipping heat pipes for the WWER (Water-Water Energetic Reactor). Imaginary design candidates were suggested for the long-term coolability of the reactor in this study. Gou et al.[8] imagined a system utilizing the heat pipes as a

pump between primary and secondary systems. Hejzlar et al.[9] attempted to use sodium heat pipe as a decay heat removal device under accident conditions. The heat pipes are designed to dissipate the decay heat from the reactor pressure vessel to earth. Dunkel et al.[10] suggested the core cooling system and ex-vessel cooling system comprises heat pipes and a heat sink. The heat pipes were installed at the guide tubes for control rod to be inserted in the core and others cover the surface of reactor pressure vessel in forms of bend heat pipe. The systems reduced temperature gradient between core and vessel wall by transporting the decay heat from the core to the heat sink. Other researches[11, 12] challenged to adapt the heat pipe to space nuclear reactors because the capillary heat pipe is passive heat transfer device using phase change and convection of the working fluid in the manner of capillary flow. Thus, heat exchange between heat source and sink could be achieved through through the heat pipe without pump.

Most of the previous studies attempted to apply the heat pipe to the nuclear power plants introduced their heat pipe-driven concepts and discussed regarding the coolabilities and efficiencies of the systems with lumped calculations. However, validations of models they used in the calculation were not conducted and physical insight on the heat pipes have not been discussed.

Table 1-1. Literatures introducing passive safety systems based on heat pipes

Researchers	Key concepts
Dunkel [10]	In-vessel heat pipe and Ex-vessel heat pipe cooling at LOCA
Mochizuki et al. [6]	Heat pipe decay heat removal system for spent fuel pool
Siviridenko [7]	Heat pipe decay heat removal system for WWER
Gou et al. [8]	Heat pipe system for heat transfer between RPV and steam supply system
Hu et al. [12]	Lithium and Potassium heat pipe for cooling system of nuclear fission reactor on Moon
Peterson et al. [11]	High temperature heat pipe for small nuclear fission reactor of spaceship
Hejzlar et al. [9]	Sodium heat pipe for heat dissipation from vessel to earth
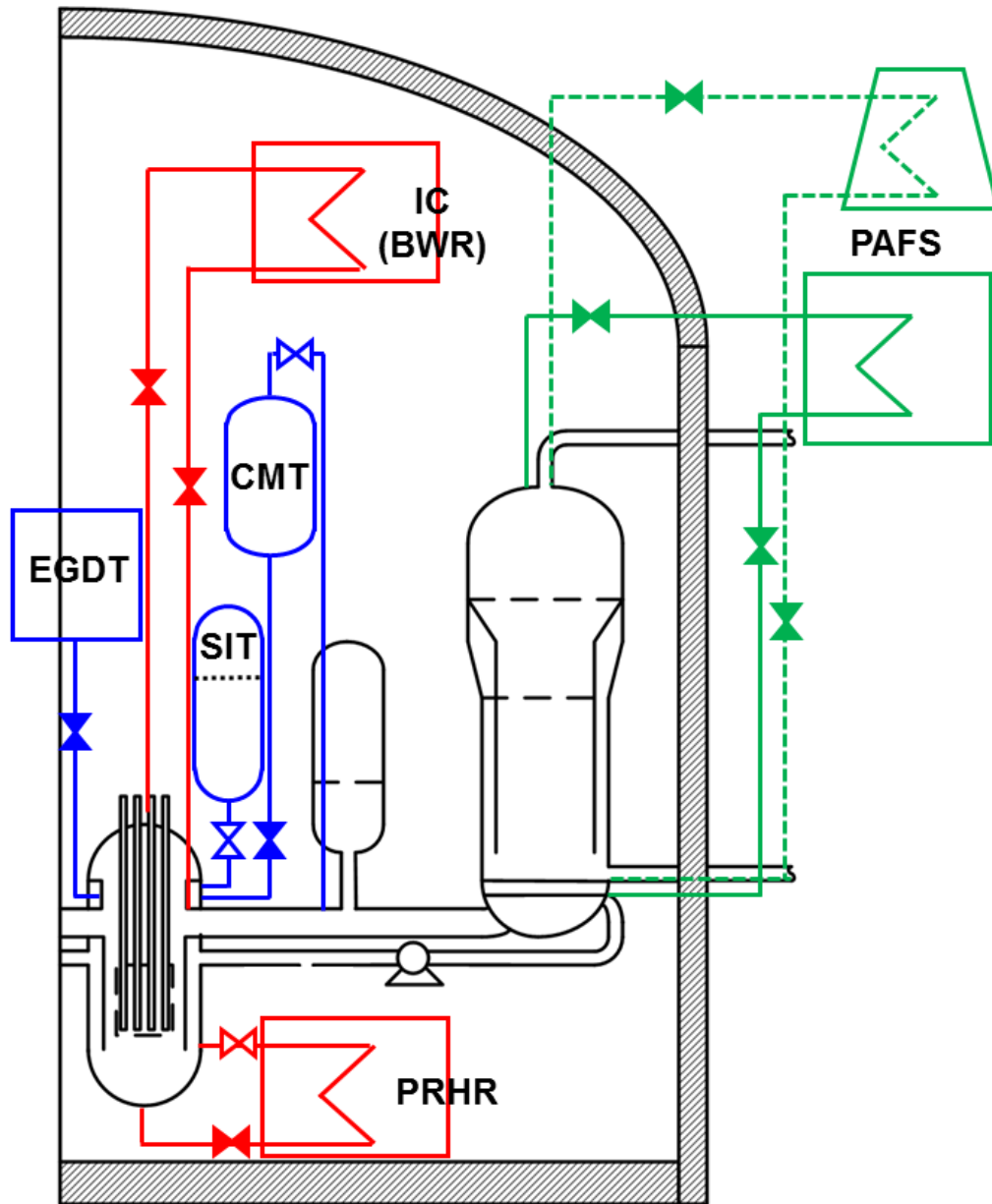
Fig 1-1. General features of passive safety systems in light water reactors

1.3 Concept of Passive IN-core Cooling System Based on Hybrid Control Rod

The passive safety systems which are under development or were installed at nuclear power plants have issues in terms of reliability, operation experience, and coolability compared to volume. For the development of passive safety system escaping from the suggested issues, conceptual designs of passive safety systems based on the use of heat pipes were proposed. Although the studies concluded that their systems are effective in accident conditions, the conclusions were derived by numerical calculations without validating the results. Thus, new type of passive safety system is necessary distinguished from the existing safety systems to supplement the weak points. The requirements for the new safety systems can be summarized as follows; i) simple working principle, ii) different working principle from existing systems, iii) simple composition of system (for the purpose of reduced possibility of failure in operation), iv) significant decay heat removal capacity.

In this study, a hybrid control rod which is a new type of thermosyphon heat pipe is proposed as a passive decay heat removal device[13]. The thermosyphon heat pipe is a type of heat pipe which transports the heat from high temperature interface to low temperature interface by phase change (evaporation and condensation) and convection of the working fluid (returning of condensed liquid from condenser to evaporator section by gravity) inside the closed metal container. The detailed schematic of the hybrid control rod is depicted in Fig. 1-2. The control rod absorbs neutrons to shutdown the fission reaction. Thus, the hybrid control rod can be defined as a heat pipe containing neutron absorber at the evaporator section which corresponds to part of core. The proposed hybrid control rod could be applied to various nuclear facilities such as commercial light water reactors, GEN-IV reactors, and spent fuel dry storage cask as shown in Fig. 1-3. The hybrid control rods are connected with control rod drive mechanism (CRDM) which controls the elevation of control rods inside the reactor pressure vessel utilizing mechanical forces or hydraulic force[14]. At normal operation of reactor, the hybrid control rod will be far from the core to maintain the criticality of reactor. When an arbitrary initiating event for anticipated operation occurrences (AOO) or design basis accidents occurs, the signal that is provided on the CRDM will be lost and the hybrid control rods will be inserted to the reactor core at the initial phase of the accidents by gravitational force. Subsequently, decay heat transported from the reactor core to the heat sink through the phase change and convection of the working fluid inside the hybrid control rod.

The hybrid control rod satisfies the requirements of new safety system because it could be operated by gravity without pumping power or driving force depending on the pressure difference. Other components helping the operation of the hybrid control rod is not necessary (passive in-core cooling system based on the hybrid control rod does not require any valves). The PINCs which comprises the hybrid control rods, heat sinks (primary and ultimate heat sinks), pipeline between the heat sinks has simple composition of system design. Consequently, the PINCs based on the hybrid control rods could be easily integrated on the nuclear facilities requiring the thermal-neutronics control[15].
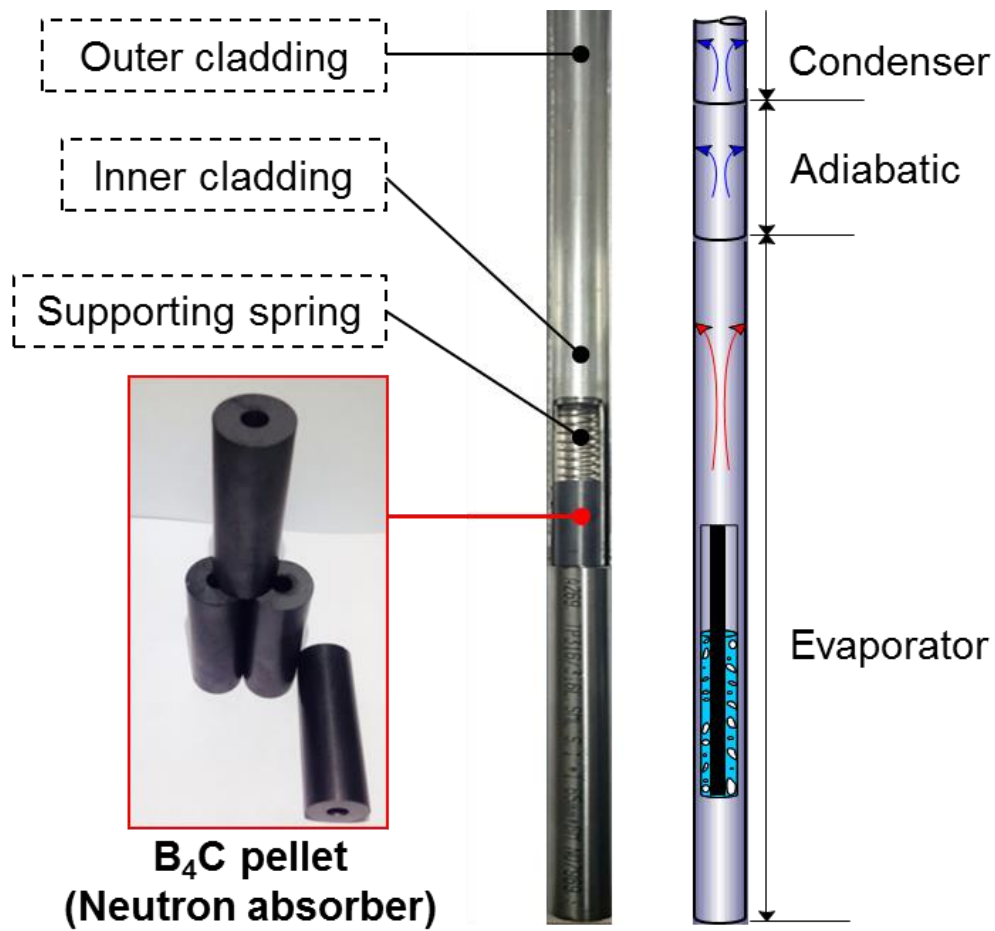
Fig 1-2. Composition and working principle of hybrid control rod
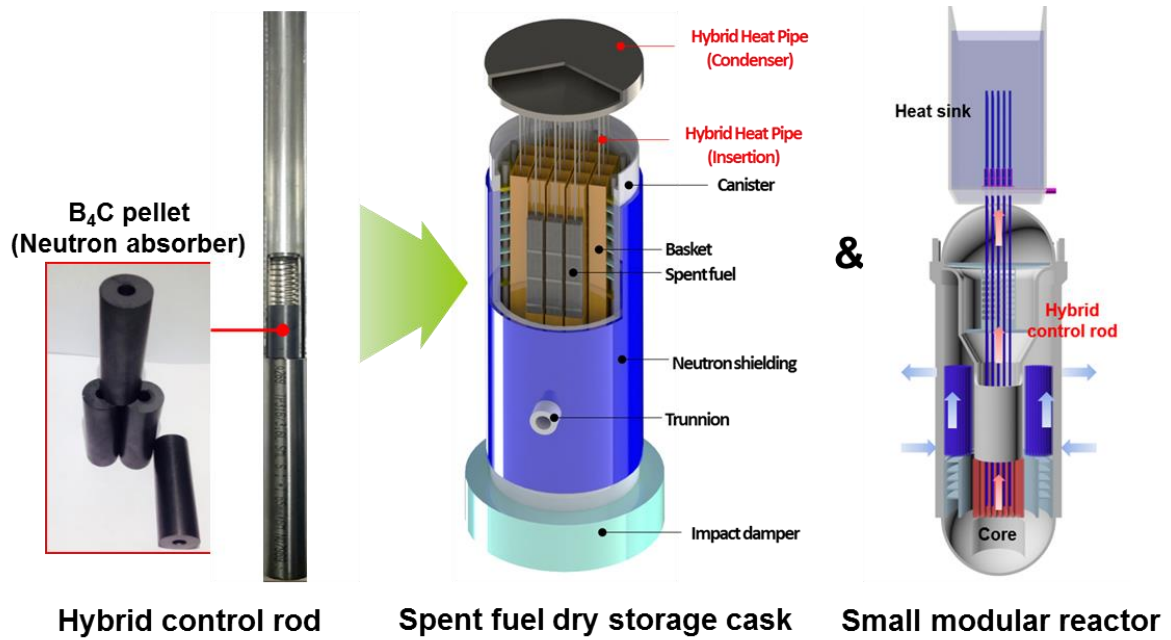
Fig 1-3. Composition and working principle of hybrid control rod

1.4 Objectives and scope

The present study aims for development of hybrid control rod for passive in-core cooling system (PINCs) that is a new type of passive safety system differentiated from the existing safety systems. This manuscript contains the researches on design and performance analysis with experimental works and modeling on thermal-hydraulics inside the hybrid control rod.

1) To design the hybrid control rod to satisfy the functional requirements as a component of passive safety system in terms of thermal-hydraulics

2) To establish operating strategy of the hybrid control rod and confirm its feasibility

3) To model the heat transfer characteristics and maximum heat removal rate of the hybrid control rod

4) To confirm the effect of PINCs on nuclear safety

Chapter 1 briefly introduces existing passive safety systems and passive in-core cooling system based on the hybrid control rod to demonstrate the motivation, necessity, and objectives of this study.

In chapter 2, research trend on the thermosyphon heat pipe was reviewed and details on the hybrid control rod designs including operating strategies (pressure control mechanism) were included. Thermal performances of the designed hybrid control rod according to pressure control mechanisms were experimentally studied. Based on the experimental data, heat transfer characteristics and maximum heat removal capacity of the hybrid control rod were analyzed for the deduction of optimal operating strategy.

In chapter 3, the analysis capability of current thermal-hydraulics code on the hybrid control rod was evaluated. After confirming the limited prediction capability of the code, previously developed correlations related to the thermal-hydraulics inside the thermosyphon heat pipes were compared with experimental results to select the optimal model or develop new models which can be implemented to thermal-hydraulics system codes. New models analyzing condensation heat transfer and flooding-based maximum heat transfer rate were developed with theoretical backgrounds specialized to the hybrid control rod. Validation works on the developed models were conducted with additional experiments and the experimental results were discussed.

In chapter 4, one of design candidates of PINCs were proposed. The scaled down mock-up was manufactured to demonstrate the UCAN (UNIST canister) design. Effects of the hybrid control rod and heat sink design on the thermal behavior inside the canister were analyzed by the experiments conducted with prepared mock-up.

The conclusions and recommendations are described in chapter 5.

Chapter 2. PERFORMANCE ANALYSIS OF PRESSRURIZED HYBRID CONTROL ROD

2.1 Introduction

The concept of the passive in-core cooling system (PINCs) based on the hybrid control rods was proposed in Chapter 1. The design of the hybrid control rod has to be conducted for the sufficient functionalities in aspects of decay heat removal and neutron absorption. The parameters contribute thermal performances of the thermosyphon heat pipe were contracted from the literatures because the performance of the hybrid control rod would be similar with the general thermosyphons excepting several unique characteristics. Besides, the understanding of the thermal-hydraulics in the thermosyphon would be helpful to design the hybrid control rod in an expected direction and analyze the measured heat transfer characteristics and maximum heat transfer rates. Composition of the hybrid control rod was designed to satisfy the functional requirements as a decay heat removal device and dimensions of the components inside the hybrid control rod were determined. Based on general design of the hybrid control rod, differences between the hybrid control rod and previously studied thermosyphons were introduced since the unique characteristics of the hybrid control rod would be crucial factor determining its performances distinguished from the concentric thermosyphons or concentric annular thermosyphons. The operating temperature and pressure of the hybrid control rod would be much higher than the heat pipes studied by previous literatures because the environment to be applied is nuclear facilities which have high operating temperature and pressure. Thus, the pressure control mechanisms were established to achieve high operating pressure. The variables that are expected to affect the pressurization were determined, and their effects on performances of the hybrid control rod were studied by experiments. The feasibility of the pressure control mechanisms was discussed with experimental data and optimal pressure control mechanism was selected considering the passive operation characteristics and performances.

2.1.1 Literatures on thermosyphon heat pipe

Thermosyphon heat pipe is defined as gravity-driven wickless heat pipe. Inside the thermosyphon, the phase changes (evaporation and condensation) of working fluid occur at high and low temperature interfaces. The driving forces of working fluid convection are gravity and vapor pressure[16]. The upward vapor flow is generated by pressure gradient from evaporator and condenser sections and the downward liquid film flow is achieved by gravity. There is countercurrent flow between upward vapor flow and downward liquid film flow exerting the shear stress at the interface between vapor and liquid film. The shear causes instability or flooding phenomenon of the liquid film that are hydraulic phenomena determining maximum heat removal capacity of the concentric thermosyphon heat pipes. There are

various types of thermosyphon modifying the forms into cylindrical, loop, rotational, U-shape, and so on because of easy working principle. The most general types of thermosyphon are concentric cylindrical heat pipe and loop type thermosyphons. Various parameters such as fill ratio of the working fluid, the inclination angle, the type of working fluid, aspect ratio, operating pressure, and condition of condenser section affect the performances of thermosyphon heat pipes.

At the evaporator section, the main heat transfer mechanisms were reported as nucleate pool boiling and evaporation at falling liquid film. When the fill ratio of the working fluid is sufficiently high and loaded heat flux is low, high volume fraction of the evaporator section will be occupied by liquid pool. The nucleate pool boiling in the manner of bubble nucleation, growth, and departure at the cavities of heater surface is heat transfer mechanism of the heat pipes. The collapsed level of liquid pool at evaporator section decreases as the fill ratio decreases and heat flux increases. The inner wall of the evaporator section`s rest volume will be covered by falling liquid film. In that condition, the evaporation will be occurred at the liquid film surface. In the medium fill ratio and heat flux conditions, the nucleate pool boiling and liquid film evaporation are combined. Thus, the effect of fill ratio, operating pressure, and geometry of test section on evaporation heat transfers characteristics have been studied[17-29].

The condensation heat transfer characteristics of the heat pipes have been studied to enhance the prediction capability of Nusselt theory through modification of the model. The condensation heat transfer models were developed by assuming that the heat is transferred in the form of falling liquid film. The thin liquid film was easily affected by shear at liquid film surface due to countercurrent flow. Therefore, the effects of waviness, film Reynolds number, and entrained droplet on the condensation heat transfer were considered in the development of condensation models to extend the flow regime from laminar to turbulent flow[30-37]. The detailed information about the previous researches focusing on the evaporation and condensation heat transfers in thermosyphon heat pipes will be demonstrated in Chapter 3.

Many researchers attempted to enhance the heat transfer rates at evaporator and condenser sections by application of nanofluids, suggestion of internal structures, and so on.

One of the method is installation of additional tube inside the outer cladding to increase the heat transfer area and enhance the thermal performances. It was a birth of concentric annular vapor-path thermosyphon containing inner tube. The hybrid control rod is a thermosyphon heat pipe with an annular vapor path at the evaporator section. Hence, the studies on annular vapor-path thermosyphon will be helpful to predict the thermal-hydraulic phenomena inside the hybrid control rod. The variables affecting the performances also can be selected by gathering the controlled parameters in the studies.

Rosler et al.[38] observed the maximum heat removal rate of a vertical annular closed two-phase thermosyphon with low fill ratios of 3 – 30 %. R113 was charged into test section as working fluid, and variation of flow patterns with heat fluxes were observed. The authors proposed a dryout-based maximum heat transfer rate model for thermosyphons having low fill ratios. The model was derived

theoretically and the experimental data validated the derived correlation. Vijra et al.[39] carried out experiments to study the thermal performance of concentric annular heat pipe. The wetted and heated perimeters of the test sections were same. Heat loads and inclination angles were controlled to observe their influence on the performances. The largest heat transfer area and efficient gravity-driven convection of vertically mounted test section attributed to the lowest thermal resistance. Lin et al.[40] studied the effect of fill ratio, condenser temperature, and evaporator length on heat transfer characteristics at the evaporator section of an annular thermosyphon. The operating pressures were below than atmospheric pressure and the heat transfer mechanism was geyser boiling. They found that the period of bubble generation, growth, departure, collapse, and return to hotter section depends on the several parameters they controlled. A correlation was proposed for the prediction of heat transfer coefficient of annular thermosyphons. Boo et al.[41] investigated the heat transfer characteristics of concentric annular thermosyphons varying the diameter ratio between the inner and outer tubes and the fill ratio of working fluid. The fill ratio influenced the thermal resistance and the effect was magnified with increase of diameter ratio. They concluded that the maximum heat removal capacity (operation limit) was proportional to fill ratio of the working fluid. Faghri et al.[42] conducted study on the flooding-based operation limit and heat transfer coefficients of concentric annular thermosyphons. They established the flooding limit of the test section by modifying the previously developed models of Imura[43], and Tien and Chung[44]. In low Reynolds number region, the established correlations had provided accurate prediction capability, while a new correlation was required for the high Reynolds number regime. Thermosyphons using water also showed significantly different experimental results compared to model predictions. Thus, they suggested a new correlation based on their experimental results and concluded the correlation must be validated with more experimental data. Nouri-Brujerdi and Layeghi[45] numerically analyzed the vapor flow inside the concentric annular heat pipes. Using the Navier-Stokes equations, the fluid flow and heat transfer in annular vapor space are simulated. Through the validation work, the vapor flow model was developed to provide good prediction accuracy in the range of low to moderate radial Reynolds number. The vapor pressure and temperature distributions according to various heat fluxes were predicted well. Yoshida et al.[46] performed experimental study with two-phase double tube thermosyphons charged with water, ethanol, and Freon 113. The effect of subcooling on the flow and heat transfer was studied. The performances were compared with single-tube thermosyphons (concentric thermosyphons) and correlated the heat transfer coefficients separately according to types of test section. In the correlation, subcooling and properties of the working fluids were well modeled. The derived correlations showed good agreement with experimental data and previous works. Ismail and Adewoye[47] did the works on numerical analysis and modeling of laminar flow in double-tube heat pipes. Several important flow parameters such as friction loss, shape of test section, and entrance were collected and the behaviors of them on the flow inside the test section were modeled.

Other researchers[48-52] analyzed the thermal performance of annular thermosyphons and annular heat pipes according to various parameters. The major parameters having sufficient influence on the thermal-hydraulics in concentric annular thermosyphons were fill ratio, operating pressure, and ratio of diameters between inner tube and outer tube. The deduced parameters will be controlled at the experimental works of the hybrid control rods, though the hybrid control rod has unique characteristics compared to the general two-phase thermosyphons.

2.1.2 Characteristics of hybrid control rod

The hybrid control rod is a new type of thermosyphon heat pipe including cylindrical neutron absorber at centerline of the evaporator section corresponding to the reactor core. The condition of the hybrid control rod is much higher than conditions that have been studied in previous researches. Thus, the hybrid control rod has unique characteristics in comparison with previously studied thermosyphon heat pipes in aspects of geometry and operating range as shown in Fig. 2-1.

There have been studies on concentric annular thermosyphon to enhance thermal performances and maximum heat removal rates. Previously studied test sections associated with the concentric annular thermosyphons had annular vapor path across the whole length of the test section and the tubes inserted at the center of the test sections were heat transfer area (evaporation and condensation heat transfers were occurred at the outer wall of inner tube and inner wall of the outer cladding)[38-42]. Therefore, the heat transfer performances or operation limits of the concentric annular-vapor path thermosyphons were analyzed assuming the annular vapor path as a cylindrical vapor path having hydraulic diameter of the annular thermosyphons because heated diameter and hydraulic diameter are coincident to each other in the geometry. However, the neutron absorber material used in this study is boron carbide (B_4C) which is a ceramic material having low thermal conductivity. The inner cladding is installed at the evaporator section to provide the interface between neutron absorber and working fluid. The inclusion of the neutron absorber inside the inner cladding protects the effect of swelling of the neutron absorber or morphology deterioration by reaction with working fluid could be neglected, and the reaction heat generated by neutron absorption could be neglected by the additional thermal resistances (gap between neutron absorber and inner tube, and cladding wall). The design on evaporator section of the hybrid control rod makes difference between heated diameter and hydraulic dimeter. As a result, the assumptions applied on the existing annular vapor-path thermosyphons could be meaningless to the hybrid control rod.

The working fluid of the hybrid control rod was determined as water due to its compatibility to cladding material (Zircaloy) and nuclear environment. Liquid metals that have been used in the heat pipes operating at high temperature environment have side effects such as reaction or explosion with reactor coolant in light water reactor. Organic fluids such as refrigerants will be dissolved in nuclear

fission environment. Other conventional fluids can produce non-condensable gas during operation owing to reaction with cladding material. Water has a high figure of merit which is a key parameter of heat transfer fluid.

The hybrid control rod charged with water must operate at high temperature and high pressure environments. Consequently, non-condensable gas would be charged inside the test section to achieve relatively high saturation temperature. The heat transfer coefficients and operation limits of the previously studied test sections were modeled in sub-atmospheric pressure range. Although several literatures focused on the effect of non-condensable gas produced by reaction between working fluid and cladding, the operating pressures were in low or moderate range. Variable conductance heat pipes utilizing the non-condensable gas for the purpose of controlling internal pressures concentrated on the maintenance of constant evaporator temperature. The operating pressures were also limited in sub-atmospheric pressure range. Hence, the quantitative observation about the effects of non-condensable gas on the thermosyphons` performances were not conducted. The heat transfer characteristics of the thermosyphon operating at high pressures with charge of non-condensable gas could be distorted from the reported heat transfer coefficients because the concentration of the non-condensable gas inside the hybrid control rod would be significantly higher than the conducted studies. Flooding limit of the thermosyphons at high operating pressures were modeled with the thermosyphons charged with refrigerants having low density ratio between vapor and liquid because the flooding phenomenon takes place in the water thermosyphons could be simulated by scaling the density ratio. While the prediction models well predicted the operation limits of thermosyphons, the experimental data measured by water thermosyphons were deviated with predictions. The difference of hydraulic diameter and heated diameter could attribute the flooding phenomenon.

In integrates, inclusion of the neutron absorber differentiates the geometrical point of the hybrid control rod from the general thermosyphons. Significantly high operating pressures achieved by charge of non-condensable gas and accumulation of water vapor are the main characteristics of the hybrid control rod.

2.1.3 Pressure control mechanism of hybrid control rod

To achieve high operating pressures of the hybrid control rod, the pressurization strategies are necessary. Loop heat pipes equipped with pressure chamber were reported in the literatures[53-55] for the maintenance of evaporator temperature or controlment of heat transfer rate. Additionally, actuator must be integrated to control the internal pressures of the test section. Pressurizers of the nuclear power plants use heater to generate vapor and the pressurization of the reactor coolant system are achieved by accumulation of the generated vapor. Safety injection system uses non-condensable gas to pressurize the tank and inject the emergency coolant to the reactor when the pressure of the reactor coolant system

is lower than storage tank pressure. For the passive controlment of operating pressure of the hybrid control rod, the non-condensable gas will be charged. However, much amount of non-condensable gas will limit the effective heat transfer length by prohibiting the reach of vapor to condenser section. If the vapor from the evaporator does not reach the condenser section, the heat transfer from evaporator to condenser section will not be taken place. Thus, controlling the volume occupied by the non-condensable gas at the condenser section is an issue on pressure control of the hybrid control rod.

Utilizing the pressurization mechanisms of pressurizer and safety injection system in light water reactors, two pressurization strategies were established for the hybrid control rod as shown in Fig. 2-2. First one is pressure regulating strategy using pressure regulator. In this strategy, the non-condensable gas is charged in the test section with a target pressure. During the operation of the hybrid control rod, the kinematic vapor pressure will be formed from the evaporator to condenser sections, the non-condensable gas initially charged in the test section will be removed through the pressure regulator that is installed at the top of the test section. The pressure regulator is a key component in the pressure regulating strategy. It has advantage in terms of easy controlment of internal pressures, on the other hand, the target pressure cannot be changed after first set-up and internal pressure will be fixed because the device cannot be extracted from the core after loading the hybrid control rod in the reactor. Second strategy is self-pressurization which uses the volume expansion and vapor accumulation of the working fluid with charge of non-condensable gas. The non-condensable gas will determine initial pressure inside the hybrid control rod, and the kinematic vapor pressure will compress the volume of non-condensable gas. There is no need to use components related to pressure regulation. The self-pressurization strategy is superior than pressure regulating strategy in a viewpoint of passive operation because it does not have any pressure regulating components having possibility of failure and the internal pressure can be controlled by boundary and initial conditions such as heat load, initial amount of non-condensable gas, fill ratio of working fluid, coolant temperature and flow rate of the condenser section, and so on.
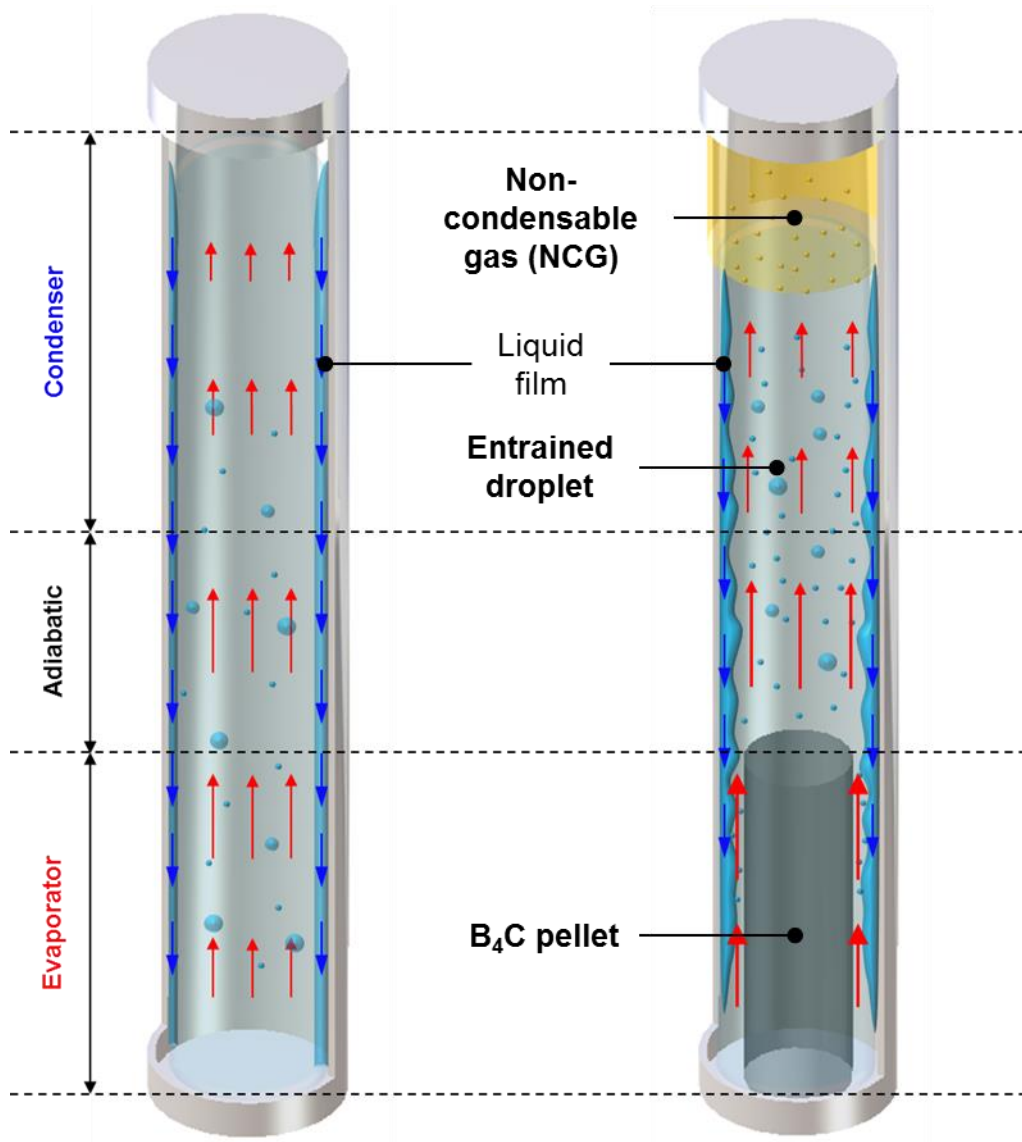
Fig 2-1. Comparison of conventional thermosyphon (left) and hybrid control rod (right)
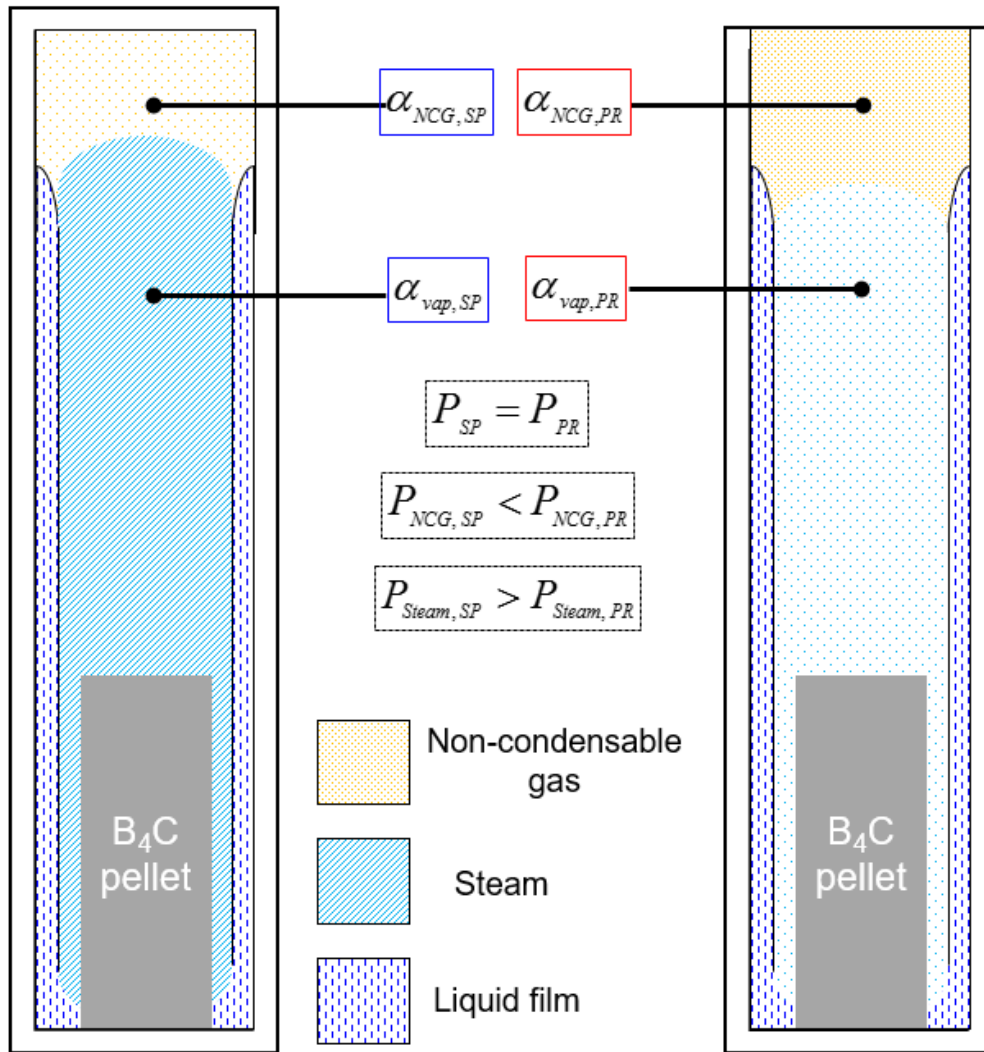
Fig 2-2. Pressurization strategies of the hybrid control rod; self-pressurization (left) and pressure regulation (right)

2.2 Experimental Setup and Procedure

Based on the established pressurization strategies, the parameters will be controlled in the experiments were summarized to observe their influence. Fill ratio of the working fluid, initial amount of non-condensable gas (initial pressure), and heat loads were selected as controlled parameters. To confirm the feasibilities of the pressurization strategies and observe the effects of controlled parameters on the pressurization phenomena in the test sections, test matrix was established as presented in Table 2-1. In this section, the details on prepared test section for the experiments were described. Information on experimental facility, test procedure, and data processing which were utilized to measure the performances of the hybrid control rods according to parameters and pressure control strategies was demonstrated. Then, experimental uncertainties were analyzed to check the accuracy of the experimentally measured results.

2.2.1 Test section

A 1-m-long stainless steel tube having sheath outer diameter of 25.4 mm and inner diameter 22.0 mm was used as outer cladding of the test section. The outer diameter of the test section was determined referring that of existing control rod in commercial light water reactor, APR-1400. Inner surface of the test section was smooth to prevent the effect of surface roughness on thermal-hydraulic phenomena. The length ratio of evaporator, adiabatic, and condenser section is 285:215:500. Inside evaporator section of the test section which corresponds to reactor core, neutron absorber, boron carbide (B_4C) pellet of 17.7 mm outer diameter was installed as shown in Fig. 2-2. Therefore, gap between inner wall of the cladding and neutron absorber is 2.15 mm. Deionized water which is working fluid of the test section fill the gap to certain fill ratios. Then, non-condensable gas, nitrogen was charged in the test section to achieve target initial pressures[56].

2.2.2 Experimental apparatus

The composition of hybrid control rod test facility is shown in Fig. 2-4. At the top and bottom of the evaporator section of the test section, two copper electrodes are connected to a DC power supply and those heat the test section by passing current (Joule heating). Water storage tank stores coolant which will be circulated to the water jacket by pump. The water jacket condenses the evaporated vapor inside the test section by forced convection at the outer wall of the condenser section. Backpressure regulator which maintains constant system pressure by removing non-condensable gas and a pipeline connected to the nitrogen gas tank were installed at the top of the test section for the pressure regulating experiments. In case of self-pressurization experiments, the backpressure regulator was removed and

valve between test section and nitrogen gas tank was closed.

Total sixteen K-type thermocouples were installed at the test section (six on evaporator section with 41 mm interval, six on adiabatic section with 30.7 mm interval, and four on condenser section with 10 mm interval) to measure the temperature variation data. Coolant temperatures at inlet and outlet of the water jacket were measured by two T-type thermocouples which will be used in the calculation of efficiency of the hybrid control rod (heat balance) with mass flow rate data recorded by turbine flow meter. A pressure transducer equipped on the top of the test section recorded the pressure variations during the experiments.

2.2.3 Test procedure and experimental uncertainty

The working fluid was filled into the test section with fill ratios of 35 and 42 % (Ratio of volume of working fluid to total volume of test section). After filling the working fluid, non-condensable gas (nitrogen) was charged on the test section until target initial pressures, $1-20$ bar for pressure regulating cases and $1-7$ bar for self-pressurization cases. The prepared test section was heated step by step achieving steady states until maximum heat transfer rates. The maximum heat transfer rates were confirmed as a heat load showing sudden increase of evaporator wall temperature. The vapor generated from the evaporator section was condensed by forced convection at the water jacket, and the heat removal rate through water jacket was calculated by Eq. (2-1). The mass flow rate of the coolant at water jacket was maintained constantly. During the pressure regulating experiments, the backpressure regulator removed nitrogen gas inside the test section to maintain constant internal pressure. Evaporation heat transfer coefficients were calculated dividing the heat flux by wall superheat as Eq. (2-2). Condensation heat transfer coefficients were obtained by removed heat flux and subcooling as Eq. (2-3).

$$Q_c = \dot{m}c_p\left(T_{in} - T_{out}\right) \tag{2-1}$$

$$h_e = IV/\pi D_e L_e\left(T_{ew} - T_{sat}\right) \tag{2-2}$$

$$h_c = \dot{m}c_p\left(T_{in} - T_{out}\right)/\pi D_c L_c\left(T_{sat} - T_{cw}\right) \tag{2-3}$$

The measurement errors in the instruments are summarized in Table 2-2. The uncertainties in the parameter measurements such as heat flux, heat transfer coefficients, thermal resistances were analyzed by the Kline and McClintock method[57] (Equation 2-4).

$$\frac{\Delta\varphi}{\varphi} = \frac{1}{\varphi}\sqrt{\sum_{i=1}^{n}\left(\frac{\partial\varphi}{\partial x_i} \times \Delta x_i\right)^2} \tag{2-4}$$

where φ is the derived parameter, x_i represents the measured variables, and Δx_i represents the error of the measured variables. The tolerances in the length and diameter of the test section were 5 mm and 1 mm, respectively. Hence, the calculated maximum uncertainty in the heat flux is 7.2%. The maximum uncertainties in the heat transfer coefficient and thermal resistance were estimated as 5.2% and 7.6%, respectively.

Table 2-1. Experimental conditions for performance analysis of hybrid control rod

	Pressure control strategies	Self-pressurization
Amount of working fluid [ml]	90	90, 110, 130
Fill ratio of working fluid [%]	29.0	29.0, 35.5, 42.0
Initial pressure [bar]	1.0 – 20.0	1.0, 5.0, 7.0
Heat load [W]	Until operation limit	
Length ratio (evaporator:adiabatic:condenser)	285:215:500	
Condenser mass flow rate [kg/s]	0.0267	

Table 2-2. Measurement uncertainties of instruments

Parameters	Instruments	Uncertainties
Temperature	Thermocouple	± 0.1 ºC
Pressure	Pressure gauge	± 0.1 kPa
Water flow rate	Turbine flowmeter	± 0.05 lpm
Voltage	Voltmeter	± 0.02 V
Current	Amperometry	± 4 A

Fig 2-3. Composition and dimensions of the test section
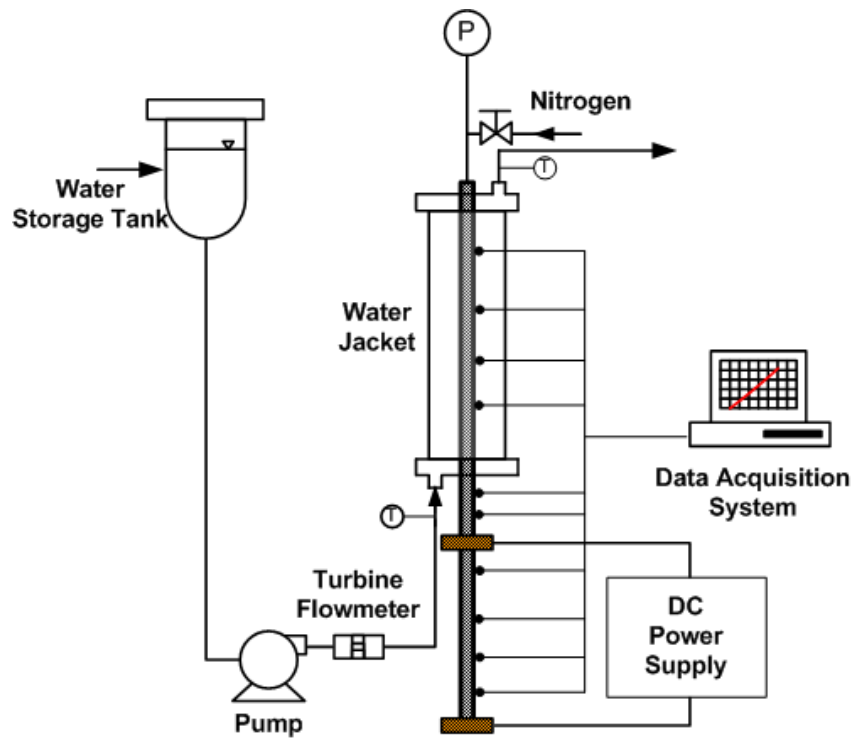
Fig. 2-4. Schematic diagram of the test facility

2.3 Results and discussion

Feasibility of the considered pressure control mechanisms were experimentally studied with measurement of effect of operating pressure, heat loads, fill ratios of working fluid on heat transfer characteristics and maximum heat transfer rates. Relations between parameters were deduced from the experimental data based on the theories reported from previous studies and assumptions. The optimal pressure control mechanism was determined by comparison of efficiency in terms of heat transfer and passive operation.

2.3.1 Heat transfer characteristics

Evaporation and condensation heat transfer coefficients of the pressure regulated hybrid control rod are shown in Figure 2-5. The evaporation heat transfer coefficients of the hybrid control rod operation at sub-atmospheric operation pressure was lower than those at operating pressures higher than atmospheric pressure owing to different heat transfer mechanisms. The vapor-liquid density ratio is very large at sub-atmospheric pressure (0.2 bar) compared to high operating pressures, consequently, the large sized-vapor would be generated at the evaporator section and it covers the inner wall of the test section forming liquid plugs and vapor slug. The liquid plug and vapor slug would be transported to the condenser section and destroyed. The destroyed liquid plug return to the evaporator section in the form of liquid film. The addressed heat transfer mechanism is defined as geyser boiling[58-60]. Thus, the bubble growth time and uncovered heat transfer area could be larger than pool boiling or liquid film evaporation heat transfer mechanisms. On the other hand, bubble sizes at pressures higher than atmospheric pressure are significantly smaller than the vacuum states. Water pool would occupy a portion of the evaporator section and liquid film would occupy the rest portion of the evaporator section. Heat transfer could be achieved by pool boiling, evaporation at falling liquid film, or combination of the mechanisms.

In general heat flux region, the heat transfer through pool boiling is lower than liquid film evaporation, while the effect of the vapor–liquid density ratio on heat transfer characteristics in the evaporator section was negligible within pressure ranges of 3–20 bar. The gap between B_4C pellet and inner wall of the cladding is 2.1 mm. If the bubble is generated and it escape the evaporator section, the vapor would be agglomerate at the center-side of the evaporator section and liquid film would be cover the inner wall. Hence, the main heat transfer mechanism is considered as liquid film evaporation which is not sensitive to the density ratio, and evaporation heat transfer coefficient according to operating pressures was similar to each other.

In aspect of condensation heat transfer, the heat transfer coefficients were inversely proportional to operating pressure (fill amount of non-condensable gas, nitrogen). Non-condensable gas dominates the condensation heat transfer because the gas is accumulated at the top of the condenser section due to

kinematic vapor pressure from evaporator section, and it impedes diffusion of steam to condenser wall or reduces the effective heat transfer length[56]. The amount of non-condensable gas is remarkably low in case of the test section operating at 0.2 bar, while in the case of high-pressure operation, the test sections are charged with nitrogen. Therefore, a noticeable difference was observed in the condensation heat transfer under sub-atmospheric pressure and normal pressure conditions.

As the heat load increases, the vapor pressure increases compressing the non-condensable gas. When the system pressure increases, the backpressure regulator which was installed at the top of the test section controls the internal pressure by removing some portion of nitrogen gas to maintain the constant operating pressure. The reduced amount of non-condensable gas extends the effective condensation heat transfer length, with the proportional tendency between condensation heat transfer coefficient and heat load as shown in Fig. 2-5(b).

The backpressure regulator is a component having possibility of the failure which could limit performance of the hybrid control rod. Thus, different pressure control mechanism is required because passive operation must be secured as a decay heat removal device. Self-pressurization strategy which utilizes the volume expansion of working fluid and accumulation of vapor is experimentally studied to confirm the feasibility and characteristics of the strategy. The effect of fill ratio and initial pressure of the test section on the heat transfer characteristics, operating pressure, and maximum heat transfer rates were observed by varying the fill ratio of the working fluid and initial pressure determined by charge of non-condensable gas.

Tendency of the measured operating pressure according to heat load, fill ratio, and initial pressure is plotted in Fig. 2-6. The operating pressures were proportional to initial pressure, fill ratio, and heat loads. The operating pressure increased as the heat load increases due to the volume expansion of the working fluid and accumulation of the steam as assumed in the establishment of pressure control strategy. As the initial pressure increases, the range of operating pressure and heat flux which the hybrid control rod works become wider because the operation limit of the hybrid control rod is proportional to the pressure. Maximum operating pressure of 20 bar that working fluid exerts maximum heat transport efficiency in terms of thermos-physical properties was achieved successfully through the self-pressurization strategy.

The evaporation and condensation heat transfer coefficients for specified conditions were depicted in Fig. 2-7. In case of evaporation heat transfer coefficients, similar heat transfer coefficient values were measured in comparison with pressure-regulated hybrid control rod as shown in Fig. 2-7(a). The heat transfer coefficients were independent on fill ratios of the working fluid and operating pressures demonstrating that the heat transfer mechanism is liquid film evaporation which is independent on the controlled parameters. The condensation heat transfer coefficients were independent on the fill ratios, and depended on the initial pressures. The inverse proportionality between heat transfer coefficient and initial amount of non-condensable gas was confirmed as observed in pressure-regulating strategy. The heat transfer coefficient values of self-pressurized hybrid control rod were slightly higher than those of

pressure-regulated hybrid control rod because the charged amount of non-condensable gas is smaller, diffusion of steam to wall may be enhanced and volume occupied by non-condensable gas is reduced.

2.3.2 Maximum heat transfer rate

Steady operation of the thermosyphon heat pipe is generally restricted by flooding phenomenon. At the liquid-vapor interface, shear between upward vapor flow and downward liquid film flow is generated. Comparison with the previously developed models on flooding limit of thermosyphon and modeling about it would be covered in Chapter 3. In this section, the maximum heat transfer rates according to pressure control strategies were qualitatively analyzed by comparison. The maxim heat removal capacities of the hybrid control rods were defined as heat loads showing sudden wall temperature excursion as shown in Fig. 2-8. Fig. 2-9 compares the operation limits of the pressure-regulated and self-pressurized hybrid control rods. As shown in the Fig, the maximum heat transfer rates increased with operating pressures. Several previous studies argued that entrainment through the shear at vapor-liquid interface determines maximum liquid velocity and the critical heat flux is determined by the maximum liquid velocity[61-63]. The explosive entrainment occurs at high vapor-liquid density ratio and the entrainment rate decreases as the density ratio decreases (that is, pressure increases). Therefore, the maximum heat transfer rates were proportional to operating pressures for both strategies. In comparison, the pressure-regulated hybrid control rods showed higher flooding limit compared to self-pressurized hybrid control rod. Fig. 2-9 demonstrates the difference of maximum heat transfer rates of pressure control mechanisms. For the self-pressurization strategy, the vapor accumulation is a main driving element of the pressurization. The mass of vapor in the self-pressurized system would be larger than that of pressure-regulated system at equal system pressure despite the same amounts of working fluid were charged to the test sections. Consequently, the liquid film thickness along the inner wall of cladding for self-pressurized test section would be thinner than pressure-regulated cases. In terms of momentum conservation, the liquid film velocity of self-pressurized hybrid control rod must be higher compared to pressure-regulating cases. The thinner liquid film thickness of the self-pressurized hybrid control rod could be confirmed by comparison of condensation heat transfer coefficients. The condensation heat transfer coefficient of the thermosyphon is dominated by the liquid film thickness, and inverse proportionality between heat transfer coefficient and film thickness is a theoretical background. The self-pressurized test sections showed slightly higher condensation heat transfer coefficients which demonstrates the thinner liquid film. The previous studies on critical heat flux of thermosyphon heat pipe reported that the liquid film become instable as the relative velocity between vapor and liquid increases and the instability of liquid film causes flooding phenomenon[64-69]. The higher liquid film velocity of the self-pressurized hybrid control rod resulted in higher entrainment rate and instable liquid film flow at relatively lower heat flux range.

Collectively, the pressure regulating strategy achieves target operating pressure with high maximum heat removal capacity through pressure regulator which is the component installed at the top of the hybrid control rod to control the internal pressure by removing the charged non-condensable gas, while the self-pressurization strategy shows relatively lower operation limits and higher condensation heat transfer coefficients. However, the pressure regulator is the component requiring setup and having possibility of malfunction. If the component is in state of malfunction, the internal pressure of the hybrid control rod cannot be controlled and decay heat removal will be not uniform and stable. The self-pressurization strategy has advantage in terms of passive operation under the reactor operation conditions. The non-condensable gas initially charged in the test section will restrict the condenser length (suppression of reach of steam) with minimization of the heat transfer rate under normal operation condition. The hybrid control rod will be inserted to the core by gravity in accident conditions, and the decay heat transferred to the rods will generate the vapor increasing the system pressure. Then, the kinematic vapor pressure will compress the non-condensable gas with extension of effective heat transfer length at the condenser section. As a result, the decay heat transfer rates and maximum heat removal capacity can be enhanced with the operating pressure passively. Thus, the self-pressurization strategy was selected as an pressure control mechanism of the hybrid control rod with consideration about passive operation characteristics.
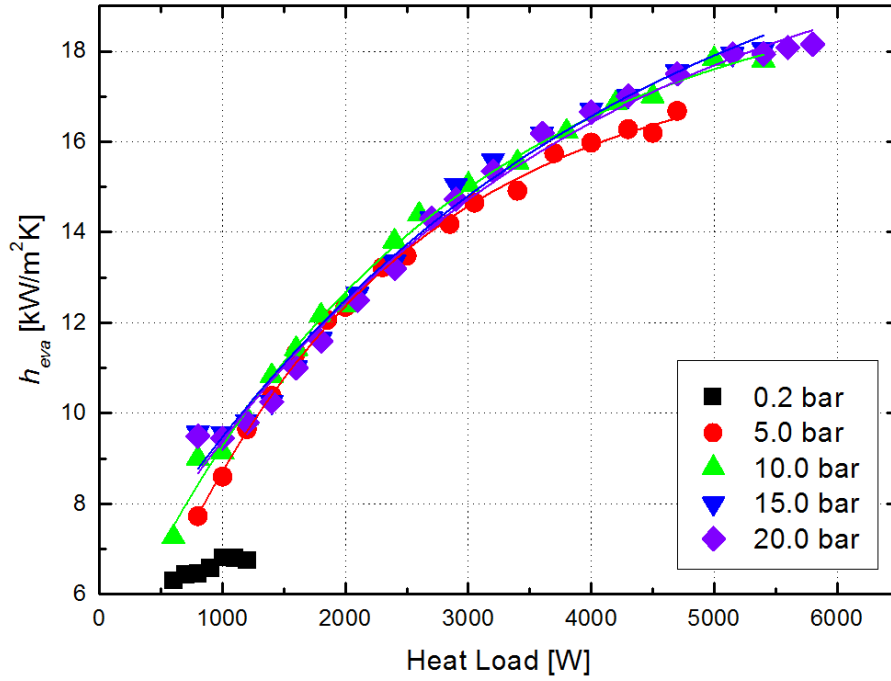
(a) Evaporation heat transfer coefficients
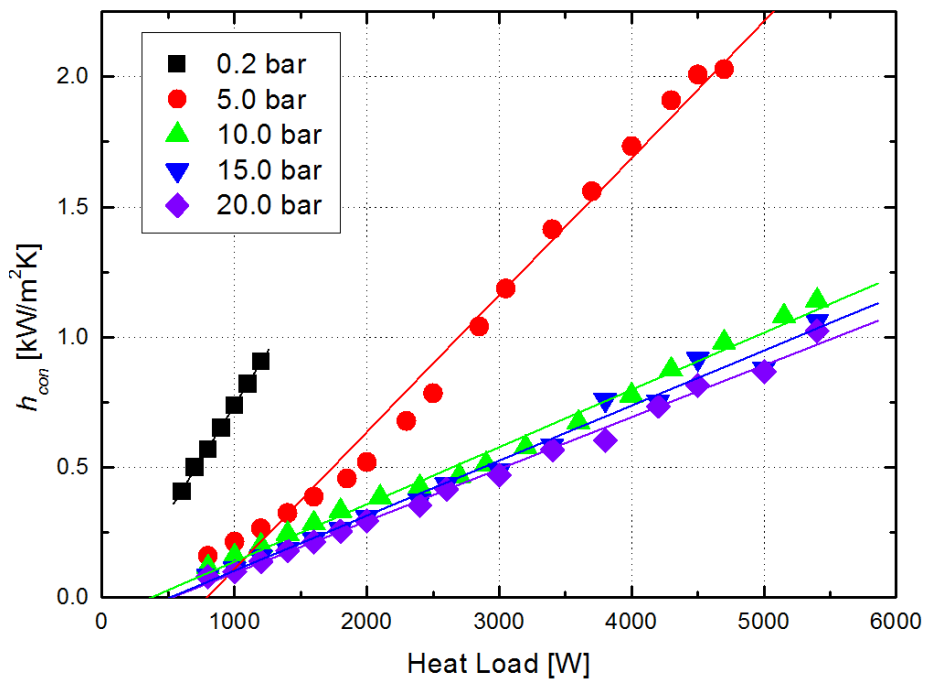
(b) Condensation heat transfer coefficients

Fig 2-5. Heat transfer coefficients of the pressure regulated hybrid control rod according to heat loads and operating pressures
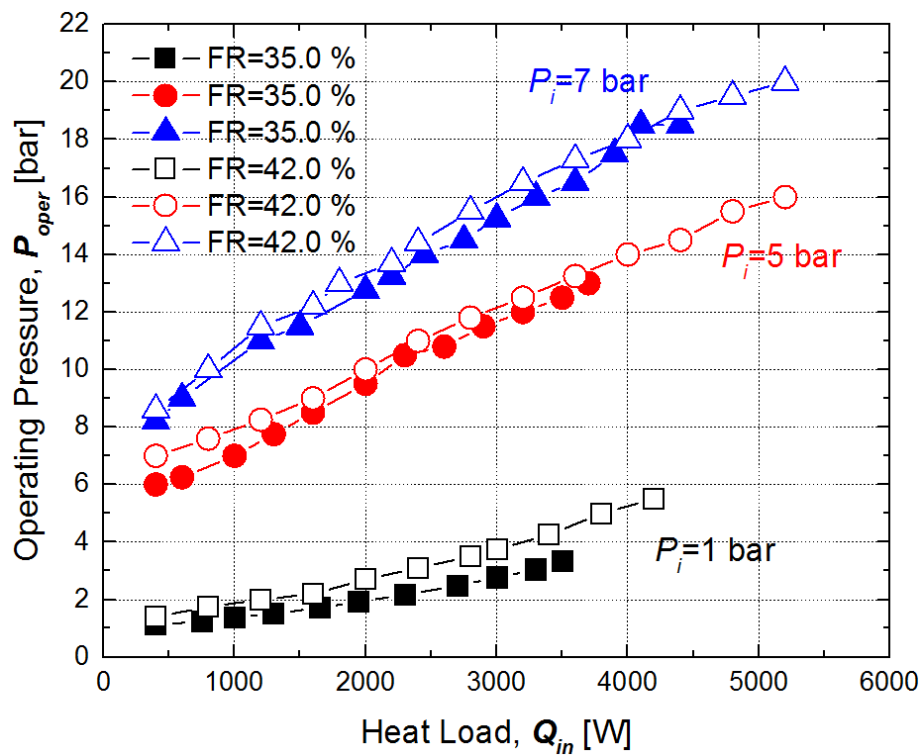
Fig. 2-6. Operating pressures according to heat loads, fill ratio, and initial pressures in self-pressurization strategy
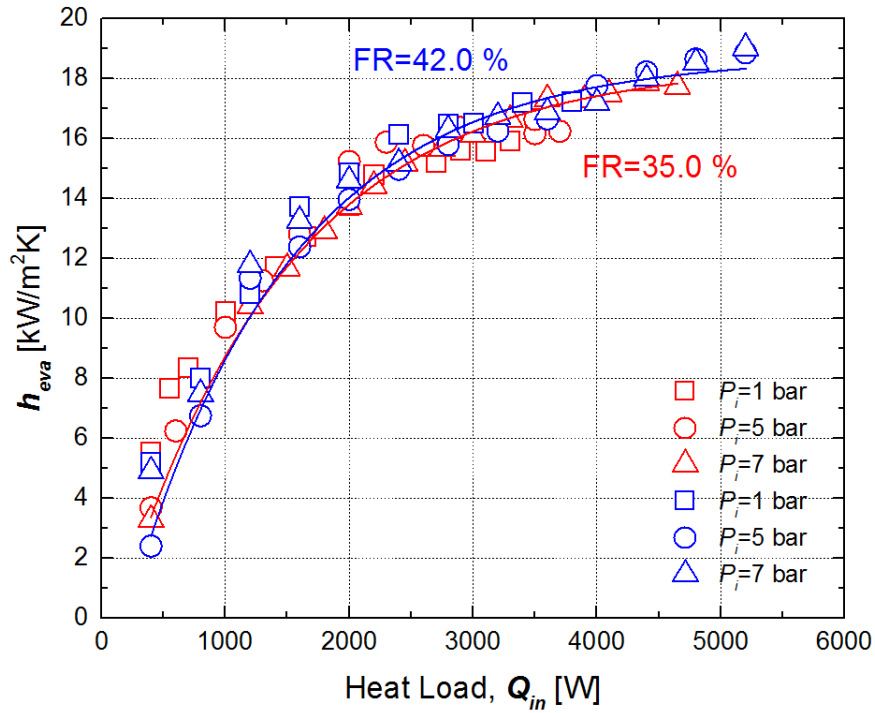
(a) Evaporation heat transfer coefficients
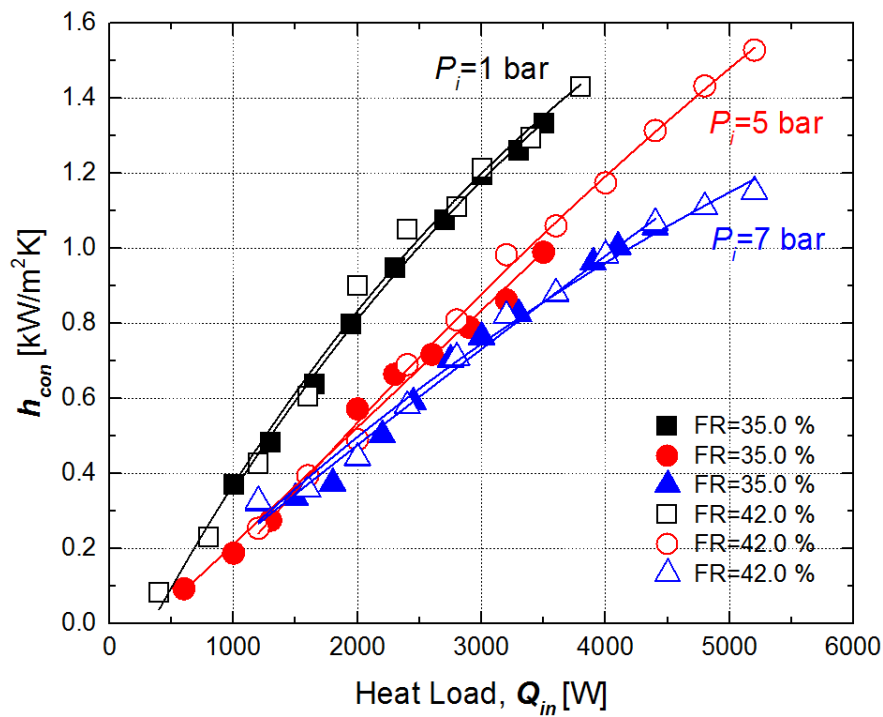
(b) Condensation heat transfer coefficients

Fig 2-7. Heat transfer coefficients of the self-pressurized hybrid control rod according to specified conditions
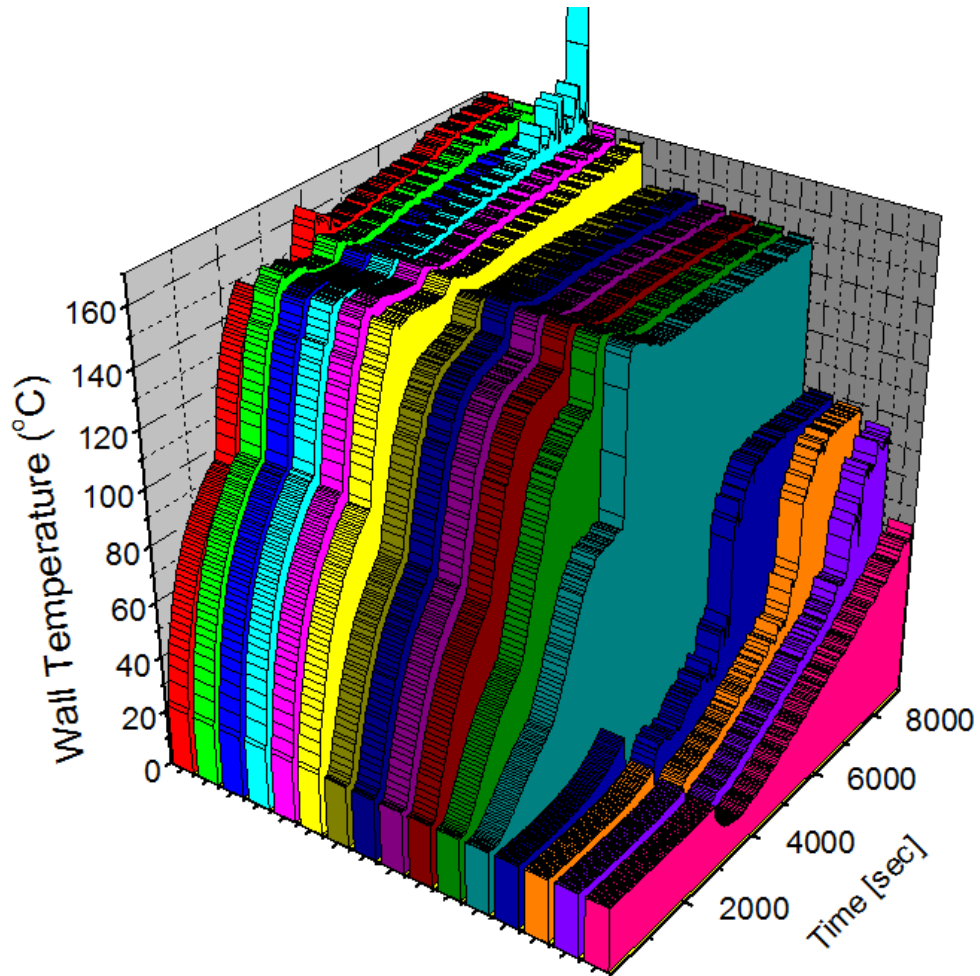
Fig 2-8. Temperature evolution during experiments and temperature excursion at operation limit
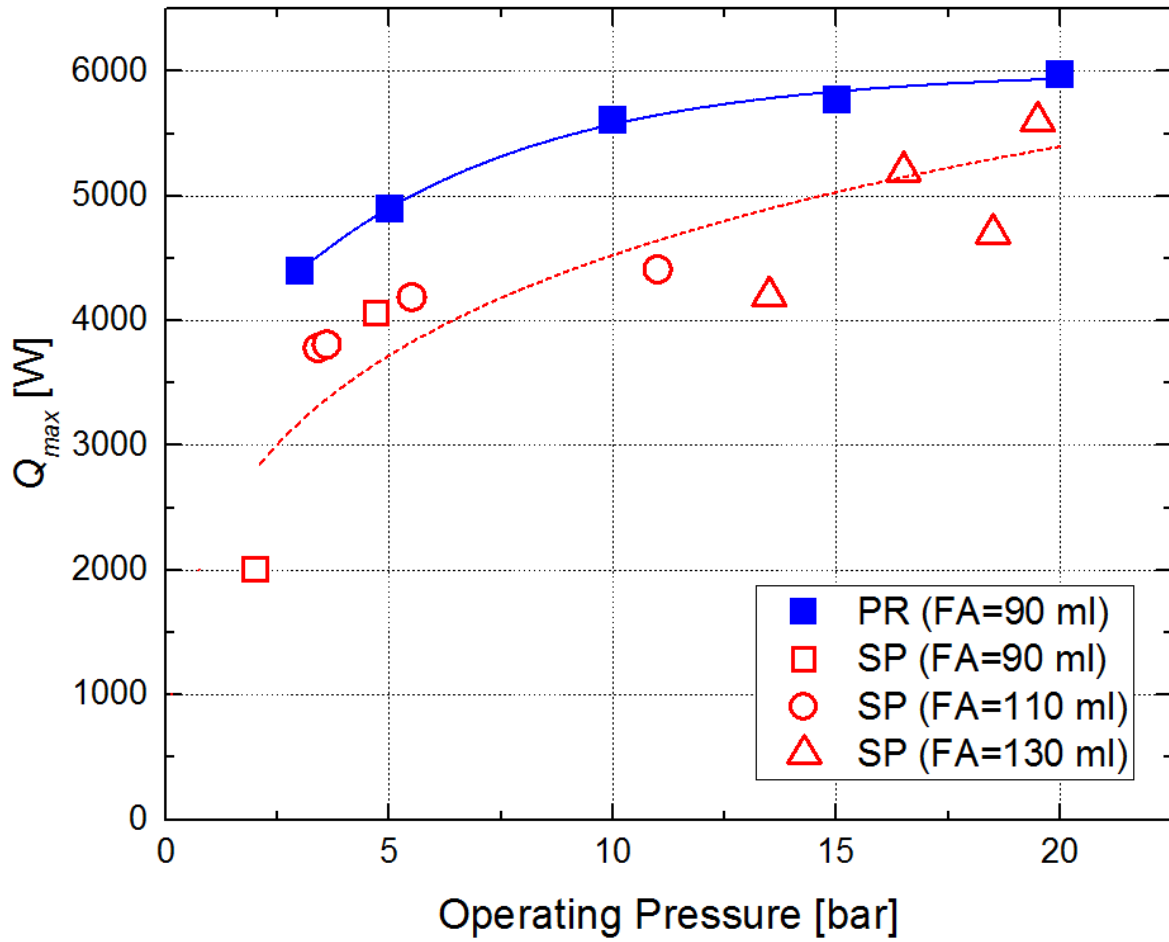
Fig 2-9. Comparison of maximum heat transfer rates of the pressure-regulated and self-pressurized hybrid control rods for various operating pressures
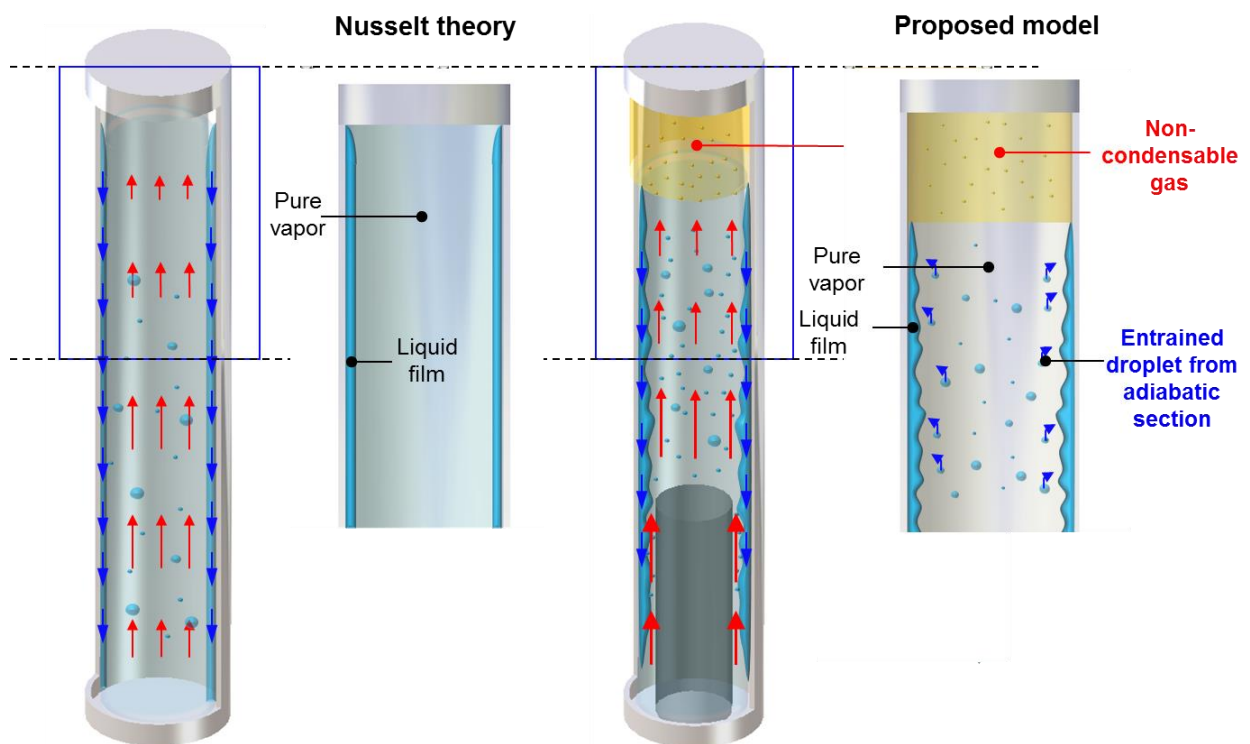
Fig 2-10. Mechanism of different maximum heat transfer rates according to pressure control strategies

Chapter 3. MODELING OF PRESSURIZED HYBRID CONTROL ROD

3.1 Introduction

Deterministic safety assessments using thermal-hydraulics system analysis codes have been conducted with postulated accidents. Through the safety analysis, the impact of installed safety systems on reactor safety including the thermal-hydraulic behaviors during transient condition can be confirmed. However, the passive safety systems have relatively high uncertainties compared to active safety systems because of randomness and complexity of their driving forces. For example, condensation heat transfer in pipelines of passive auxiliary feedwater system (PAFS) were not predicted accurately by the condensation models in the safety analysis code[70, 71]. Also, the codes have limitations in prediction of steam condensation at the inner wall of containment through passive containment cooling system despite it is crucial phenomenon determining containment pressure during loss of coolant accidents (LOCAs). For the accurate safety assessment, performances of the passive safety systems have been analyzed by experiments, and models associated with the thermal-hydraulic phenomena inside the systems were developed. The models were implemented in various safety analysis codes and they were utilized in the analyses.

Most of safety analysis codes concentrated on the two-phase flow and heat transfers solving mass, momentum, energy conservation equations. For the special hydraulic phenomena such as onset of nucleate boiling, critical heat flux, countercurrent flow, critical flow, etc. are solved by specified models. Although various safety systems using the heat pipes have been proposed, the models specified to the thermal-hydraulic phenomena inside the heat pipes have not been implemented. The heat pipes have unique characteristics compared to general two-phase flow because the heat is transferred in the countercurrent flow conditions along the whole length. Recently, NUSMOR+ project attempts to develop the models related to heat pipes and implement them to safety analysis codes for the purpose of application of heat pipes on passive containment cooling system.

For the application of the passive in-core cooling system utilizing hybrid control rods, the safety assessment with the safety analysis code must be carried out, and its effect on accident progress will be followed. The geometry and operating conditions of the hybrid control rod are differentiated from the previous researches on the heat pipes. The different heat transfer characteristics and hydraulic phenomena are expected compared to the previously developed models. Thus, the experimental results discussed in Chapter 2 were compared with the existing models. From the comparison work, the optimal models have to be selected or new models reflecting the unique characteristics of the hybrid control rod must be derived. The representative characteristics of the heat pipe, evaporation and condensation heat transfer, pressure variation, and flooding-based maximum heat removal rate will be analyzed.

3.2 Analysis of Hybrid Control Rod using MARS Code

To evaluate prediction capability of the current system safety code, the experiments conducted with self-pressurized hybrid control rod were simulated. Multi-dimensional analysis for reactor safety (MARS) code which is a thermal-hydraulic analysis code developed by Korea atomic energy research institute (KAERI). Two-component and two-phase flow could be analyzed based on the mass, momentum, and energy conservation equations, total six governing equations in one-dimension problems. Various models on thermal-hydraulic phenomena of two-phase flow are implemented in the code and the code has been used to observe the reactor behavior during design basis accidents. The code was validated by wide range of separate effect tests and integral effect tests. Through the evaluation of prediction capability of the MARS code against the performance of the hybrid control rod, weak points or limitations of the currently implemented models could be deduced. The hydraulic states inside the test section such as flow velocity for each phase, void fraction, and pressure gradient which parameters are difficult to predict, visualize, and quantify by the measurement during experiments also can be analyzed. Effectiveness of theoretical backgrounds including assumptions in the models against the hybrid control rod can be observed, and the work can give insight in improvement or development of models related to the thermal-hydraulics in the hybrid control rod.

3.2.1 Analysis models and conditions

The simulations were conducted with MARS V1.4. MARS nodalization of the hybrid control rod is depicted in Fig. 3-1. The evaporator section of the hybrid control rod is modeled by annulus component because the B_4C pellet is located at the center of the evaporator section and flow path of the working fluid is gap between B_4C pellet and inner wall of the cladding. Constant heat flux was entered as a boundary condition. The adiabatic and condenser sections were modeled as a pipe component. For the condenser section, the heat exchange was occurred through convective heat transfer with constant coolant mass flow rate in accordance with the experimental condition. Initial amount of the working fluid was modeled by collapsed water level and the initial pressure of the test section was given. The number of nodes along the test section was fit to the thermocouple locations of the experiments to compare the temperature distributions and internal pressures.

The default heat transfer models were applied to evaporator and condenser sections. At the evaporator section, Chen correlation as expressed in Eq. (3-1) was used in prediction of nucleate boiling[72].

$$q'' = h_{mac}\left(T_w - T_{sat}\right)F + h_{mic}\left(T_w - T_{sat}\right)S \qquad (3\text{-}1)$$

$$h_{mac} = 0.023\left(\frac{k}{D}\right)\mathrm{Re}^{0.8}\,\mathrm{Pr}^{0.4} \qquad (3\text{-}2)$$

35

$$h_{mic} = 0.00122 \left(\frac{k_f^{0.79} C_{pf}^{0.45} \rho_f^{0.49} g^{0.25}}{\sigma^{0.5} \mu_f^{0.79} h_{fg}^{0.24} \rho_g^{0.24}} \right) \Delta T_w^{0.24} \Delta P^{0.75} \qquad (3\text{-}3)$$

Churchill-Chu correlation predicted the natural convection by Eq. (3-4) during the transient phase until onset of nucleate boiling[73].

$$Nu = \left\{ 0.825 + \frac{0.387 Ra^{1/6}}{\left[1 + (0.492/\text{Pr})^{9/16} \right]^{8/27}} \right\}^2 \qquad (3\text{-}4)$$

Colburn-Hougen condensation heat transfer model (Eq. (3-5)) which calculate the condensation heat transfer in presence of non-condensable gas[74] was applied.

$$q'' = h_m h_{fg} \rho_v \ln \left(\frac{1 - P_{vi}/P}{1 - P_{vb}/P} \right) \qquad (3\text{-}5)$$

$$h_m = \frac{0.04053}{D} \frac{\left(\frac{1}{M_v} + \frac{1}{M_n} \right)^{0.5} T^{1.75}}{P \left[(\varepsilon_v)^{1/3} + (\varepsilon_n)^{1/3} \right]^2} \qquad (3\text{-}6)$$

For the analysis of the countercurrent flow between vapor and liquid film, Wallis model which can be simply expressed as Eq. (3-7) was selected as a default CCFL model, and CCFL models developed by Kutateladze or Bankoff were used in the sensitivity study to fit the experimental data. The beta value is zero for Wallis and unity for Kutateladze model. Bankoff model considers the both effects of channel diameter and surface tension on countercurrent limitation.

$$j_g \left[\frac{\rho_g}{gw(\rho_f - \rho_g)} \right]^{1/2} + m j_f \left[\frac{\rho_f}{gw(\rho_f - \rho_g)} \right]^{1/2} = C \qquad (3\text{-}7)$$

$$w = D_j^{1-\beta} \left(\frac{\sigma}{g(\rho_f - \rho_g)} \right)^{\beta/2} \qquad (3\text{-}8)$$

3.2.2 Simulation results

The evaporator wall temperature distributions according to heat loads and operating pressures are plotted with experimental data in Fig. 3-2. The predicted wall temperatures at evaporator and adiabatic

section showed good agreement with experimental data meaning the internal pressure and heat transfer in evaporator section can be well predicted by MARS code.

Based on the validated predictability of the boiling heat transfer, the liquid fractions along the evaporator and adiabatic sections were analyzed to confirm the flow state and working fluid distributions as shown in Figs. 3-3 and 3-4. Through the liquid fraction analysis, it was confirmed that the initial amount of working fluid inside the test section is well modeled in the analyses. As the heat load increases, the liquid fraction at evaporator section was decreased which demonstrates the vapor generation and increase of void fraction. The liquid fraction was decreased with elevations, and the analysis implies that the flow pattern at upper part of evaporator section is close to the annular film flow because the clearance between B_4C pellet and inner wall of cladding is narrow and void fraction at high operating is extensively high. In low heat flux region, liquid pool is observed in the low elevation of evaporator section, however the flow pattern was transferred to annular film as the heat load increases. The decrease in liquid fraction at adiabatic section explains the vapor accumulation with increase of operating pressure and transport of the working fluid to condenser section. The oscillation of the liquid fraction at evaporator and adiabatic section means the oscillatory flow pattern or effect of countercurrent flow. The amplitude of oscillation at adiabatic section is larger than that of evaporator section because the highest relative velocity between downward liquid film flow and upward vapor flow is observed at adiabatic section.

In aspect of the condensation heat transfer, the predicted condenser wall temperature distributions showed large deviation from the experimentally measured temperature data as shown in Fig. 3-5. The condenser wall temperatures were fit to experimental data by controlling the multiplication factor on the mass transfer coefficient in the Colburn-Hougen condensation model. However, the multiplication factor according to simulation conditions did not have any tendency about the parameters. Therefore, the reason of limited predictability of the default model on condensation inside the hybrid control rod will be discussed later.

The heat flux that wall temperature excursion was observed during the simulation was determined as a maximum heat transfer rates of the test section. In MARS code, the sudden decrease of heat transfer rate from the nucleate boiling heat transfer is predicted by critical heat flux, and the CHF look-up tables or several correlations are used in the predictions. However, the calculated CHFs were deviated from the measured maximum heat transfer rates. The deviation was attributed to the different critical phenomena. Countercurrent flow limit which restricts the liquid return from the condenser section to evaporator section was pointed out as a critical phenomenon of the test conditions. The countercurrent flow limits analyzed by Wallis model[75] were higher than experimental data, and the deviations become larger as the system pressure increases. Kutateladze CCFL condition was applied on the simulation to observe the sensitivity of CCFL according to model, and the results also showed deviation from the experimental results as plotted in Fig. 3-6. Through the iterative simulations, the optimal constants in

Wallis model were deduced. The deduced values for *m* and *C* in Eq. (3-7) were 2.0 and 1.08 with the zero value of beta. The optimized Wallis CCFL model showed agreement with experimental data within 20 %. However, there is no physical meaning for the suggested constants.

3.2.3 Limitation in prediction capability of MARS code

The limited prediction capability of MARS code on condensation heat transfer inside the heat pipe was confirmed by the simulation. Colburn-Hougen model is a diffusion method which is used to solve for the liquid-gas interface temperature in the presence of non-condensable gases. To solve for the temperature at the interface between the steam and water film, iterative diffusion calculation scheme is used. The assumptions of Colburn-Hougen diffusion model is as follows:

(1) Neglect the sensible heat transfer through the diffusion layer to the interface.
(2) Neglect stratification of the non-condensable gas in steam vapor by buoyancy.
(3) Analogy between the heat and mass transfer is applied to obtain the mass transfer coefficients.
(4) The non-condensable gas is not dissolved in the condensate.

The non-condensable gas boundary layer covers the liquid film and the vapor diffuses to the liquid film passing the gas boundary layer. Therefore, the diffusivity of vapor and non-condensable gas is a key parameter influencing the condensation heat transfer rate of MARS code.

In thermosyphon heat pipes, there is upward vapor flow and it could be stratified due to buoyancy of the steam vapor. It could be considered that the assumption of Colburn-Hougen diffusion model is not appropriate in terms of ignorance of non-condensable gas stratification in steam. Previous studies developing the condensation heat transfer models inside the heat pipes assumed the stratification of the non-condensable gas by the vapor flow. One-dimensional flat front model or two-dimensional front models were applied to reflect the condition of non-condensable gas` accumulation at the top of the heat pipes.

In case of flooding-based maximum heat transfer rate of the hybrid control rod, MARS code used Wallis, Kutateladze, or Bankoff models to predict the CCFL. The models related to the CCFL calculate the relative velocity between vapor and liquid at a junction (cross-section). While the vapor velocity is dominated by the cross-sectional area at the evaporator section and liquid velocity is developed from condenser and adiabatic section. When the superficial velocities for vapor and liquid phase at a cross-sectional area, the sudden change of superficial velocities could be analyzed because the cross-sectional areas of evaporator section and adiabatic section is large for the hybrid control rod due to presence of neutron absorber at the evaporator section. The dramatic change of superficial velocities according to cross-sectional areas cannot consider the velocity profiles in real condition.
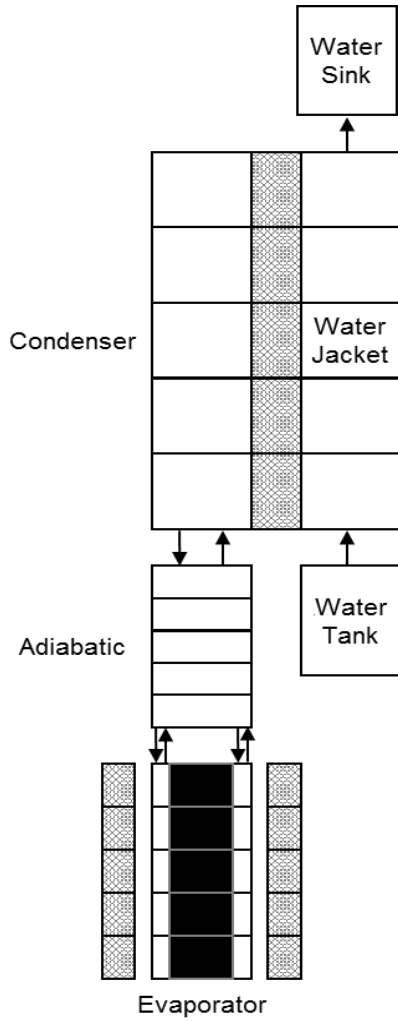
Fig. 3-1 MARS nodalization of hybrid control rod
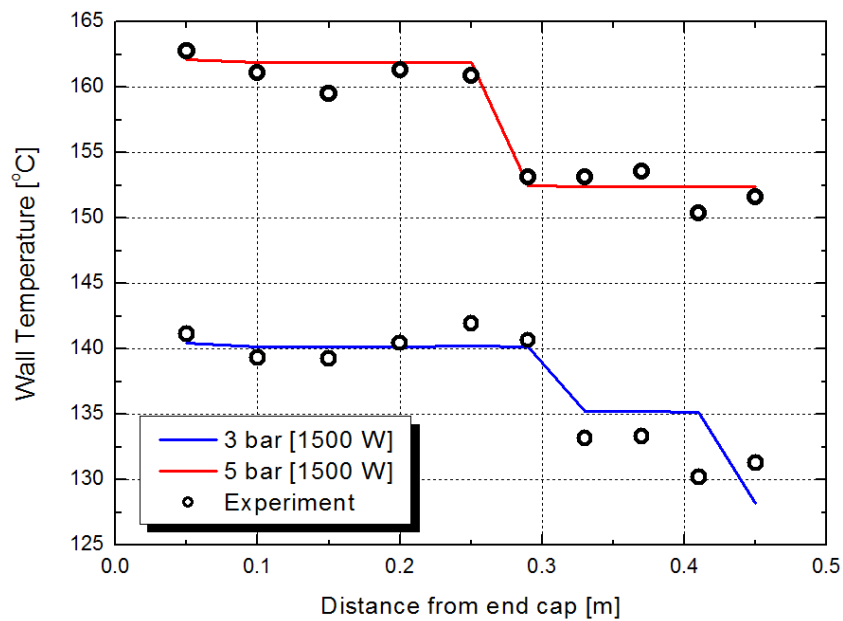
Fig. 3-2 Comparison of predicted evaporator wall temperature distributions with experimental data
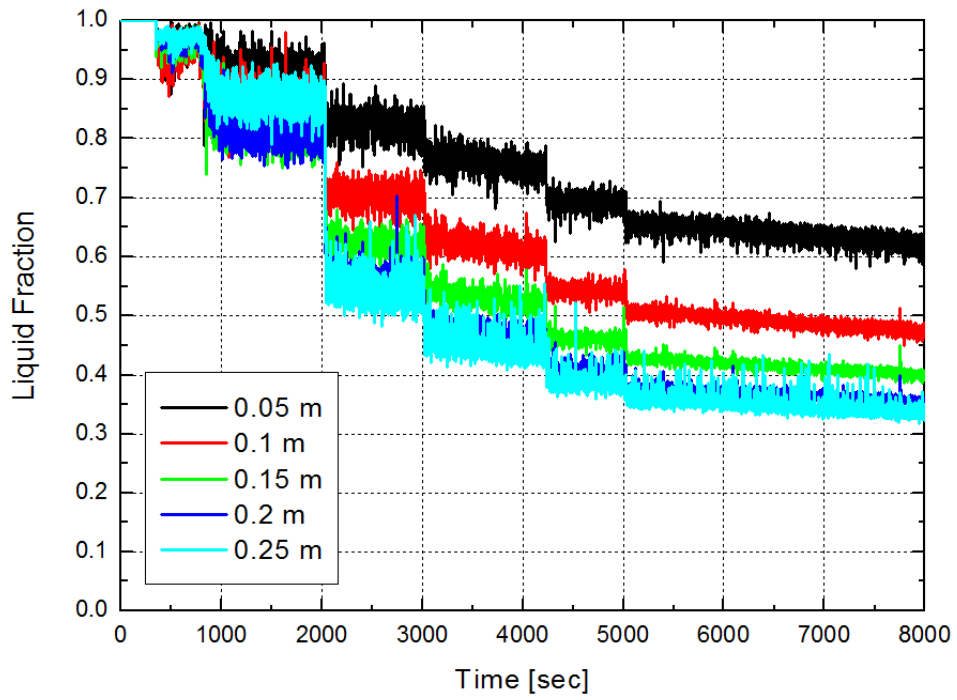
Fig. 3-3 Predicted liquid fraction at evaporator section of the hybrid control rod
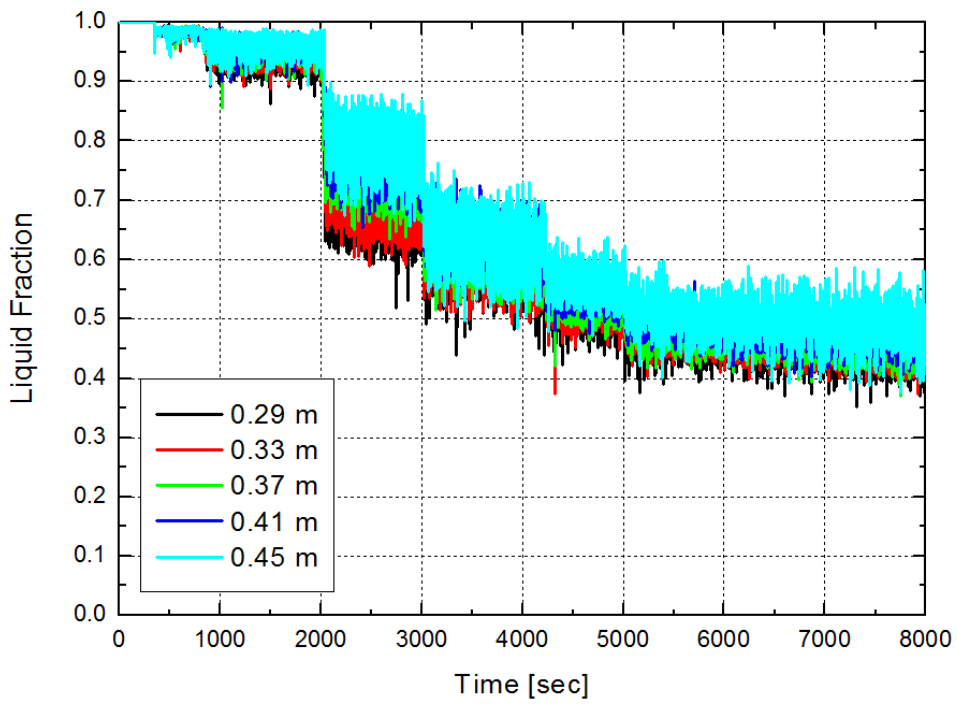
Fig. 3-4 Predicted liquid fraction at adiabatic section of the hybrid control rod
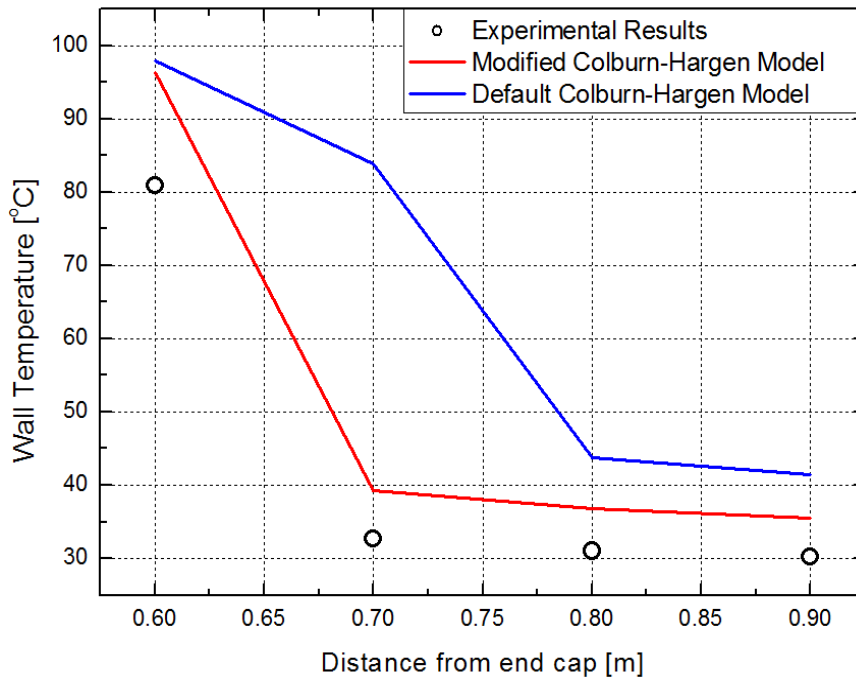
Fig. 3-5 Comparison of predicted condenser wall temperature distributions with experimental data
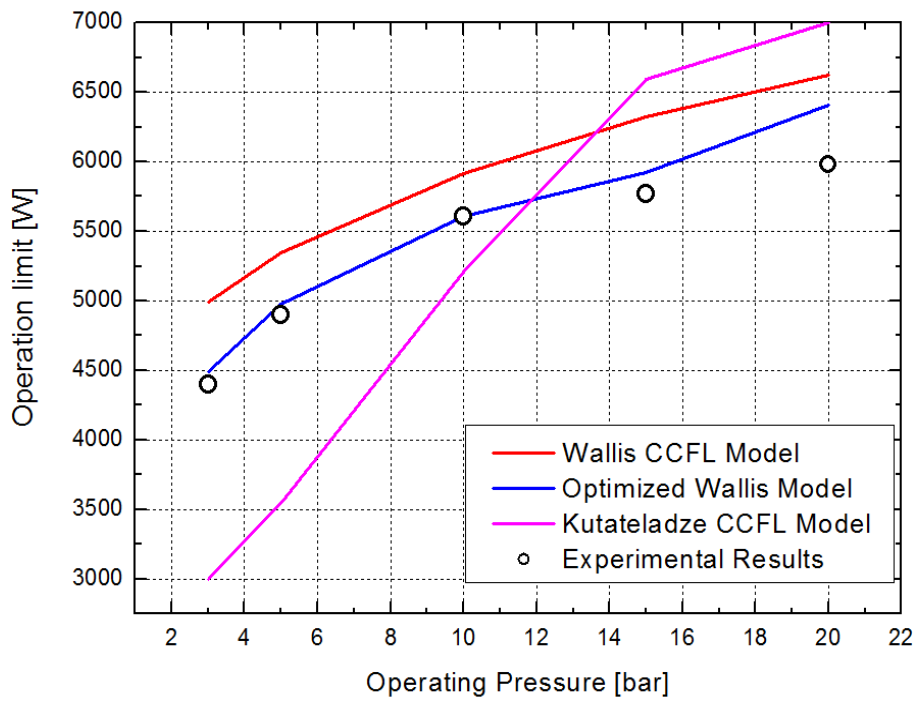
Fig. 3-6 Comparison of CCFLs of experiments and predictions by MARS

41

3.3 Development of Models on Performance of Hybrid Control Rod

Various models predicting the performances of the thermosyphon heat pipe have been developed because the performances of the heat pipe depend on wide range of parameters such as fill ratio and kind of working fluid, geometry (dimensions and shape), operating pressure, inclination angle, non-condensable gas, and so on. The hybrid control rod has several unique characteristics compared to general types of thermosyphons due to its specialized requirements. It must contain neutron absorbing material, working fluid, and non-condensable gas in a cladding because it operates at high temperature and high pressure environment with reactor shutdown ability. The containment of various elements makes it difficult to analyze or predict the thermal-hydraulics inside of the hybrid control rod. Nevertheless, the heat transfer characteristics and hydraulic phenomena that occurs in the hybrid control rod should be analyzed and modeled to observe effects of the passive in-core cooling system equipped with the hybrid control rod on safety of nuclear facilities. The development of models analyzing the performances of the hybrid control rod would be helpful to enhance the prediction capability of the system safety analysis codes such as MARS, SPACE, and RELAP5. In other ways, independent in-house code could be developed with integration of the models. Thus, the representative heat transfer characteristics (evaporation and condensation heat transfers) and hydraulic phenomenon (flooding or entrainment phenomenon) were analyzed by comparison of previously developed models on thermosyphon with experimental data of the hybrid control rod. The optimal models could be selected if the model predictions show good agreement with experimental data. If not, the theoretical background and assumptions used in the modeling were reexamined with taking into account the different conditions of the hybrid control rod, then new models applying distinct characteristics of the hybrid control rod were developed. This section demonstrates the selected models or newly proposed models on thermal-hydraulics of the hybrid control rod.

3.3.1 Evaporation heat transfer

Heat transfer at the evaporator section of heat pipe would be varied with operating conditions. Before phase change of the working fluid takes place, heat will be transferred by single phase natural convection. After certain heat fluxes, the bubble and vapor will be generated by phase change. The two-phase heat transfer of the heat pipes could be divided into several representative mechanisms.

(1) Pool boiling
(2) Evaporation at the surface of pool
(3) Evaporation at the falling liquid film
(4) Combination of pool boiling and liquid film evaporation

When a certain portion of the evaporator section is submerged by pool, bubbles grow at the cavities of inner wall of cladding. At that time, evaporation of working fluid occurs at the surface of pool. In the condition of low collapsed level of water pool owing to high vapor velocity or high heat flux, the evaporation will be occurred at the surface of falling liquid film. In middle heat flux range, the pool boiling heat transfer and liquid film evaporation can be occurred simultaneously.

With the physical insight on the heat transfer at evaporator section, several models were developed as summarized in Table 3-1.

The models were validated within limited operating pressure region about water. The comparative study between the models shows deviations of prediction results each other. The reason why there is difference between the predictions could be guessed as follows: i) the error of measurement and the error of measuring instruments. ii) heat loss during experiments. iii) determination of saturation temperature, iv) geometry of the test section, v) fill ratio and types of working fluid, vi) operating pressure. Error by measurement and instruments and heat loss would contribute to deviations within 10 % due to their information on uncertainties and heat balance. Saturation temperature is an important parameter which affect the heat transfer coefficients. The previous studies measured the saturation temperature by assuming the temperature at adiabatic section is equal to vapor temperature, measuring vapor temperature, or calculating the saturation temperature based on measured internal pressure of the test section. Determining saturation temperature is too difficult because there is pressure gradient along axial direction of the test section. Thus, the difference in measurement method of saturation temperature occupies large portion of uncertainties and deviations. Finally, the tendency of heat transfer coefficients with experimental conditions including geometry and element of test section, and operating condition are not clarified yet.

Representative models on evaporation heat transfer coefficients were compared with experimental data of present study as shown in Fig. 3-7. The correlations which were developed with assumption of nucleate boiling heat transfer showed relatively higher deviations in comparison with measured evaporation heat transfer coefficients. Generally, the correlations based on evaporation at falling liquid film calculated the higher evaporation heat transfer coefficients than those of nucleate boiling. The experimentally measured evaporation heat transfer coefficients were independent on fill ratio and initial pressures at heat flux region close to maximum heat transfer rates which implies the heat transfer mechanism is liquid film evaporation (annular film flow). The most accurately predicting model was Imura`s correlation which put the basis on liquid film evaporation because it did not include any factors related to the pool boiling heat transfer. Imura`s correlation showed agreement with experimental data by maximum deviations of 30 % as compared in Fig. 3-8. The ratio between predictions and experiments were lower than unity. The underprediction is thought as effect of countercurrent flow. The upward vapor flow would reduce the liquid film velocity and the thicker liquid film would be formed

(in aspect of momentum continuity) along the wall of the evaporator section. Imura`s correlation was selected as an evaporation heat transfer model of the hybrid control rod since the overall trend of heat transfer coefficients was coincident with that of experiments, though the prediction were lower than experimental results.

3.3.2 Condensation heat transfer

Condensation heat transfer in thermosyphons have been analyzed by Nusselt theory-based models[77]. The suggested models on condensation heat transfer are presented in Table 3-2. The specified conditions of the experiments which were conducted to validate their models and the hydraulic phenomena considered in their models were described. The Nusselt liquid film condensation theory closely represents experimental data conducted on vertical plates with conditions of no ripples or non-condensable gases and laminar film flow. The condensate film begins at the top and flows downward by gravity. During the downward flow, new condensate is added. The laminar film flow is assumed to be fully developed from the leading edge. As a result, one-dimensional heat conduction across the film to the wall can be assumed because the temperature profile across the film is linear. Other assumptions are as follows:

(1) Vapor temperature is saturation temperature and it is uniform,
(2) Force affecting on film is only gravity (solve force balance between gravity and wall shear)
(3) Vapor is stagnant and it does not exert any drag force
(4) Fluid properties are constant
(5) Neglect the sensible heat
(6) Interface curvature is negligible.

Simple solution for the condensation heat transfer coefficient is derived as Eq. (3-9).

$$h_c = 0.943 \left[\frac{\rho_l (\rho_l - \rho_v) g h_{fg} k_l^3}{\mu_l L_c (T_{sat} - T_w)} \right]^{1/4} \qquad (3\text{-}9)$$

However, the above equation has limits due to many assumption. Especially, the forces considered at the force balance is only gravity and shear force at wall. Many researchers compared their experiments with prediction of Nusselt`s analysis, however, the deviations were reported. Therefore, the effects of curvature of interface, waviness, interfacial shear due to vapor flow on condensation heat transfer were modeled. The Nusselt`s theory was also extended to the turbulent region. In presence of

the non-condensable gas, one-dimensional flat front model, two-dimensional flat front model, two-dimensional mixed models were developed. The waviness at the vapor-liquid interface enhanced the film Reynolds number and consequently higher heat transfer coefficients were observed compared to Nusselt theory while the interfacial shear between vapor and liquid reduced the heat transfer. The difference in assumptions made deviations according to various parameters.

The measured condensation heat transfer coefficients according to specified conditions were compared with the prediction values by existing models as shown in Fig. 3-9. Nusselt theory and other correlations considering the effect of entrainment on the condensation cannot follow tendency of the experimental data because the assumed conditions of the models seem to be not appropriate to take into account the phenomena inside the hybrid control rod. Inclusion of non-condensable gas and modification of the liquid film thickness by entrained droplet were pointed out as two main mechanism inducing the deviations between experimental results and predictions. Hence, new models analyzing the condensation heat transfer in the hybrid control rod is suggested as follows:

$$h_c = \text{Re}_f^{0.1} \exp\left(-0.0003\frac{\rho_l}{\rho_v}\right) \times \left\{0.943\left(\rho_l(\rho_l - \rho_v)gk_l^3 h_{fg} \Big/ \mu_l(T_v - T_c)\left(l_c - \frac{nRT}{PA_{cs,c}}\right)\right)^{1/4}\right\} \qquad (3\text{-}10)$$

The theoretical backgrounds of Nusselt`s film analysis and model suggested in this paper is shown in Fig. 3-10. The non-condensable gas would be accumulated at the top of the test section by kinematic vapor flow from evaporator section and the accumulated non-condensable gas prohibit the reach of vapor across the total length of condenser section. Ideal gas law was applied to the non-condensable gas and the reduction of effective heat transfer length owing to accumulation of the non-condensable gas was reflected in the heat transfer coefficient calculated by Nusselt theory. In Nusselt`s falling film analysis, the liquid film thickness is calculated along the flow direction by force balance between gravitational force and wall shear on liquid film. Then, the profile on liquid film velocity is calculated. The heat balance between one-dimensional heat conduction and phase change at the vapor-liquid interface is solved to calculate the local heat transfer coefficients. Integral of the local heat transfer coefficients throughout the total condenser length give a total condensation heat transfer coefficient. In this model, the local heat transfer coefficients were integrated with the length scale excepting the non-condensable gas region. The derived heat transfer coefficient considering the non-condensable gas is third term of Eq. (3-10).

Second phenomenon included in this model is entrainment at vapor-liquid interface. In countercurrent flow condition, the instability at the vapor-liquid interface would be generated. At low heat flux region, the instability of the liquid film exerted by entrainment would be magnified because the relatively thin liquid film would be formed across the inner wall of condenser section. Influence of

45

instability on condensation heat transfer was weighted by film Reynolds number which is arranged in first term of the model.

The entrained droplets from the liquid film at adiabatic or evaporator sections could be reached the condenser section by pressure gradient between evaporator and condenser section. The reached droplets would be deposited on the condensate film at the condenser section forming the thicker liquid film than entrainment effect-neglected conditions. In general, the entrainment rate is inversely proportional to density ratio of vapor and liquid. Thus, the effect of entrained droplet on condensation heat transfer was expressed as an exponential function of density ratio which is second term of the proposed model. The validity of the assumptions about non-condensable gas and entrainment on condensation heat transfer will be discussed in Section 3.4. The prediction results with newly proposed condensation heat transfer were showed good agreement with experimental data within 30 % deviation range as shown in Fig. 3-11.

3.3.3 Maximum heat transfer rate

Operation of the thermosyphon is limited by several critical phenomena; viscous limit, sonic limit, boiling limit, and flooding limit. At the initial phase of operating heat pipe, the vapor velocity may reach sonic values with certain high temperature liquid metal heat pipes. The sonic velocity limits the performance of heat pipe (sonic limit). At low operating temperature, the vapor pressure in the evaporator is very low and the difference in vapor pressure between evaporator and condenser section is insignificant to overcome the viscous and gravitational force (viscous limit). The boiling limit can be defined as critical heat flux of the thermosyphon. At certain radial heat fluxes, the inner wall of evaporator section will be covered by vapor blanket and the heat transfer rate through the phase change of working fluid is dramatically reduced. When the vapor velocity is highly increases with a high heat flux, the liquid return from condenser to evaporator sections can be entrained and liquid supply to the evaporator cannot be achieved. This operation limit is defined as entrainment limit or flooding limit.

The most typical phenomenon limiting the performance of the thermosyphon is flooding (or entrainment). The flooding-based maximum heat transfer rate models were developed in analytical method or semi-empirical correlation. In analytical methods, there are two main different mechanisms; maximum liquid envelope velocity and instability of vapor-liquid interface. The models predicting the maximum heat transfer rate by finding the solution about maximum falling liquid rate due to envelope procedure or instability divide the control volumes as two parts. At control volume 1 (total cross section), the force balance between vapor pressure, wall shear, and gravity is solved. For the control volume 2 (cross-section from center to liquid-vapor interface), interfacial shear, gravity, and pressure gradient are force balanced. Combination of the momentum equations and mass continuity arranges the equation about void fraction, interfacial shear, wall shear, densities, and superficial velocities. Unknown

variables in the derived equation are void fraction and superficial velocity. Additional equation is needed to solve the equation, and it is the differentiation of the equation with respect to void fraction in the envelope procedure models. The void fraction which makes zero value of differentiated equation is a point expressing the maximum liquid rate (superficial velocity). In instability models, the instability criterion introduces additional equation replacing the differential equation of the envelope model. Helmholtz instability is backbone of the instability criterion. Various researchers defined the instability criterion providing a relationship between wavelength and liquid film thickness. However, the solution of the analytical methods is complex and easy to approach. Thus, various semi-empirical correlations were proposed.

There are two representative semi-empirical correlations on countercurrent flow limitation; Wallis model and Kutateladze criterion. Wallis model suggested dimensionless number which is results of force balance between inertia and hydrostatic force. The relation between dimensionless superficial velocity was derived as Eq. (3-11).

$$\sqrt{j_v^*} + m\sqrt{j_l^*} = C_w \qquad (3-11)$$

The values of m and C_w which are constants of the equation were proposed by liquid-gas experiment in open system. From the relation of dimensionless superficial velocities, the following flooding limit model (Eq. (3-12)) is derived.

$$Q_{max} = C_w^2 h_{fg} A \rho_v^{1/2} \left[gD(\rho_l - \rho_v) \right]^{1/2} \left[1 + m\left(\frac{\rho_v}{\rho_l}\right)^{1/4} \right]^{-2} \qquad (3-12)$$

The flooding limits of the thermosyphons having narrow flow channel were coincident with Wallis model. However, the Wallis correlation showed insufficient predictability on experimental data of thermosyphon which is a closed system. The proposed constants were varied with experimental conditions and there is no tendency of constants with variables because the experiments were conducted in open systems within confined range of experimental conditions. Ignorance of the surface tension in the force balance may affect the predictability of the model. Kutateladze suggested the separate model with Kutateladze number this is a dimensionless number by balancing inertia, surface tension, and buoyant forces. The relation between Kutateladze numbers for vapor and liquid is similar with the Wallis model as expressed in Eq. (3-13).

$$\sqrt{K_v} + \sqrt{K_l} = C_k \qquad (3-13)$$

$$Q_{\max} = C_k^2 h_{fg} A \rho_v^{1/2} \left[g \sigma (\rho_l - \rho_v) \right]^{1/4} \left[1 + m \left(\frac{\rho_v}{\rho_l} \right)^{1/4} \right]^{-2} \tag{3-14}$$

The final equation calculating flooding limit of the thermosyphon is Eq. (3-14) and it showed deviations from the measured maximum heat transfer rates of the experimental works. In the model, the effect of channel diameter is ignored, while the Wallis model neglected the effect of surface tension. Based on these two representative correlations, several researchers attempted to develop new models on flooding-based maximum heat transfer rates of the thermosyphon heat pipes as summarized in Table 3-3. Tien and Chung[44] introduced Taylor instability and Bond number to combine the Wallis model and Kutataeladze model. since the effects of channel diameter and surface tension on the flooding phenomenon were not considered simultaneously in previous models (Wallis and Kutateladze). As a result, the correlation showed good agreement with experimental data of several working fluids excluding water. Imura[43] suggested the critical heat flux model of thermosyphon based on flooding. This model modified the Kutateladze number as a function of density ratio between vapor and liquid by gathering wide range of experimental data for operation limit of closed two-phase thermosyphon. The collected experimental data were rearranged with several variables to observe the tendencies. The developed model showed good agreement with various experimental results, making it as the most accurate model predicting the flooding-based operation limit. Faghri[42] enhanced the prediction capability of model proposed by Tien and Chung[44]. According to operating conditions and working fluids, the Kutateladze number was varied with revision of constants in front of Bond number of Tien and Chung to unity. Consequently, predictions by Faghri model was coincident to experiments against the various working fluids. Especially, this model was also validated for concentric annular vapor-path thermosyphons. Monde[78] developed the new critical heat flux model in the open thermosyphon systems. Theoretical background of the model is maximum liquid velocity due to envelopment procedure. The double-tube open thermosyphon was used as test section for the analysis of new critical heat flux. The clearance between outer wall of inner tube and inner wall of outer cladding on the critical heat flux was modeled with observation about the flow pattern inside the tubes utilizing visualization works. ESDU[36] proposed the empirical correlation collecting the wide range of data from literatures and rearranged them according to variables of Bond number, pressure, inclination angle. Three dimensionless factors were suggested and its values were drawn in the form of graphs. Therefore, the model has strong predication ability in spite of the absence of physical meaning.

The previously suggested models were used to predict the measured operation limits of the hybrid control rod. In the calculations, the hydraulic diameter of evaporator section was utilized as a diameter of channel because the vapor velocity (relatively higher velocity than liquid film, affect the flooding limit dominantly) is dominated by cross-sectional area of their escaping section (evaporator section).

As show in Fig. 3-12, Wallis correlation showed excellent agreement with experimental data in low operating pressure region. However, the developed models were deviated from the experiments at high operating pressure region.

Typically, the flooding limit correlations of closed two-phase thermosyphons were validated with experimental data at low operating pressures in the case of water was used as working fluid. The hydraulic diameter of the evaporator section was used in the calculation of the maximum heat transfer rates which means that the whole test section including adiabatic and condenser sections has cross-sectional area of the evaporator section. Although the vapor velocity is dominant parameter affecting the entrainment, the superficial velocities could not reflect the variation of the vapor and liquid velocities across the axial direction of the test sections. The superficial velocities considered in the existing models are defined at a cross-section because the void fraction is implied in the terms as follows:

$$j_v = \alpha u_v = \frac{\dot{m}_v}{\rho_v A}, \qquad\qquad j_l = (1-\alpha)u_l = \frac{\dot{m}_l}{\rho_l A} \qquad\qquad (3\text{-}15)$$

There are uncertainties in void fraction because the void fraction could not be measured in the conducted experiments. In the hybrid control rod, the neutron absorber is located at the center of evaporator section. The cross-sectional area of the evaporator section is difficult to adiabatic section. If the cross-sectional areas of the adiabatic and condenser sections are equal to evaporator section, the superficial velocity of liquid film is higher than that of larger cross-sectional area as shown in Fig. 3-13. The liquid film is developed from condenser section and it will be accelerated by gravity. Thus, the superficial velocity of the liquid film must be defined at the cross-sectional area of adiabatic section. In terms of vapor flow, superficial velocity of the vapor has to be defined at the cross-section of evaporator section because the vapor velocity would be highest at evaporator section (in other words, the vapor is generated from the evaporator and reduced as the elevation increases due to pressure loss). Very thin liquid film thickness than diameter of the test section makes the assumption that superficial velocities of liquid film at adiabatic section and evaporator section are almost same possible. This assumption forms new superficial velocities (Eq. (3-16)) in the model of maximum heat transfer rate.

$$j_v = \alpha u_v = \frac{\dot{m}_v}{\rho_v A_{eva}} = \frac{Q}{\rho_v A_{eva} h_{fg}}, \qquad j_l = (1-\alpha)u_l = \frac{\dot{m}_l}{\rho_l A_{adia}} = \frac{Q}{\rho_l A_{adia} h_{fg}} \qquad (3\text{-}16)$$

Substituting the previous superficial velocities with newly suggested superficial velocities, the Kutateladze numbers of vapor and liquid is derived as Eq. (3-17):

$$K_v = \frac{Q}{\rho_v^{1/2} A_{eva} h_{fg}} \left[g\sigma(\rho_l - \rho_v) \right]^{-1/4}, \quad K_l = \frac{Q}{\rho_l^{1/2} A_{adia} h_{fg}} \left[g\sigma(\rho_l - \rho_v) \right]^{-1/4} \qquad (3\text{-}17)$$

Rearranging the Kutateladze CCFL criterion, Eq. (3-13), Eq (3-18) which could reflect the influence of different cross-sectional areas along evaporator and adiabatic sections on flooding phenomenon.

$$Q_{\max} = C_k^2 h_{fg} \left[g\sigma(\rho_l - \rho_v) \right]^{1/4} \left[\rho_l^{-1/4} A_{adia}^{-1/2} + \rho_v^{-1/4} A_{eva}^{-1/2} \right]^{-2} \qquad (3\text{-}18)$$

The previous studies which developed the models on maximum heat transfer rate through modification of the Kutateladze number suggested various C_k in Eq. (3-14). Density ratio, Bond number, and ratio of diameter between inner tube and outer cladding are the examples of the parameters for C_k. Controlled parameter of the experiments were pressure and the entrainment rate is proportional to density ratio. Thus, the density ratio of the vapor and liquid was selected as a variable of C_k. Consequently, the flooding-induced maximum heat transfer rate of the hybrid control rod which has different cross-sectional areas across the sections is suggested as Eq. (3-19).

$$Q_{\max} = \left(\frac{\rho_l}{\rho_v} \right)^{0.14} h_{fg} \left[g\sigma(\rho_l - \rho_v) \right]^{1/4} \left[\rho_l^{-1/4} A_{adia}^{-1/2} + \rho_v^{-1/4} A_{eva}^{-1/2} \right]^{-2} \qquad (3\text{-}19)$$

The predicted flooding limits of the hybrid control rod were compared with experimental data. The model showed good agreement with experiments within 20 % error range as shown in Fig. 3-14.

Table 3-1. Existing models on evaporation heat transfer of the thermosyphons

Researcher	Correlations	Operating pressures [bar]	Remarks
Imura et al. (1979)	$h_e = 0.32 \left(\dfrac{\rho_l^{0.65} k_l^{0.3} C_{pl}^{0.7} g^{0.2}}{\rho_v^{0.25} h_{fg}^{0.4} \mu_l^{0.1}} \right) \left(\dfrac{P_v}{P_{atm}} \right)^{0.3} q^{0.4}$	~ 1.0	Based on falling filmy evaporation (Neglect nucleate boiling)
Shiraishi et al. (1981)	$h_e = 0.32 \left(\dfrac{\rho_l^{0.65} k_l^{0.3} C_{pl}^{0.7} g^{0.2}}{\rho_v^{0.25} h_{fg}^{0.4} \mu_l^{0.1}} \right) \left(\dfrac{P_v}{P_{atm}} \right)^{0.23} q^{0.4}$	0.05 – 0.2	Based on falling filmy evaporation (Neglect nucleate boiling)
Kaminaga (1990)	$h_e = 0.0154 \left(\rho_g / \rho_l \right)^{0.4} R^{(1-p/p_c)} \dfrac{\lambda}{l_m} \left(\dfrac{p}{p_c} \right)^{0.35} \left(\dfrac{q l_m}{\rho_g r v} \right)^{0.7} \left(\dfrac{p l_m}{\sigma} \right)^{0.7}$	0.05 – 1.2	Based on nucleate boiling
Rohsenow (1952)	$h_e = q^{2/3} \Big/ \left\{ \left(\dfrac{C_{s,f} h_{fg}}{C_{pl}} \right) \left(\dfrac{L_b}{h_{fg} \mu_l} \right)^{0.33} \mathrm{Pr}_l^{1.7} \right\}$	1.0 – 17.0	Based on nucleate boiling
Kutateladze (1990)	$h_e = 0.44 \left(\dfrac{k_l}{L_b} \right) \left(\dfrac{10^4 g P}{g h_{fg} \rho_v \mu_l} \dfrac{\rho_l}{\Delta \rho} \right)^{0.7} \mathrm{Pr}_l^{0.35}$		Based on nucleate boiling
Labuntsov (1972)	$h_e = 0.075 \left[1 + 10 \left(\dfrac{\rho_v}{\rho_l - \rho_v} \right)^{0.67} \right] \left(\dfrac{k_l^2}{\upsilon_l \sigma (T_{sat} + 273.15)} \right)^{0.33} q^{0.67}$		Based on nucleate boiling
Kruzhilin (1952)	$h_e = 0.082 \left(\dfrac{k_l}{L_b} \right) \left(\dfrac{h_{fg} q}{g T_{sat,abs} k_l} \dfrac{\rho_l}{\Delta \rho} \right)^{0.7} \left(\dfrac{T_{sat,abs} C_{pl} \sigma \rho_l}{h_{fg}^2 \rho_v^2 L_b} \right)^{0.33} \mathrm{Pr}_l^{-0.45}$		Based on nucleate boiling
Grob (1990)	$h_e = 3.47 \times 10^4 M^{-0.5} \dfrac{(p/p_c)^{0.12}}{[-\lg(p/p_c)]^{0.55}} \left[\dfrac{q}{10^4} \right]^{0.7}$		Combined nucleate boiling and falling liquid film evaporation
Chowdhury et al. (1997)	$h_e = 11.43 (\mathrm{Re}_b)^{0.72} (\mathrm{Pr}_l)^{0.42} \left(\dfrac{\rho_v}{\rho_l} \right)^{0.5} \left(\dfrac{k_l}{D} \right)$	0.06 – 0.97	Combined nucleate boiling and falling liquid film evaporation

Table 3-2. Previously developed condensation heat transfer models of the thermosyphons

Researcher	Correlations	Operating pressures [bar]	Remarks
Nusselt (1916)	$h_c = 0.943 \left(\dfrac{\rho_l (\rho_l - \rho_v) g k_l^3 h_{fg}}{\mu_l (T_v - T_c) l_c} \right)^{1/4}$	$0.085 - 2.1$	Basic liquid film condensation theory
Hashimoto and Kaminaga (2002)	$h_c = 0.85 \mathrm{Re}_f^{0.1} \times \left\{ 0.74057 - 4.77089 \times 10^{-5} \left(\dfrac{\rho_l}{\rho_v} \right) \right\} \times h_{Nusselt}$	~ 1.0	Considered the effect of entrainment
Jouhara et al. (2012)	$h_c = 0.85 \mathrm{Re}_f^{0.1} \times \left\{ 0.86906 - 5.5987 \times 10^{-5} \left(\dfrac{\rho_l}{\rho_v} \right) \right\} \times h_{Nusselt}$	$\sim 0.04 - 0.19$	Considered the effect of entrainment
Gross (1992)	$h_c = \dfrac{k_l}{\left((v_l^2/g) \rho_l/(\rho_l - \rho_v) \right)^{1/3}} \left(\left(\dfrac{0.925 \mathrm{Re}^{-1/3}}{1 - 0.63 p^{*3.3}} \right)^2 + \left(0.044 \mathrm{Pr}_l^{2/5} \mathrm{Re}^{1/6} \right)^2 \right)^{1/2}$	~ 7.0	From laminar to turbulent flow
ESDU (1981)	$h_c = 0.651 \left(\dfrac{L}{d} \right)^{1/3} \left(\dfrac{\rho_l (\rho_l - \rho_v) g k_l^3 h_{fg}}{\mu_l (T_v - T_c) l_c} \right)^{1/4}$	~ 7.0	From laminar to turbulent flow
Uehara (1983)	$h_c = 0.884 \mathrm{Re}^{1/12} \left(\dfrac{\rho_l (\rho_l - \rho_v) g k_l^3 h_{fg}}{\mu_l (T_v - T_c) l_c} \right)^{1/4}$	~ 2.0	Considered the effect of waviness

Table 3-3. Summary on flooding limit models of the thermosyphons

Researchers	Correlations	Operating pressures [bar]	Remarks
Wallis (1969)	$Q_{Wallis} = C_w^2 h_{lv} A \rho_v^{1/2} [gD(\rho_l - \rho_v)]^{1/2} \left[1 + m\left(\dfrac{\rho_v}{\rho_l}\right)^{1/4}\right]^{-2}$	-	Water-air experiment
Kutateladze (1972)	$Q_{Kutateladze} = C_k^2 h_{lv} A \rho_v^{1/2} \left[g\sigma(\rho_l - \rho_v)\right]^{1/4} \left[1 + m\left(\dfrac{\rho_v}{\rho_l}\right)^{1/4}\right]^{-2}$	-	Water-air experiment
Tien and Chung (1978)	$Q_{Tien\&Chung} = 3.2 \tanh\left(0.5 Bo^{1/4}\right) h_{lv} \rho^{1/2} [\sigma g(\rho_l - \rho_v)]^{1/4} \dfrac{d_e / l_e}{\left[1 + (\rho_l / \rho_v)^{1/4}\right]^2}$	-	Combined the Wallis and Kutateladze criterion (Based on Helmholtz instability)
Imura et al. (1983)	$Q_{Imura} = 0.64 \rho_v H_{lv} A \left(\dfrac{D}{4L}\right)\left(\dfrac{\rho_l}{\rho_v}\right)^{0.13} \left[\sigma g (\rho_l - \rho_v)/\rho_v^2\right]^{1/4}$	$0.07 \sim 1.0$	Proposed the C_k^2 as a function of density ratio of working fluid
Faghri et al. (1986)	$Q_{Faghri} = \left(\dfrac{\rho_l}{\rho_v}\right)^{0.14} \tanh^2 Bo^{1/4} h_{lv} A [\sigma g(\rho_l - \rho_v)]^{1/4} \left[\rho_v^{-1/4} + \rho_l^{-1/4}\right]^{-2}$	$0.12 \sim 1.0$	Modified the Tien and Chung model to fit the experimental data about water
Monde et al. (1994)	$Q_{Monde} = \dfrac{0.16}{1 + 0.075(L/D_h)} \rho_v h_{fg} A \left[\dfrac{\sigma g(\rho_l - \rho_v)}{\rho_v^2}\right]^{1/4}$	1.0	Modeled the flooding phenomenon in open thermosyphon
ESDU (1983)	$Q_{ESDU} = f_1 f_2 f_3 A h_{fg} \rho_v^{1/2} [\sigma g(\rho_l - \rho_v)]^{1/4}$	~ 2.25	Empirical correlation
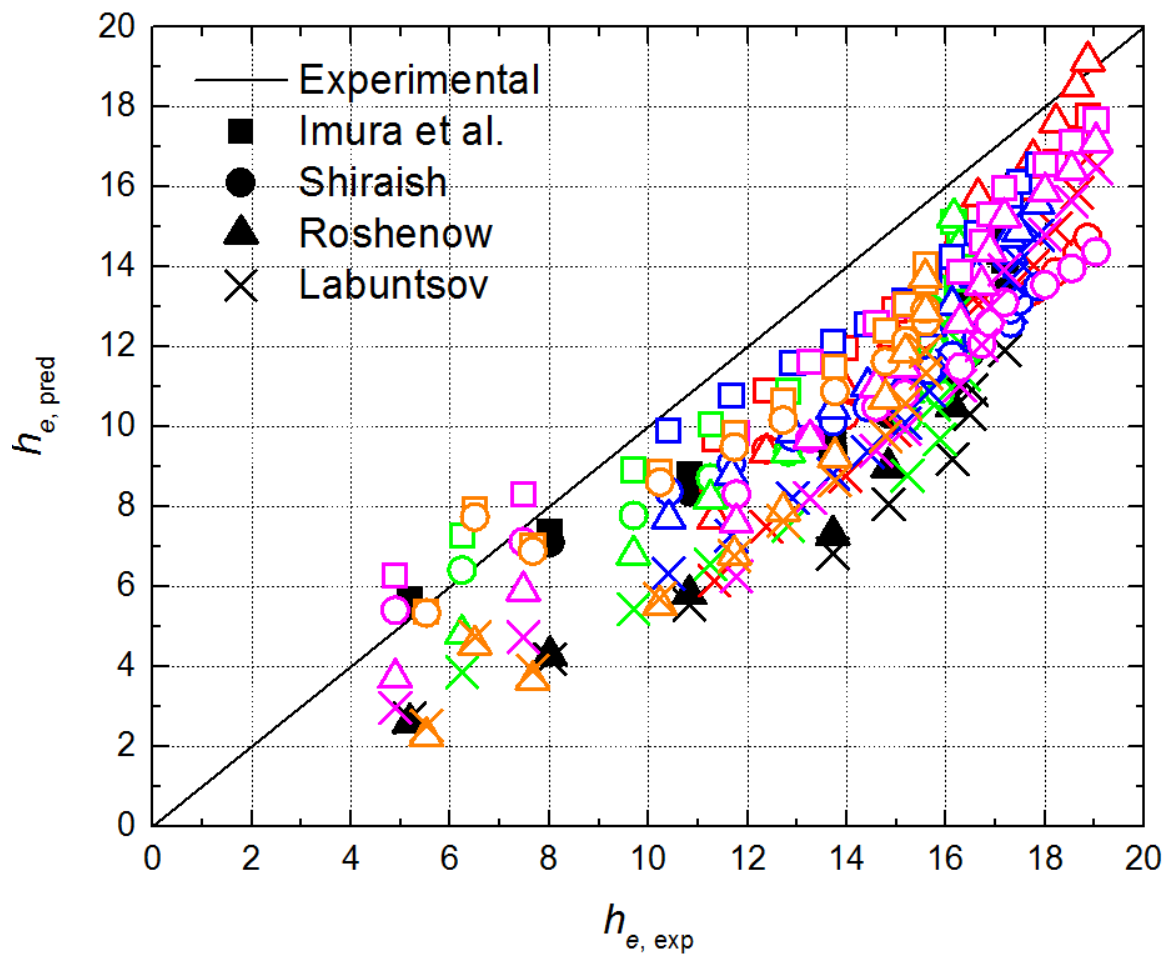
Fig. 3-7 Comparison of predicted evaporation heat transfer coefficients of existing models with experimental data
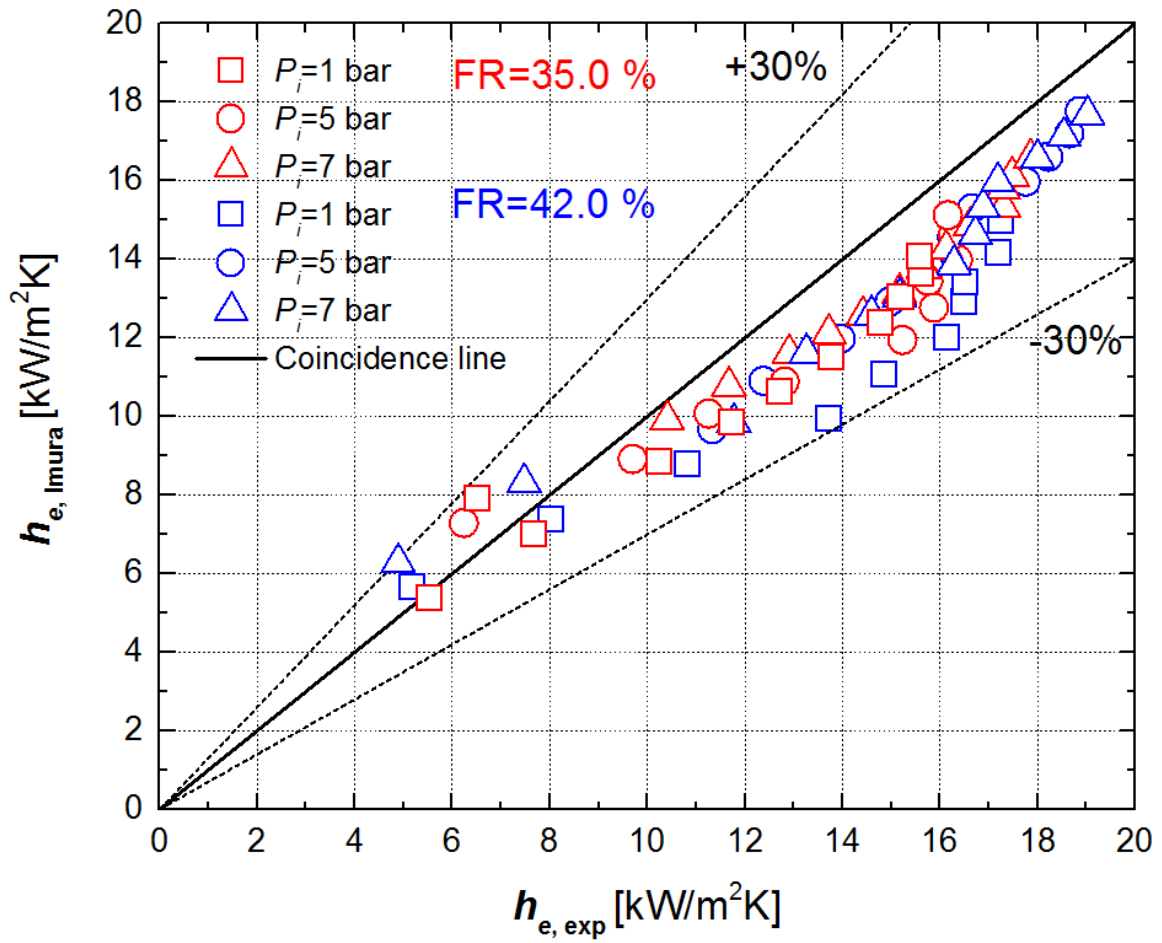
Fig. 3-8 Comparison of predicted evaporation heat transfer coefficients of Imura`s correlation with experimental data
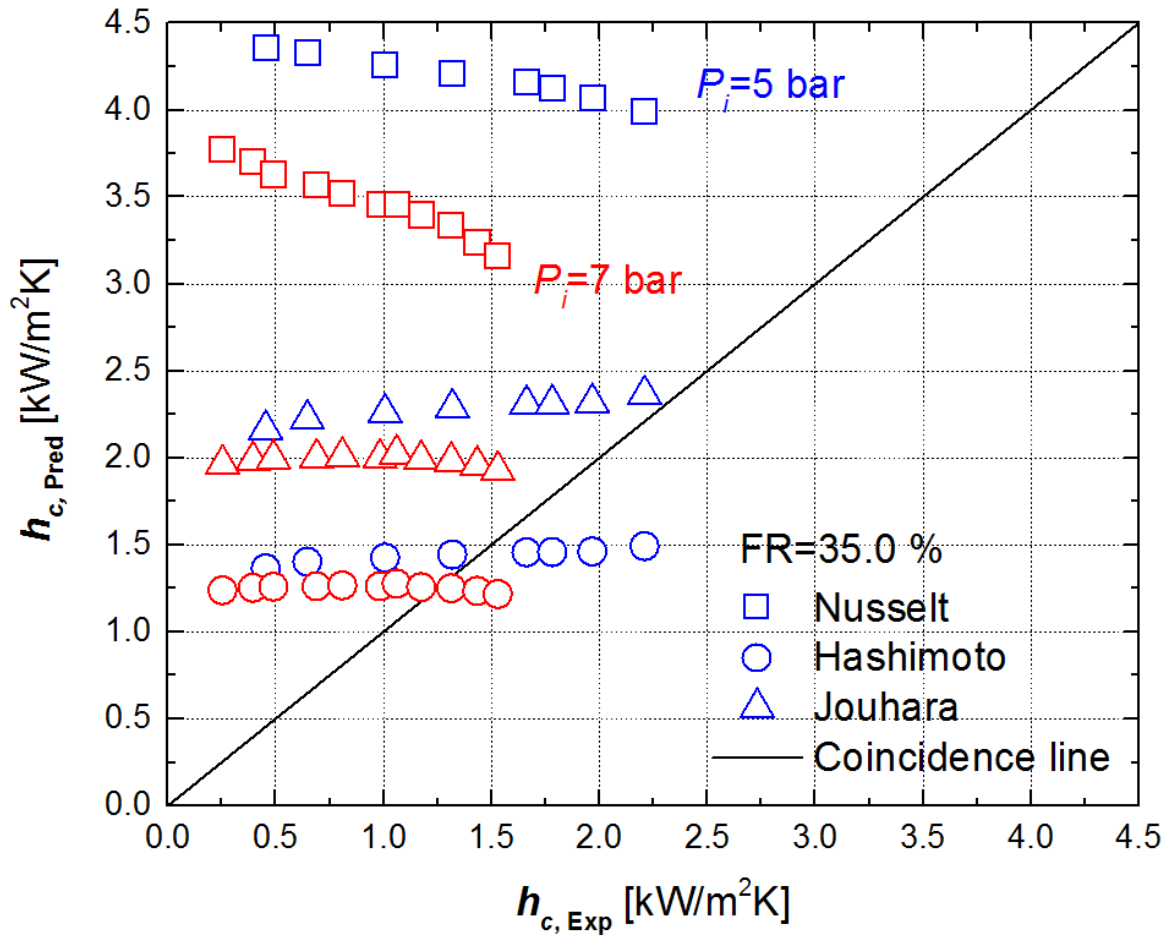
Fig. 3-9 Comparison of predicted condensation heat transfer coefficients of existing correlation with experimental data
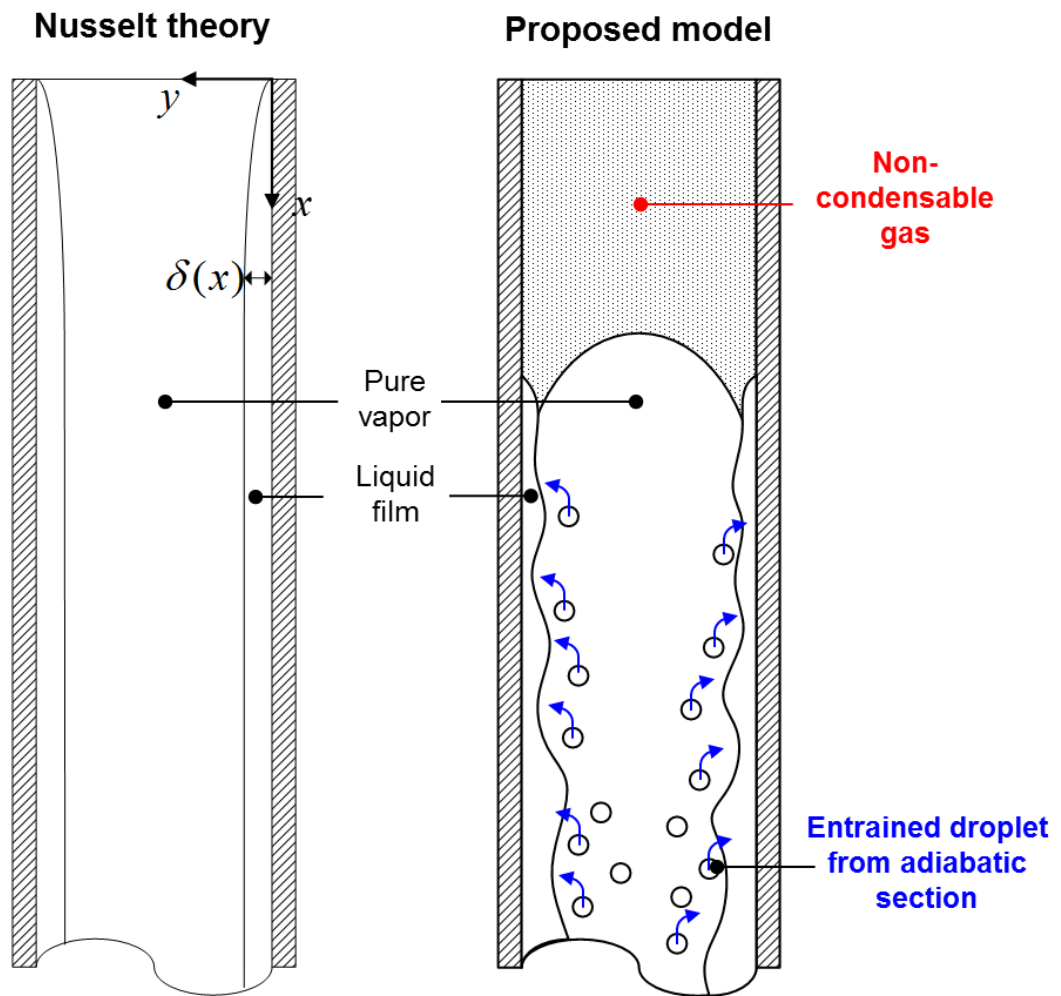
Fig. 3-10 Theoretical backgrounds of Nusselt theory (left) and proposed model (right)
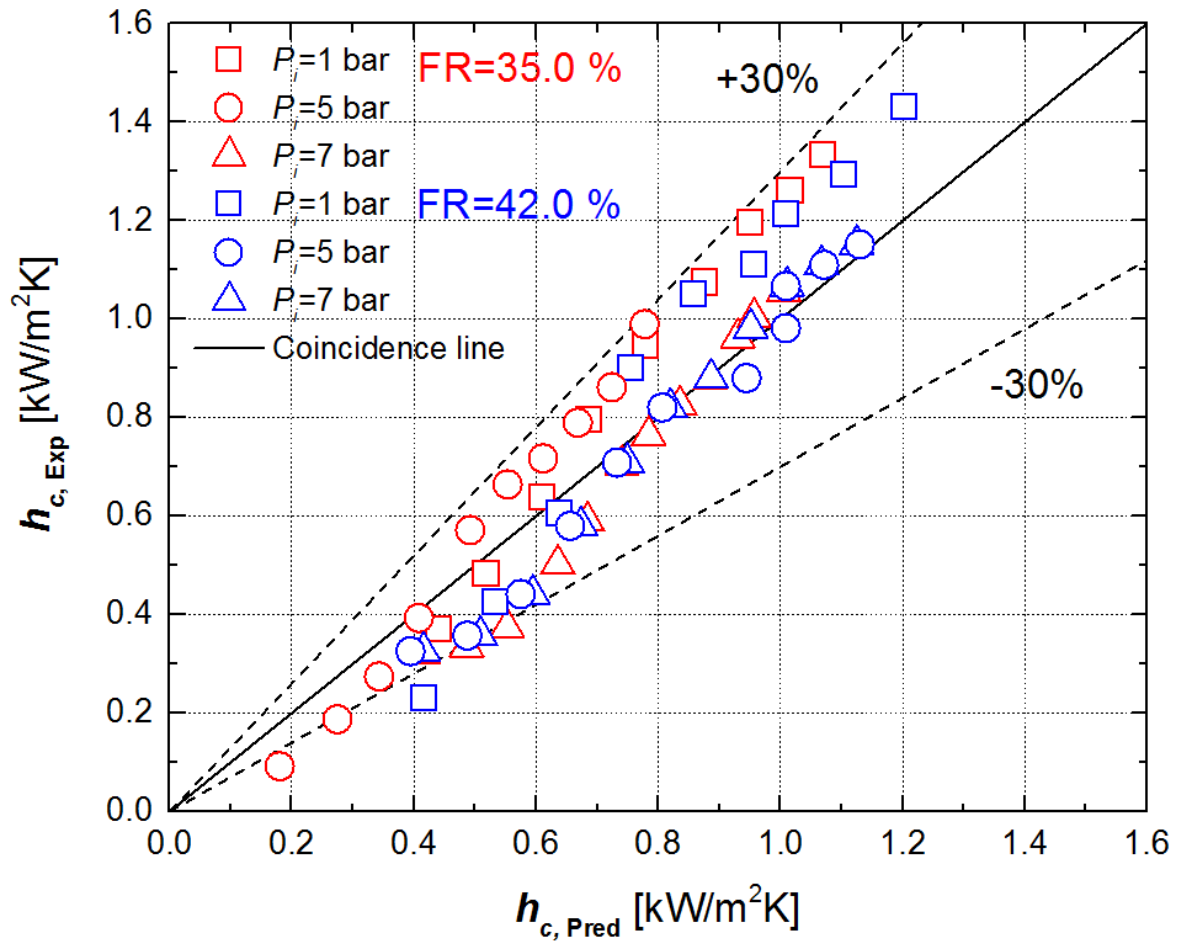
Fig. 3-11 Comparison of predicted condensation heat transfer coefficients by proposed model and experimental results
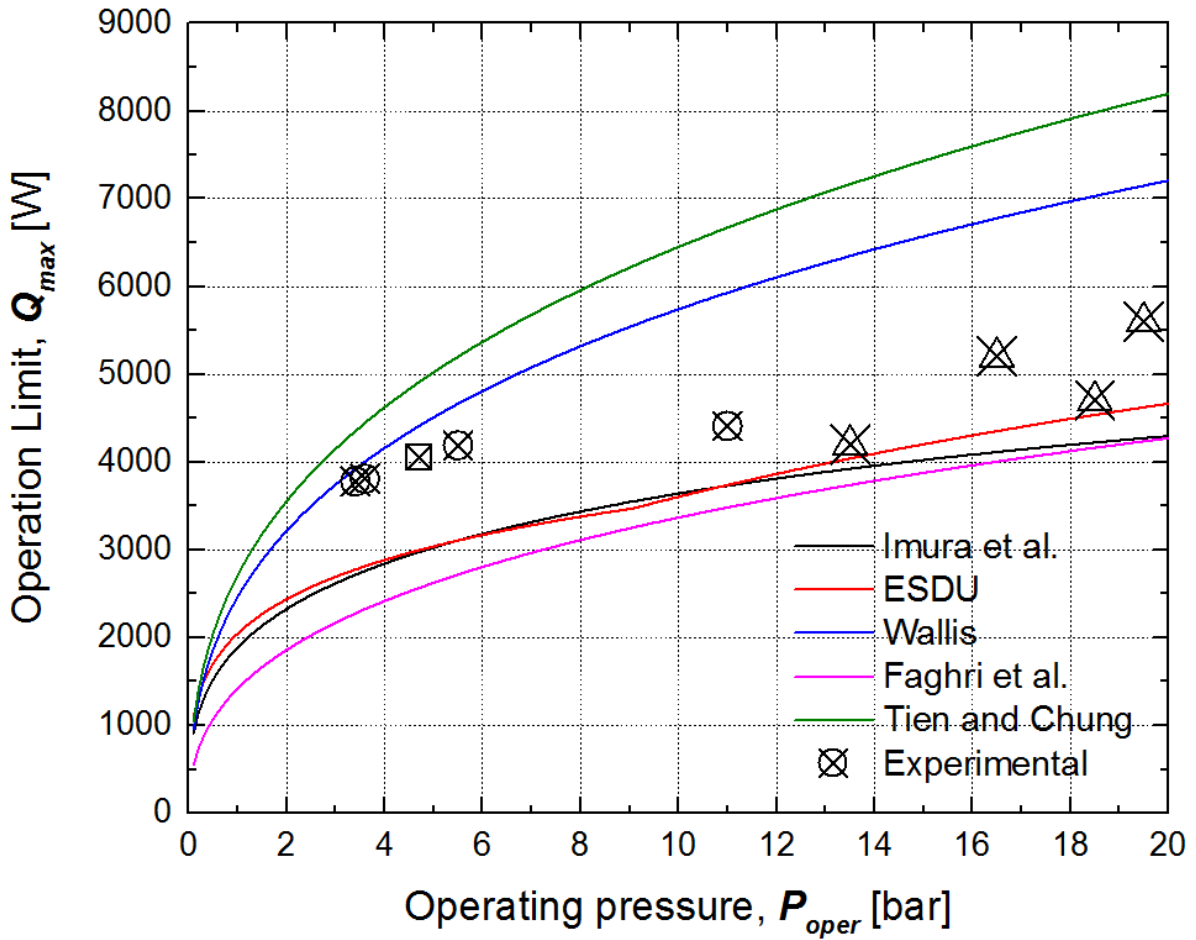
Fig. 3-12 Measured maximum heat transfer rates and predictions by existing flooding limit model
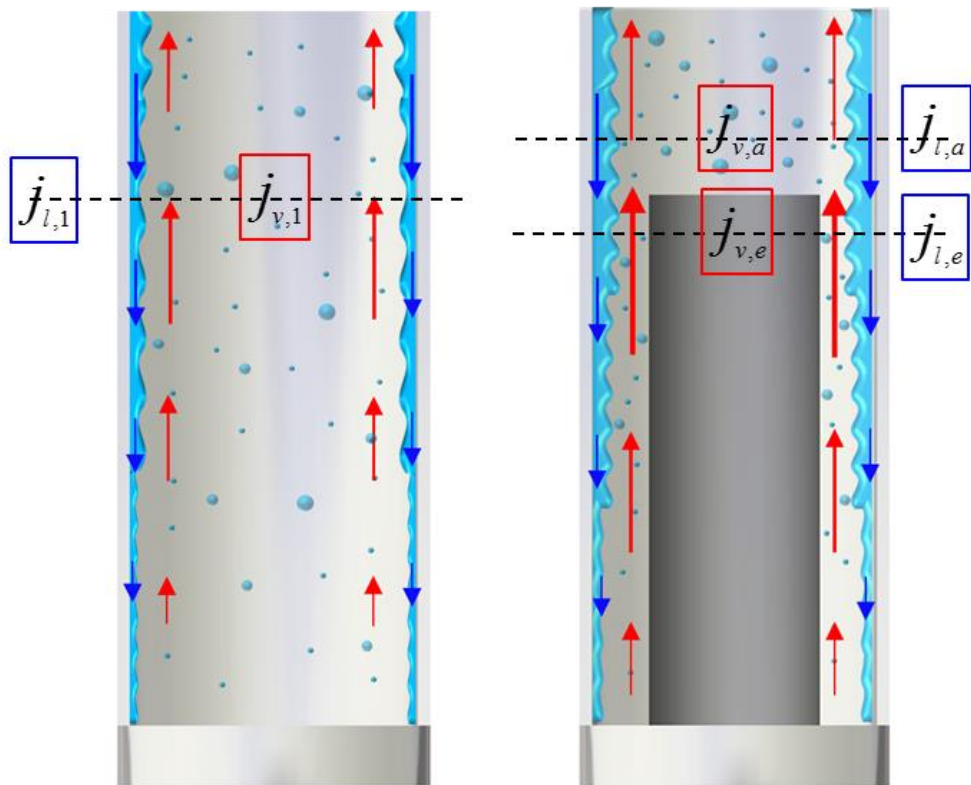
Fig. 3-13 Superficial velocities of concentric thermosyphon and hybrid control rod
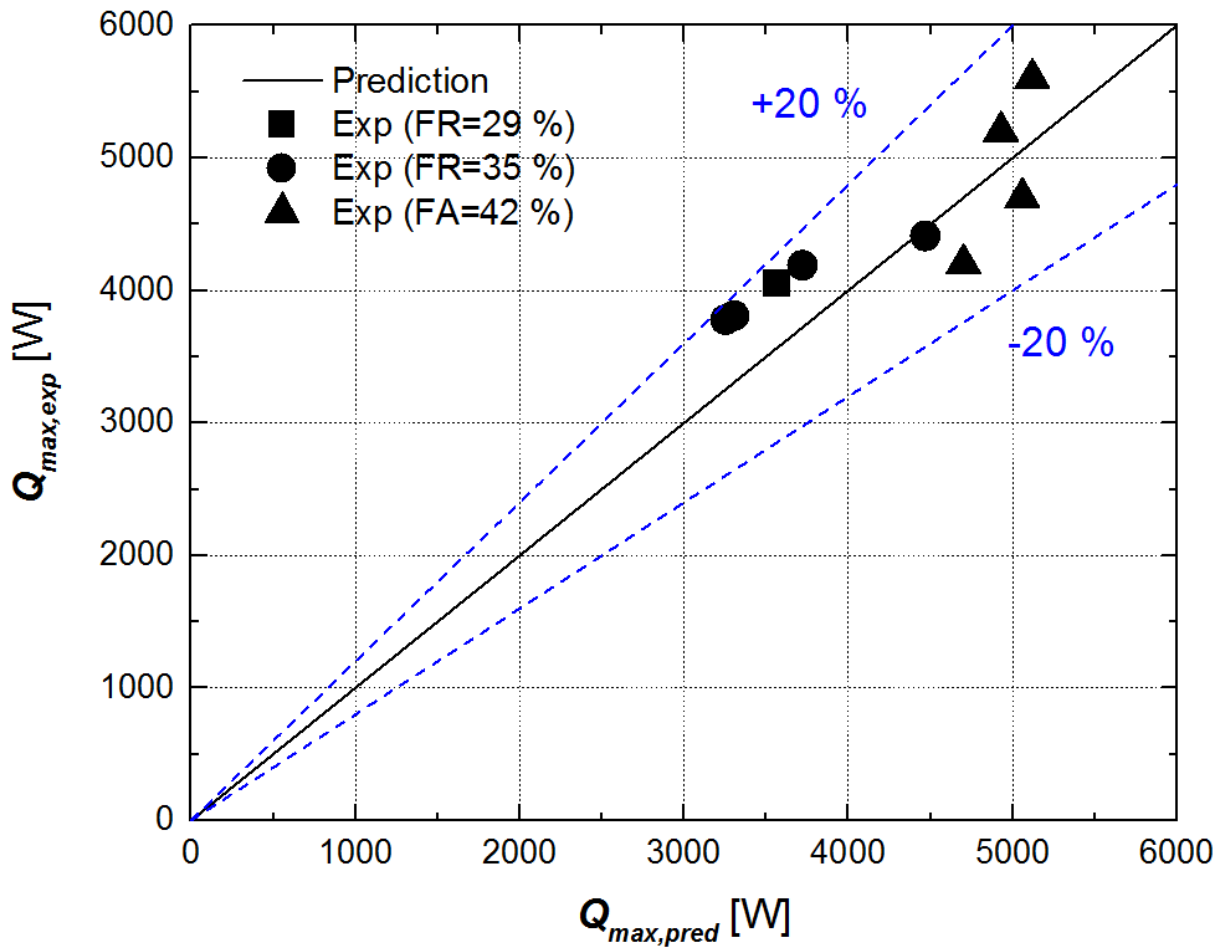
Fig. 3-14 Comparison between measured operation limits of hybrid control rod and predictions of proposed model

3.4 Validation of Models

New condensation heat transfer model was suggested for the hybrid control rod containing the non-condensable gas. In the proposed model, variation of the effective heat transfer length due to the volume occupied by the non-condensable gas was considered. The non-condensable gas was assumed as ideal gas and one-dimensional flat front model (there is no condensation heat transfer at the volume occupied by the non-condensation heat transfer) was applied. The effect of entrainment on the condensation heat transfer was reflected with suggestion of functions of density ratio and film Reynolds number on the condensation heat transfer coefficient predicted by Nusselt`s theory. For flooding-based maximum heat transfer rate model, the superficial velocities of the Kutateladze number were modified to depend on the cross-sectional areas of adiabatic and evaporator sections. The relation between Kutateladze numbers of liquid and vapor was defined as a function of density ratio. However, there is narrow range of available data to validate the models because of the unique characteristics of the hybrid control rod in comparison with conventional thermosyphon heat pipes. Therefore, the main assumptions on the models should be validated with extended experimental data. Table 3-4 presents the test matrix for the experiments validating the proposed models. Equal fill ratios of the working fluid, initial pressures, length ratio of test section, and coolant mass flow rate through condenser with self-pressurization experiments were varied for both experiments. Helium was introduced in the test section replacing the nitrogen gas to validate the condensation heat transfer model, nevertheless, the diameter of the boron carbide pellet was 17.7 mm. In the experiments for the validation of flooding-based maximum heat transfer rate model, diameter of the B_4C pellet was varied from 14.0 to 15.0 mm to change the cross-sectional area of evaporator section. The detailed information about the experiments will be described by following subsections.

3.4.1 Validation of condensation heat transfer model

The ideal gas assumption on the non-condensable gas will be verified if the variation of effective heat transfer length according to system pressure is independent on the kind of non-condensable gas. The helium gas was selected as a comparative gas for the validation of ideal gas assumption. The molecular weight of nitrogen is heavier than helium about seven times. Water molecule is also lighter than nitrogen about 64 %. The nitrogen gas can be settled down owing to its heavier molecular weight than water. In this model, the kinematic vapor pressure from the evaporator section is assumed to be higher than gravity. Thus, the helium was used in the experiment to utilize its light weight and non-reactive property with working fluid. To exclude other parameters that can affect the condensation heat transfer, dimensions of neutron absorber, initial pressure, and fill ratios of non-condensable gas were varied within the ranges of self-pressurization experiments.

Fig. 3-15 shows the assumed phenomenon inside condenser section of the hybrid control rod. When the internal pressure of the test section increases with heat load on evaporator section, the non-condensable gas will be compressed. The compressed volume of non-condensable gas was determined by ideal gas assumption. From the calculated volume of non-condensable gas according to internal pressure, the effective condensation heat transfer length can be deduced as Eq. (3-20).

$$L_{c,eff} = L_c - \frac{nRT}{PA} \qquad (3\text{-}20)$$

The vapor generated from the evaporator section will reach the higher elevation of condenser section compared to relatively lower pressure. Then, sudden temperature increase will be observed by thermocouples attached on the higher elevation due to formation of continuous falling liquid film will as shown in Fig. 3-16. The heat loads that temperature increases of the thermocouples are indicated by Fig. 3-17. The term of 'temperature increase' means the higher temperature than coolant temperature at outlet of water jacket. The elevations of thermocouples (TC-01, TC-02, TC-03, and TC-04) were 0.1, 0.175, 0.24, and 0.3 m from the bottom of condenser. In the specified experimental condition (initial pressure is 5 bar with helium and fill ratio of 35 %), thermocouple of lowest position of condenser (TC-01) recorded temperature increase at 1200 W heat load. The temperature increases of TC-02 and TC-03 were observed at heat loads of 2450 and 3600 W. The effective heat transfer length of condenser was calculated by ideal gas law assumption and measured internal pressures at each steady state. The calculated effective condensation heat transfer lengths according to heat loads were plotted in Fig. 3-18. The comparison between the calculated heat transfer lengths and elevations of thermocouples indicating temperature increase were in good agreement. Other experimental conditions also showed good agreement between predictions and experimental data. Hence, the ideal gas assumption is valid in the newly proposed condensation heat transfer model.

The rest theoretical background of the proposed condensation heat transfer model is deterioration of the heat transfer by entrainment. Countercurrent flow induces interfacial shear between upward vapor flow and downward liquid film flow. The interfacial shear entrains droplets and the droplets would return to condenser section by kinematic vapor pressure from evaporator section. The returned droplets would be deposited on the liquid film at condenser section and thicker liquid film would be formed. The effect of entrained droplet was weighted by exponential function of density ratio between vapor and liquid. The reason why weighting the entrainment effect exponentially can be explained by observing the instability of liquid film exerted by differences in densities and velocities of the phases. Amplitude of the instable liquid film could be expressed as sinusoidal function. The sinusoidal function can be rearranged in terms of exponent by Euler`s formula as shown in Eq. (3-21).

$$\eta = \eta_0 \exp(ikx + at) \qquad (3\text{-}21)$$

The lagrangian derivative of wave amplitude is the rate of ripple growth which can be rearranged as Eq. (3-22).

$$\frac{D\eta}{Dt} = \eta_0 e^{ikx+\mathrm{Im}(at)} e^{R(at)} R(a) = \eta R(a) \qquad (3\text{-}22)$$

where R(at) is real part of the exponent. The entrainment was assumed to be occurred at the ripple of the liquid film. Thus, the entrainment will be proportional to the ripple growth rate. Then, the entrainment rate is proportional to the growth rate of the ripples multiplied by liquid density as Eq. (3-23).

$$\varepsilon = \frac{D\eta}{Dt} \rho_f = \eta \rho_f R(a) \qquad (3\text{-}23)$$

Taylor[79] applied the growth of ripples to obtain the entrainment rate. In the linear instability model, Kelvin-Helmholtz`s theory was improved by considering the effect of liquid viscosity. The analysis was based on the fasted growing or 'most dangerous' wave. As the liquid viscosity become small enough to show the asymptotic behavior, solution of Taylor is close to Kelvin-Helmholtz`s model. In this case, the fastest growth rate of the ripple (real part of exponent) is Eq. (3-24)

$$R(a) = 0.384 k_0 u_g \sqrt{\frac{\rho_g}{\rho_f}} \qquad (3\text{-}24)$$

Hence, the effect of entrainment on condensation heat transfer was correlated in a form of exponent employing the density ratio as parameter. In general models[80,81] related to the entrainment rate under two-phase flow condition (especially annular flow regime), Weber number of gas phase, film Reynolds number, and viscosity ratio were considered as main parameters determining the entrainment fraction and rate as expressed in Eq. (3-25) and (3-26).

$$\frac{\varepsilon D}{\mu_f} = k \left[We_g \left(\frac{\Delta\rho}{\rho} \right) \left(\mathrm{Re}_{lf} - \mathrm{Re}_{lfc} \right) \right]^{0.925} \left(\frac{\mu_g}{\mu_f} \right)^{0.26} \qquad (3\text{-}25)$$

$$\frac{\varepsilon D}{\mu_f} = 6.6 \times 10^{-7} \, \mathrm{Re}_f^{0.74} \, \mathrm{Re}_{fc}^{0.185} \, We^{0.925} \left(\frac{\mu_g}{\mu_f} \right)^{0.26} \quad for \quad (\mathrm{Re}_{lf} < \mathrm{Re}_{lf\infty}) \quad\quad (3\text{-}26)$$

However, the correlations were derived in the range of Weber number above second order. As shown in Fig. 3-19, gas Weber numbers (We_g) were below 6.0 during the experiments of the pressurized hybrid control rod. Thus, Weber number was not considered in the modeling of entrainment effect on liquid film condensation heat transfer.

Constant in the exponential function is -0.0003 which could be thought as meaningless value. However, as shown in Fig. 3-20, the term on entrainment effect was meaningful in the pressures that experiments were conducted. The value was varied from 0.4 to 0.95 at pressure ranges of atmospheric pressure to 20.0 bar.

The condensation heat transfer coefficients measured by experiments of helium charged-test sections were compared with the self-pressurization experiments conducted with nitrogen. The test sections charged with helium gas showed similar heat transfer coefficients with the nitrogen gas as shown in Fig. 3-21 validating the assumptions of ideal gas and consideration about the entrainment effect. As a result, the experimental data showed agreement with prediction results within 30 % as shown in Fig. 3-22. Therefore, it can be concluded that the assumed thermal-hydraulic phenomena at the condenser section of the hybrid control rod are valid.

3.4.2 Validation of flooding limit model

Existing correlations related to the prediction of maximum heat transfer rate of thermosyphon heat pipes were developed assuming the critical phenomenon as a flooding. The dimensionless numbers balancing the forces between gravity and drag forces were proposed. The representative dimensionless number is Kutateladze number and it depends on the superficial velocities of vapor and liquid. Relation between Kutateladze numbers of liquid and vapor were defined by many researchers. They developed the correlations as functions of density ratio, Bond number, length to diameter ratio, and clearances. However, the superficial velocities were defined at a cross-section in the previous models. The superficial velocities defined at a cross-section could not predict the liquid film velocity developed from condenser section and vapor velocity generated from the evaporator section accurately because the hydraulic diameters at evaporator, adiabatic, and condenser section are different for the hybrid control rod. The predictions using the existing correlations were conducted by employing the cross-sectional area of the evaporator section. As a result, all of existing correlations predicted high deviations from the experimental data.

To consider the effect of different cross-sectional area across evaporator and condenser sections, liquid superficial velocity at adiabatic section was assumed to be equal to that of evaporator section since the liquid film would be very thinner than diameter of the test section. New Kutateladze numbers were proposed and their relation was defined as a function of density ratio between vapor and liquid. The proposed model predicted experimental data within 20 % error range.

For the purpose of validation of the model, the cross-sectional area of the evaporator section was varied maintaining the cross-sectional area of the adiabatic section. Although the effect of fill ratio on the flooding-based maximum heat transfer rate was ignored in the model, the fill ratio of working fluid was varied to verify the neglection. Initial pressures were determined to maintain the equal values with self-pressurization experiments. Nitrogen gas was charged in the test section for double-check on condensation heat transfer model.

As the initial pressure increases, the internal pressure was increased and flooding-based maximum heat removal capacity was enhanced. The increase of fill ratio resulted in the achievement of higher internal pressure according to heat loads. Consequently, the fill ratio affect the flooding limits in terms of increasing operating pressures. Reduction of diameter of neutron absorber (magnification of cross-sectional area for the evaporator section) induced enhanced operation limits due to lower vapor velocity compared to the test sections of narrow channel. Fig. 3-23 showed that the experimentally measured operation limits of the hybrid control rod were agreed with predictions by model proposed in this study. The maximum deviation was 20 % as shown in Fig. 3-24. Thus, the prediction capability of the model was confirmed in following conditions; i) operating pressure = 1.0 – 20.0 bar, ii) fill ratio = 29.0 – 45.0 %, iii) initial charge of non-condensable gas = 1.0 – 7.0 bar, and iv) diameter of neutron absorber = 13.0 – 17.7 mm in outer cladding of 1 in" diameter.

Table 3-4. Experimental conditions for performance analysis of hybrid control rod

	Condensation model	Flooding limit model
Fill ratio of working fluid [%]	35.5, 42.0	35.5, 42.0
Heat load [W]	400 – 4000	Until operation limit
Diameter of neutron absorber [mm]	17.7	14.0, 15.0
Non-condensable gas	Helium	Nitrogen
Initial pressure [bar]	1.0, 5.0, 7.0	1.0, 5.0, 7.0
Length ratio (evaporator:adiabatic:condenser)	285:215:500	
Condenser mass flow rate [kg/s]	0.0267	
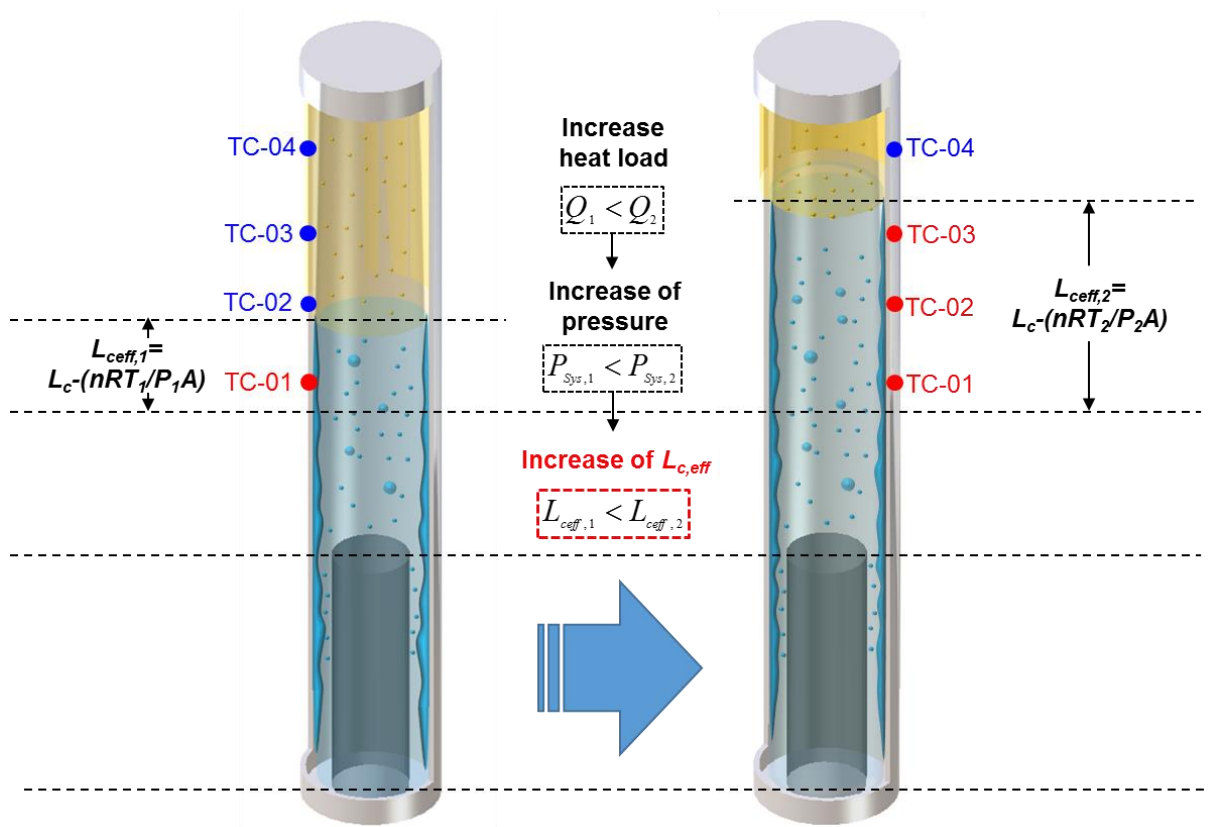
Fig. 3-15 Distributions of liquid film, entrained droplet, and non-condensable gas at the condenser section with increase of heat load and internal pressure
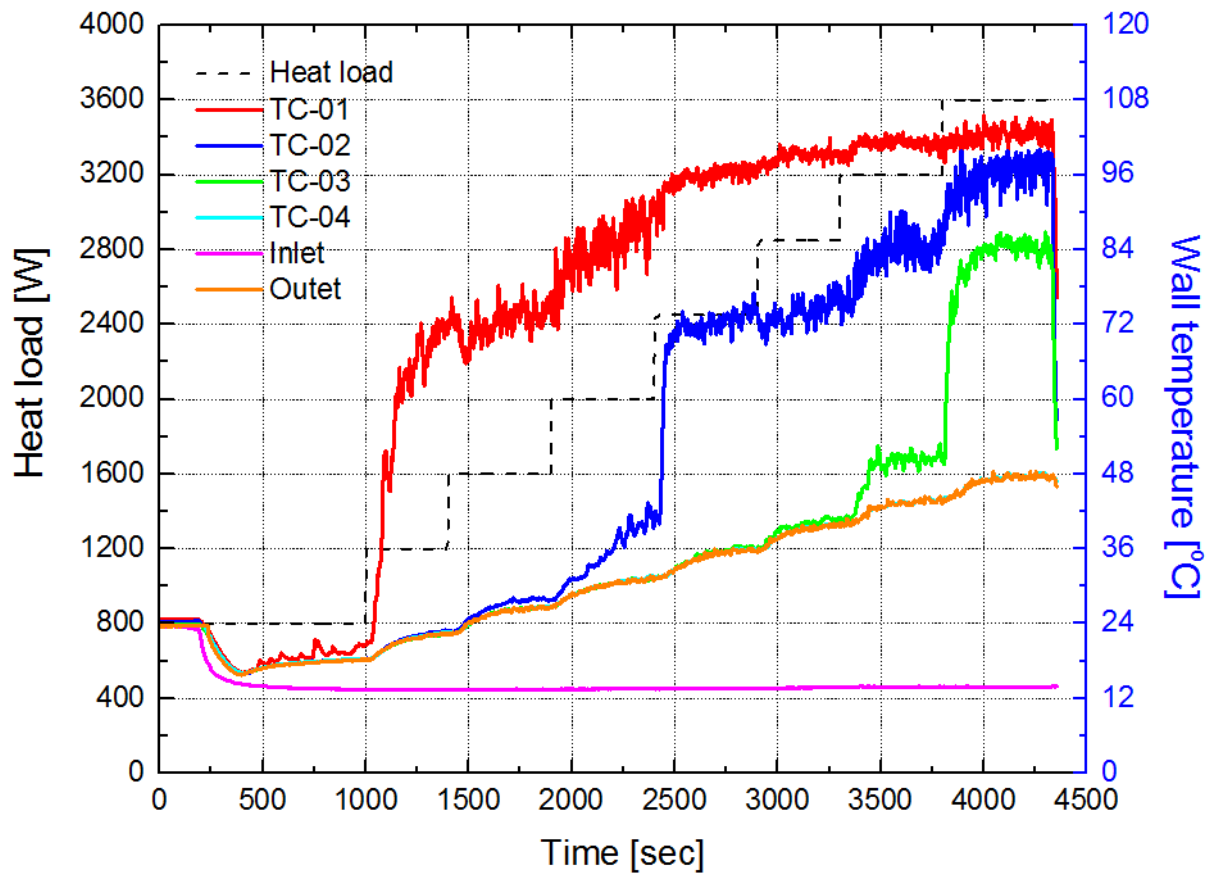
Fig. 3-16 Temperature variations of the thermocouples installed at the condenser section according to heat loads
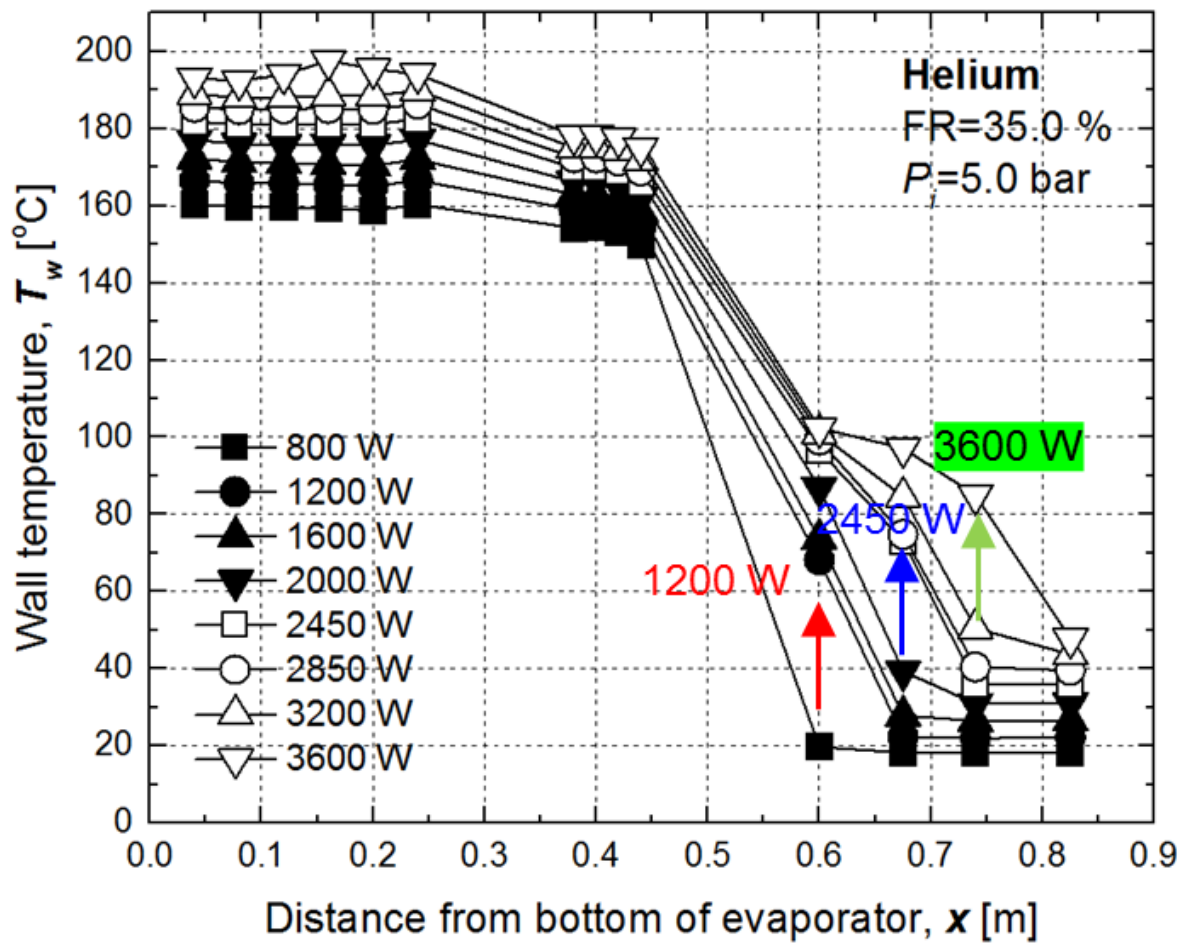
Fig. 3-17 Wall temperature distributions at steady states during experiment (FR=35 %, initial pressure=5.0 bar, Helium charged)
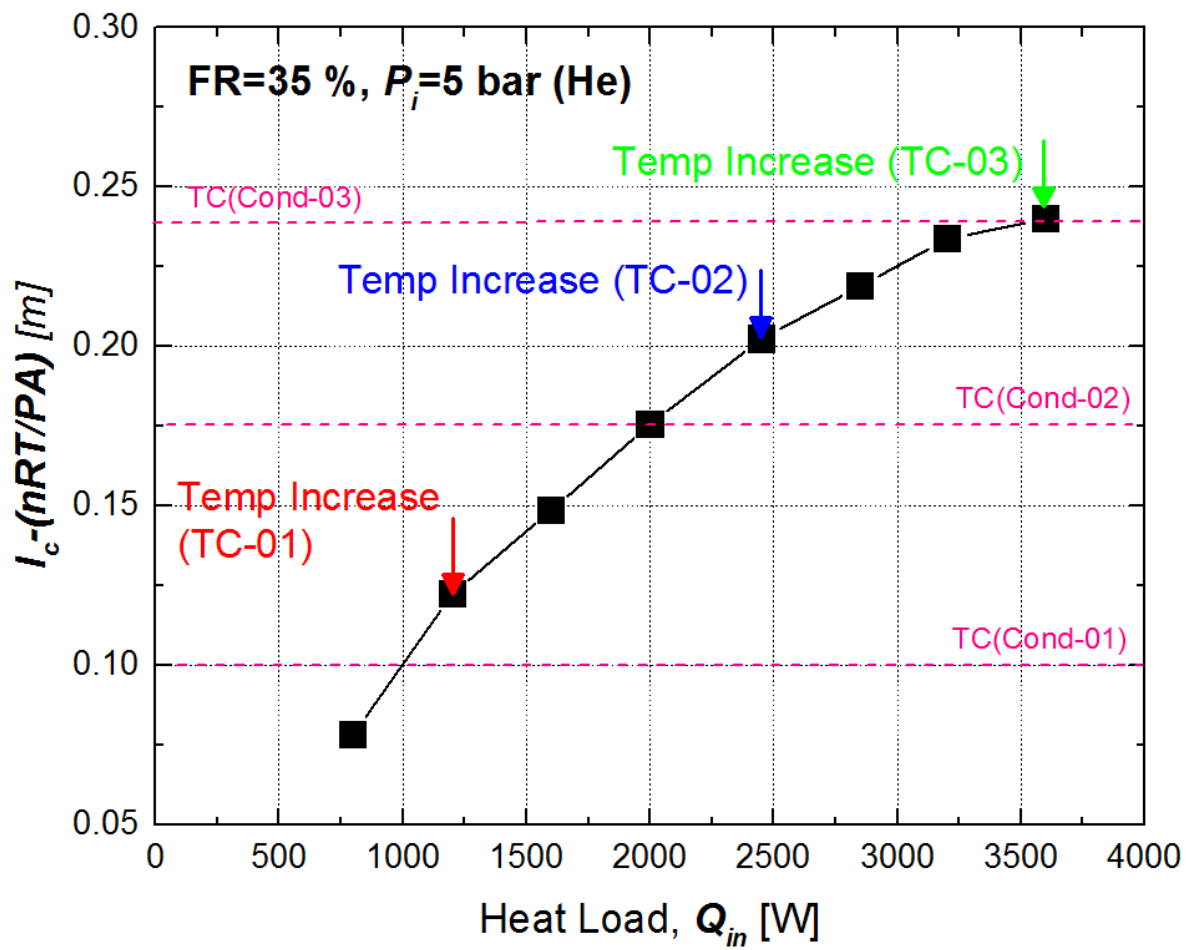
Fig. 3-18 Calculated effective condensation heat transfer lengths according to heat loads and temperature increase points of thermocouples during experiment.
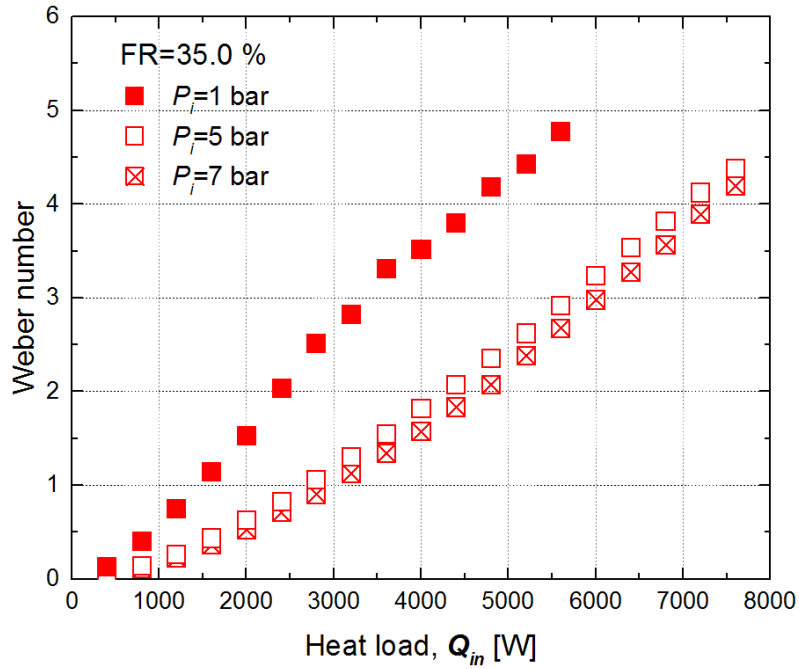
(a)
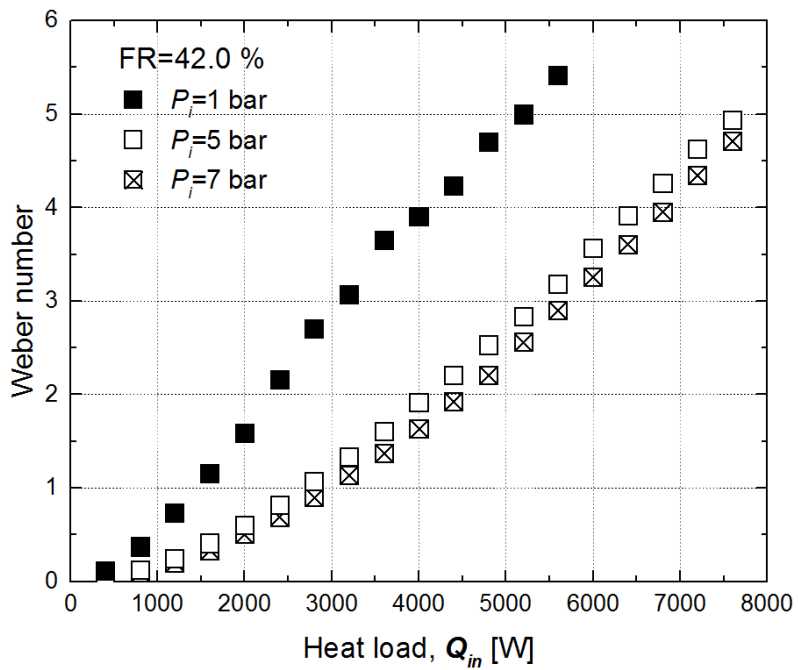
(b)

Fig. 3-19 Weber numbers according to heat loads, fill ratios, and initial pressures during helium-charged experiments: (a) FR=35.0 %, (b) FR=42.0 %
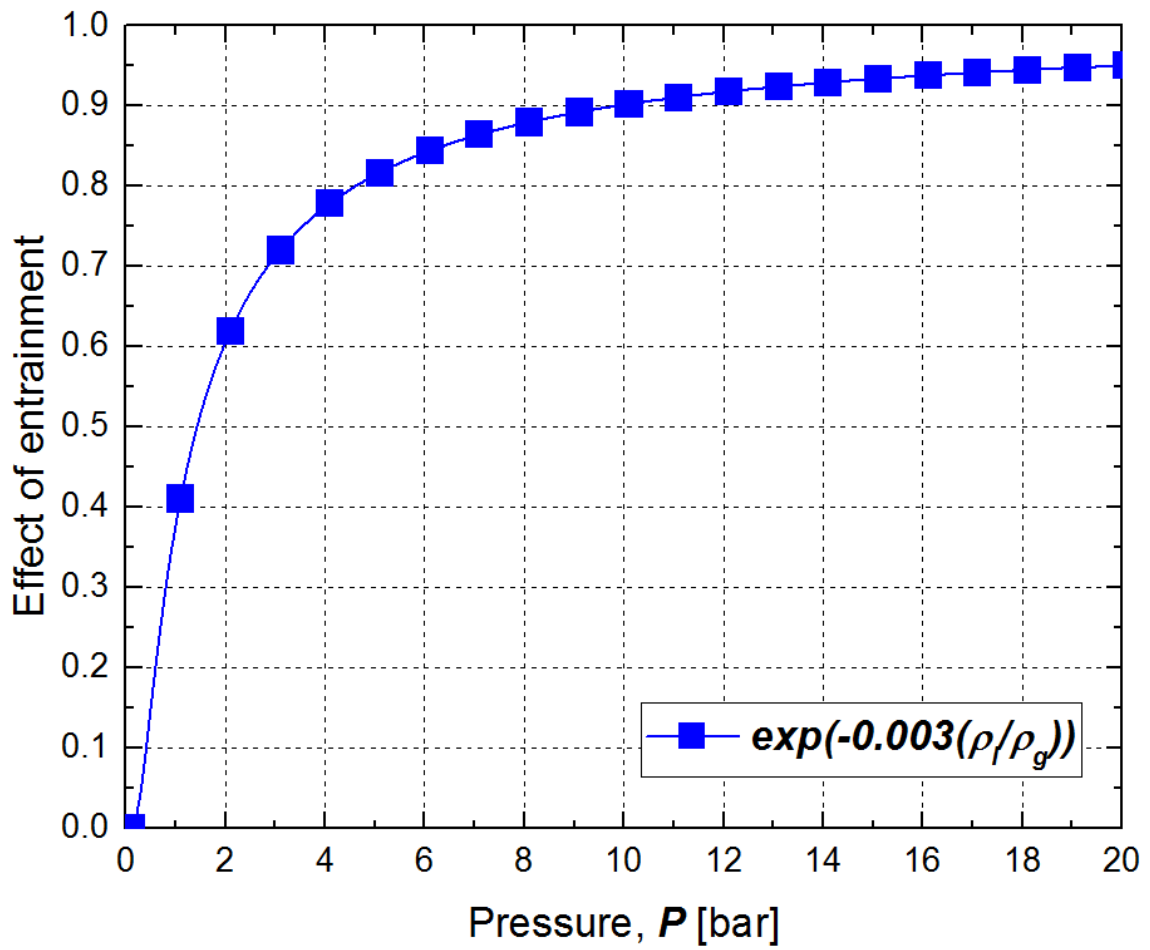
Fig. 3-20 Values of exponential function in proposed model
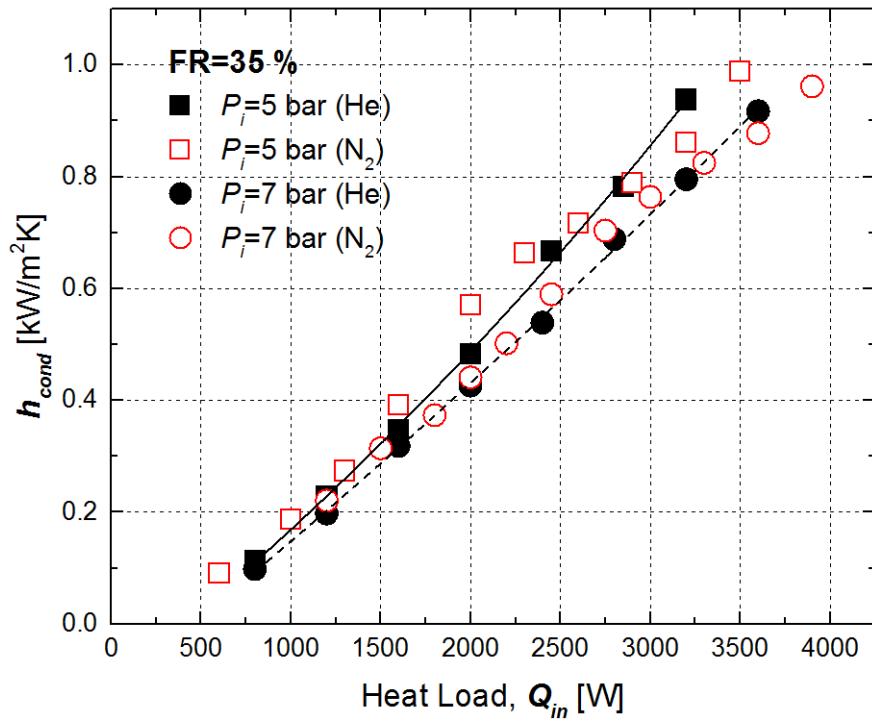
(a)
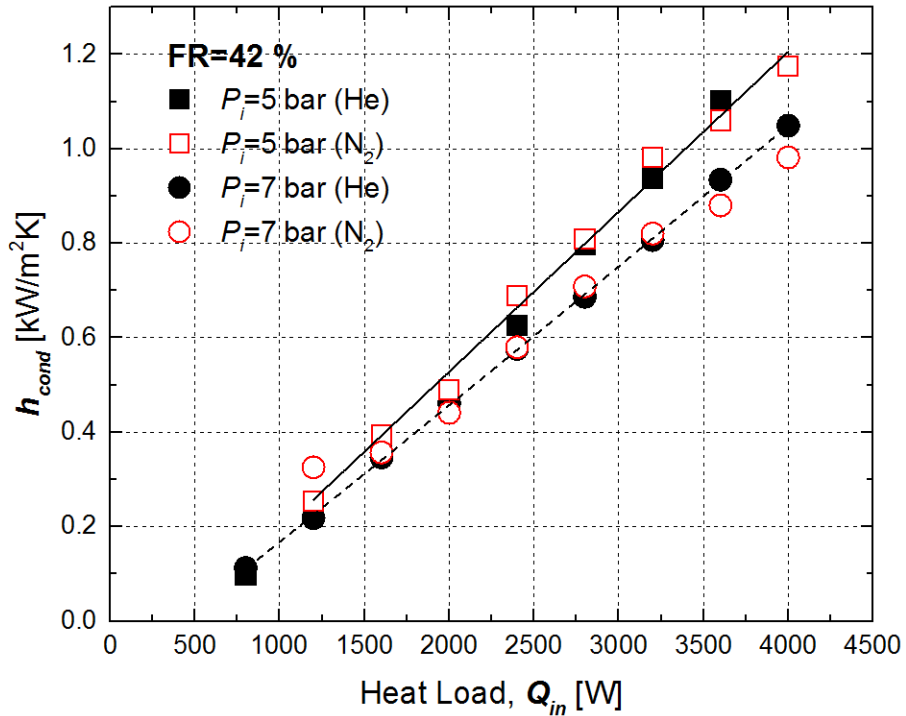
(b)

Fig. 3-21 Comparison of condensation heat transfer coefficients with different non-condensable gases, fill ratios, and initial pressures: (a) Fill ratio=35 %, (b) Fill ratio=42 %
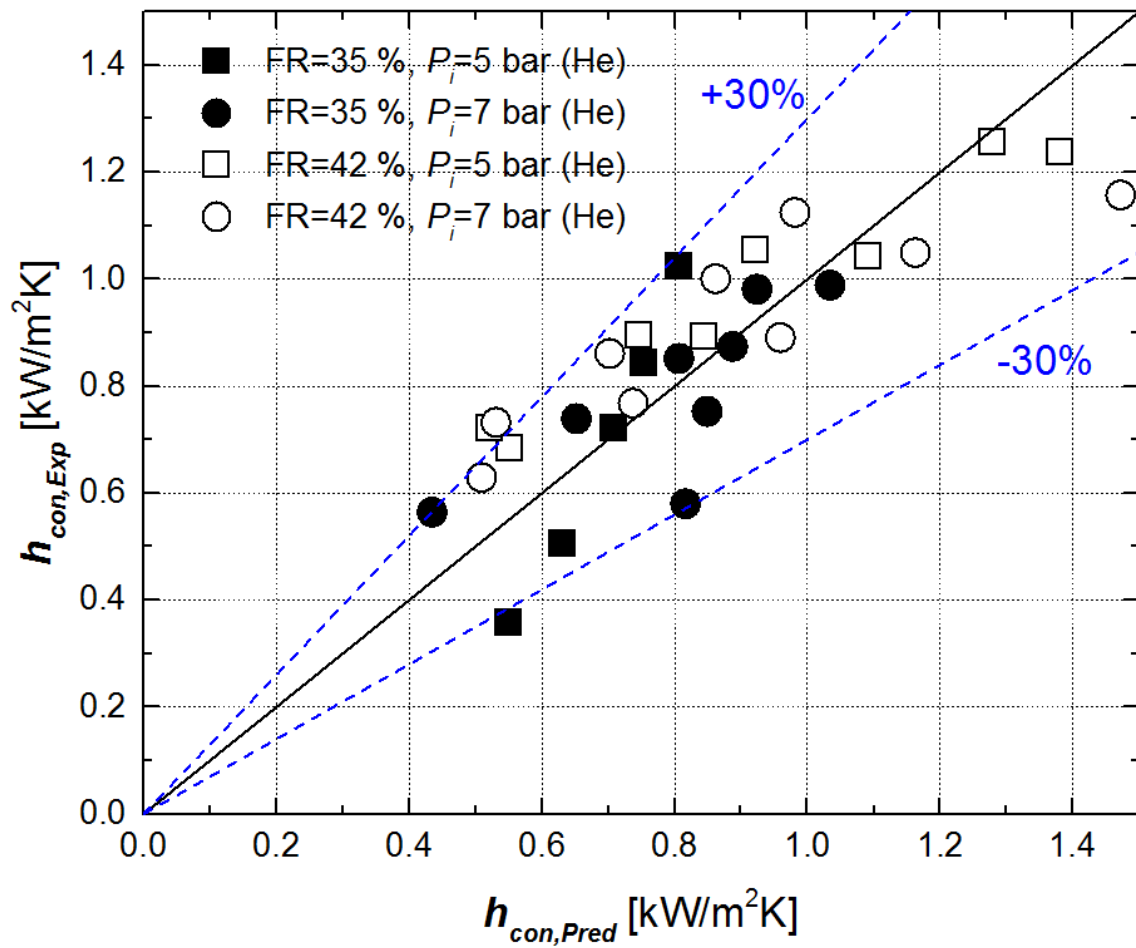
Fig. 3-22 Comparison of measured condensation heat transfer coefficients and predictions by proposed model
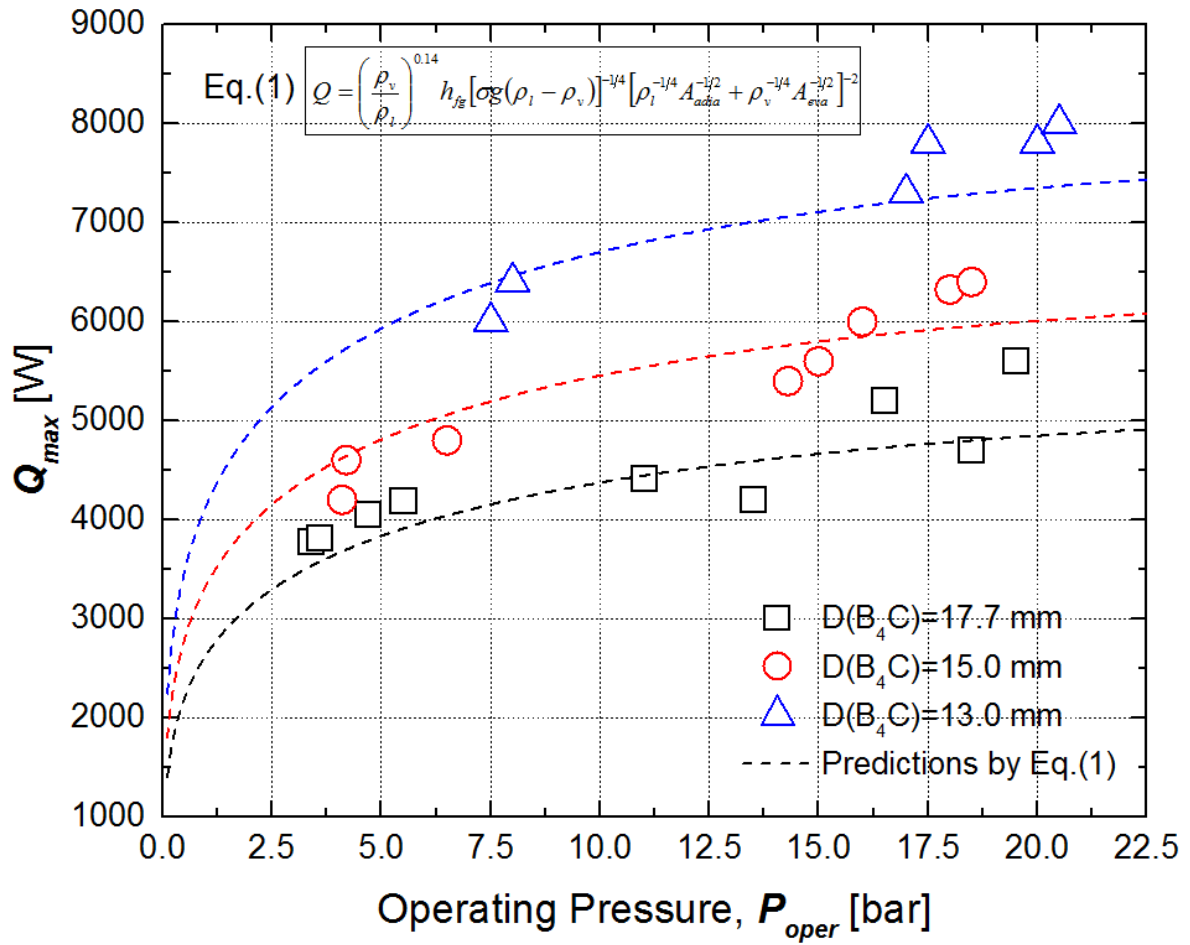
Fig. 3-23 Maximum heat transfer rates of the hybrid control rod according to diameters of neutron absorber and operating pressures

Fig. 3-24 Comparison of measured maximum heat transfer rates and predictions by proposed model

3.5 Guideline for Hybrid Control Rod Design

The thermal performances including the maximum decay heat removal capacity were modeled with theoretical assumptions considering the parameters affect the thermal-hydraulic phenomena. For the specific application of the hybrid control rods on various nuclear facilities, the controlled parameters such as initial pressure, fill ratio of the working fluid, dimensions of the test section (diameters of neutron absorber, inner tube and outer cladding), and types of working fluid in the experiments could be varied. Therefore, a guideline for hybrid control rod design was established based on the experimental results and proposed models as shown in Fig. 3-25.

If the environmental conditions such as temperatures at core and heat sink, decay heat, system pressure, and required reactivity worth are determined, the diameter of neutron absorber (cross-sectional area of the vapor-path at evaporator section with determination of diameter of outer cladding referring the geometry of guide tube for control rod) must be initially calculated to secure the sufficient reactor shutdown capability. Then, the core temperature which corresponds to the evaporator section of the hybrid control rod will determine the optimal operating pressure of the hybrid control rod. The internal pressure of the hybrid control rod was varied with the heat load at evaporator section, fill ratio of the working fluid, initial pressure, and diameter ratio between neutron absorber and outer cladding during the experiments. The system pressure was proportional to the initial pressure, heat load, fill ratio, and diameter ratio with magnitudes of arranged order. The relationship between internal pressure and parameters which dominate the operating pressure was summarized.

The decay heat generated from the core during reactor shutdown phase should be compared with the maximum heat removal capacity of the hybrid control rod to confirm the stable decay heat removal capability. In this step, newly proposed model for maximum heat removal rate of the hybrid control rod can be used. If the predicted maximum heat transfer rates of the hybrid control rods at the determined pressure is lower than required decay heat removal capacity, the initial pressure, diameter ratio, and fill ratio will be reconstructed. When the maximum heat removal rate through PINCs satisfies the efficient decay heat removal, the heat transfer coefficients at evaporator and condenser sections of the hybrid control rod have to be calculated to quantify the coolant temperatures at the different temperature interfaces. At the evaporator section, Imura`s correlation which was developed with basis of evaporation at falling liquid film will be applied. In case of the condenser section, newly developed model in this study which considers the effects of variations of effective heat transfer length due to presence of non-condensable gas, and liquid film thickness because of the entrainment can be used to predict the condensation heat transfer rate.

Boundary conditions at the evaporator and condenser sections have to be assumed appropriately. Although the convective conditions in the section of heat source will be determined by the analysis results of thermal-hydraulics system code during accident condition, the boundary condition at heat

sink should be determined with design of heat exchanger system including the ultimate heat sink condition. Consequently, the predicted temperatures at the interfaces of heat source and sink will be compared to the target temperatures and the design of the hybrid control rod will be confirmed with iterative calculation to meet the functional requirements of target nuclear facilities.

It is expected that the design of the hybrid control rods according to requirements of the application system would be possible using the proposed guideline. However, there would be limited usability due to assumptions and limited experimental range. The guideline does not include the effect of length ratio between the evaporator, adiabatic, and condenser sections assuming the length ratio effect is negligible. The assumption about length ratio must be evaluated and validated with further works. Besides, the working fluid is restricted to water and range of fill ratio is 29.0 – 42.0 %. The models on heat transfer coefficients and flooding limit were validated within operating pressures from 1.0 to 20.0 bar. Hence, design of the hybrid control rod using the proposed guideline is recommended to be conducted within the suggested ranges.

Initial conditions
Fill Ratio of Working fluid, Initial charge of NC,
Diameter of B_4C pellet, Heat load

Calculate system pressure, P_{sys}

$$P_{sys} = P_{initial} + (1/4)(D_{B_4C}/D_{i,Clad})Q + \left(V_{fluid}^+/V_{tot}\right)$$

Calculate maximum heat removal rate, Q_{max}

$$Q = \left(\frac{\rho_l}{\rho_v}\right)^{0.14} h_{fg}\left[\sigma g(\rho_l - \rho_v)\right]^{-1/4}\left[\rho_l^{-1/4}A_{adia}^{-1/2} + \rho_v^{-1/4}A_{eva}^{-1/2}\right]^{-2}$$

Q > Q_{max}   **Yes**

No

Calculate evaporation heat transfer

$$h_e = 0.32\left(\frac{\rho_l^{0.65}k_l^{0.3}C_{pl}^{0.7}g^{0.2}}{\rho_v^{0.25}h_{fg}^{0.4}\mu_l^{0.1}}\right)\left(\frac{P_v}{P_{atm}}\right)^{0.3}q^{0.4}$$

Calculate condensation heat transfer

$$h_c = Re_f^{0.1}\exp\left(-0.0007\frac{\rho_l}{\rho_v}\right)\times\left\{0.943\left(\rho_l(\rho_l - \rho_v)gk_l^3h_{fg}\middle/ \mu_l(T_v - T_c)\left(l_c - \frac{nRT}{PA_{cs,c}}\right)\right)^{1/4}\right\}$$

Calculate temp. difference between heat source and heat sink

No

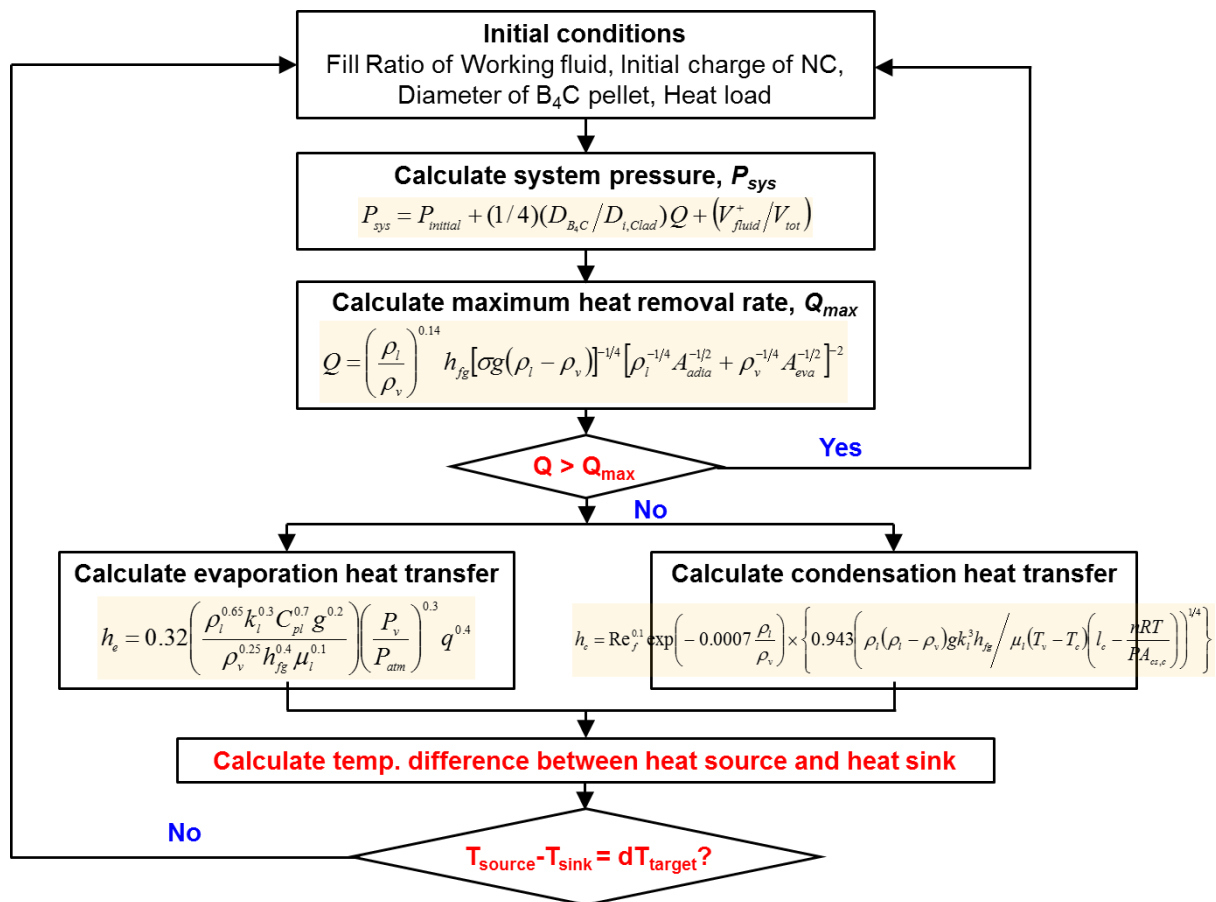**$T_{source}-T_{sink} = dT_{target}$?**

Fig. 3-25 Proposed flowchart for hybrid control rod design

Chapter 4. APPLICATION STUDY OF HYBRID CONTROL ROD

4.1 Introduction

Spent fuel storage problem become an important issue in society due to its radioactivity, increasing amount of spent fuel, and space for storage. Interim spent fuel dry storage casks have been developed and installed for the purpose of spent fuel storage until reprocessing and usage of the spent fuel.

For concrete type of spent fuel dry storage casks, the natural air convection through the gap between canister and cask is a cooling strategy. Despite the concrete cask cannot be used in the transportation of spent fuels, they are widely used in the fields due to their ensured integrity in terms of radiation shielding. The analyses[82-84] on natural convection through the flow path in normal and off-normal conditions have been conducted. The analyses were combined with thermal analysis on peak cladding temperatures and temperatures of structural components to guarantee their design safety against the acceptance criteria provided by nuclear regulatory commission (NRC).

Metal spent fuel dry storage casks are promising type of the casks because it could be utilized under transportation and normal storage conditions. In metal cask, decay heat from the spent fuel is managed by conduction and radiation from basket to atmosphere.

Kim et al.[85] conducted computational fluid dynamics to find optimal prediction methods for peak cladding temperature and effective thermal conductivity in spent fuel assemblies of transportation/storage casks. According to types of spent fuel assemblies (B&W type, CE type, and WH type), optimal models predicting the peak cladding temperature and effective thermal conductivity of the cask were found with discussion about the models. Kim et al.[86] evaluated the heat transfer on spent fuel dry cask during short-term operations; i) wet condition, ii) vacuum drying condition, iii) dry condition. The short-term operations are related to loading spent fuels in the cask. FLUENT code was used to observed the appropriate working times for the conditions. Vacuum drying condition showed the highest temperature distributions and evolution compared to other cases due to its poor heat transfer mechanism. Kang et al.[87] analyzed the performances of fin installed at the outer wall of cask to optimize the heat transfer from cask to environment. At normal operation, fins reduce the cladding temperature, but, the fins increase cladding temperature inside the canister during fire accident condition. They deduced the optimal number of fins with sensitivity study on normal and accident conditions. Lee et al.[88] studied on the integrity of the dry storage cask using FATE code in off-normal conditions. The assumed off-normal conditions were loss of flow and forced helium dehumidification. 1/8 section is modeled with five unique channels (basket, upper plenum, downcommer, gap, and heat sink). The analysis results showed that both cases satisfy peak cladding temperature below than limiting PCT. Frano et al.[89] carried out simulation on thermal behavior of a spent fuel cask in different transport conditions. A 9-m drop impact event onto a flat, unyielding, horizontal surface, in the most damaging

orientation) and rigorous fire events (full exposure to an engulfing fire for 30 min or to an environment at 800 °C temperature) were selected off-normal cases. The integrity of AGN-1 cask system was ensured by ANSYS analysis results.

However, it has been observed that the decay heat removal mechanism through the wall is inefficient due to thick walls which are determined in terms of radiation shielding. The long-term exposure of the spent fuel in high temperature condition could result in material problems such as embrittlement. Therefore, UCAN which is a new type of spent fuel dry storage cask integrating hybrid control rod was proposed to solve the possible material issues of spent fuel in storage casks by enhancing the thermal margin. Impact of the proposed design on cask safety was tested with 1/10 scaled-down mock-up. The test results showed that the hybrid control rod could enhance the thermal margin of the cask by providing additional heat transfer path. Efficiency of the decay heat removal through the hybrid control rod according to design of condenser was also demonstrated in this study.

4.1.1 Issues on spent fuel dry storage cask

Construction and operation of commercial nuclear power plants generate spent fuels which have fission products. Increase of demand for energy requires more number of nuclear power plants, and more spent fuels will be generated. Disposal of the spent fuel generating decay heat and radioactivity becomes an essential ingredient. Technologies related to reprocessing and further use of the spent fuel are under development for the disposal of spent fuels. Until the complete development of the technology and facilities, the spent fuel must be managed in appropriate manners. Therefore, interim spent fuel storage casks are operating to manage the spent fuels. The interim spent fuel storage facilities have been designed in the form of dry storage cask to maintain the sub-criticality of the spent fuel assemblies. The casks have to remove the decay heat significantly satisfying acceptable component temperatures, sub-criticality, and radiation shielding.

The designed interim spent fuel dry storage casks must be verified by submitting safety analysis report (SAR) to US nuclear regulatory commission (US NRC). The following design bases should be included as operating controls and limits. In normal operations, the effect of ambient temperature on cooling capacity of the cask must be evaluated. Off-normal conditions are can be arranged as follows; i) variations in temperatures beyond normal, ii) failure of 10 percent of the fuel rods combined with off-normal temperatures, iii) failure of one of the confinement boundaries, iv) partial blockage of air vents, v) human error, vi) out-of-tolerance equipment performance, vi) equipment failure, vii) instrumentation failure or faulty calibration. The safety of cask must be ensured against the postulated accident conditions as follows; i) cask drop, ii) cask tipover, iii) fire, iv) fuel rod rupture, v) leakage of the confinement boundary, vi) explosive overpressure, v) air flow blockage. The natural phenomena events such as flood, tornado, earthquake, burial under debris, and lightning are also must be considered in the

design.

The spent fuel dry storage casks must meet the acceptance criteria provided by US NRC in terms of structural, thermal, confinement, shielding, criticality, and material.

The passive cooling system for decay heat removal have to be equipped on the casks and its performances must be quantified by analyses through experiments and simulation. The analyses results will be compared with the acceptance criteria in terms of temperature limits for each component. Maximum fuel cladding temperature should not be exceeded 400 °C during normal operation or short-term operations such as cask drying and backfilling to guarantee cladding integrity of zirconium-based alloy. For off-normal and accident conditions, the maximum zirconium based cladding temperature should not exceed 570 °C. In aspect of criticality design, the effective neutron multiplication factor should not exceed 0.95 under all credible normal, off-normal, and accident level conditions.

However, the dry storage casks have limited coolability due to poor heat transfer mechanisms (radiation and air convection) and thick wall which is designed in terms of radiation shielding. As a result, thermal analyses reported the low temperature margins of the components including fuel cladding compared to the acceptance criteria provided by US NRC. Long-term exposure of the spent fuel in high temperature condition could cause the material problems such as thermal embrittlement, then failure of the radiation shielding would be occurred.

The criticality of the spent fuels stored in the casks is controlled by neutron absorber. The general methodology controlling the criticality is coating of neutron absorber at the outer wall of the baskets. The coating technology is a key technology in maintenance of subcriticality to prevent the chain reaction and ensure the integrity of fuel. However, the coating layer of the neutron absorption material provides additional thermal resistance in cooling. The addition of thermal resistance increase radial temperature gradient from spent fuel to cask wall with reduced effective thermal conductivity. The current designs considering the combined issues associated with thermal, material, shielding, and critical viewpoint restrict the efficient decay heat management.

4.1.2 Concept of UCAN based on hybrid control rod

The existing designs on spent fuel storage casks have inefficient cooling capacity owing to their wall thickness, thermal resistances based on wall thickness and coating layer of the neutron absorber material. The cooling strategies using the natural air convection or radiation are common. The different coping strategies were applied on the existing spent fuel dry storage casks in aspects of controlments of neutron flux and decay heat management. If the hybrid control rod which is a passive decay heat removal device having the functionalities of neutron absorption is applied to the casks, the cooling and subcriticality of spent fuel assemblies can be achieved simultaneously. The guide tubes in spent fuel assemblies are vacancies in currently installed casks, and the space can be used as passage for insertion of hybrid

control rods. The integration of the hybrid control rod on spent fuel dry storage cask have several advantages compared to previously developed casks. First, the thermal resistance due to coating layer of neutron absorbing material on the basket can be eliminated. The neutron absorber inside the hybrid control rod has reactivity worth of reactor shutdown which is sufficient value on reactivity control for spent fuel assemblies replacing the coating layer. The cost to form the coating layer also can be reduced. Second, the additional decay heat removal path will be secured. The radial heat conduction through wall, convective heat transfer by air convection, radiation from cask wall to environment are main heat transfer mechanisms of the existing metal casks or concrete casks. The phase change and convection of working fluid between spent fuel and heat sink will provide the decay heat management passage in axial direction. Consequently, the temperature of the components inside the cask will be reduced and the temperature margin will be extended. Third, the transferred decay heat through the hybrid control rod can be reused. If the stored energy inside the heat sink of the hybrid control rod is reused, power generation system or power plant can be constructed in the basement of spent fuel dry storage cask cluster. For the regeneration process, the thermoelectric module, stirling engine, or heat pumps could be combined with the heat sink. At that points, the hybrid control rod acts as heat transfer medium and heat sink of the cask play a role of heat source.

The design having the hybrid control rod on spent fuel dry storage cask with replacement of cask lid to heat sink is defined as UCAN (UNIST canister). The detailed information on the UCAN is drawn in Fig. 4-1. Impact damper is on the bottom of UCAN to mitigate the impact which could be applied to the cask in off-normal or accident conditions such as cask drop or cask tipover. A canister storing 21 baskets and a cask. The heat sink replaces the cask lid of the previously developed casks. The hybrid control rods are installed at the guide tubes of spent fuel assemblies and they are connected to the heat sink.
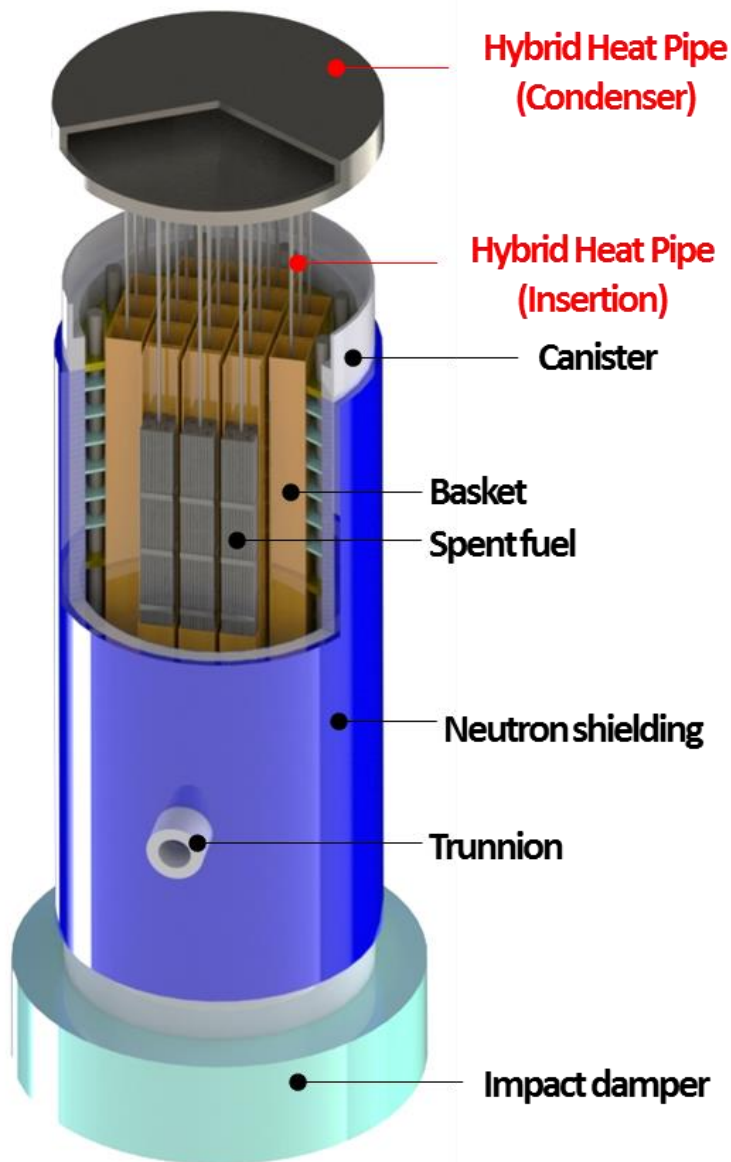
Fig. 4-1. Schematic diagram of UCAN

4.2 Experimental Setup and Procedures

To observe the effect of UCAN design on safety of spent fuel dry storage cask, UCAN mock-up was prepared for the experimental works. The UCAN mock-up was designed to be scaled-down to 1/10 of dimension of metal cask developed by KORAD in as presented in Table 4-1. Length and diameter of the components were scaled-down with equal linear power density. Fig. 4-2 shows the inner structures of the UCAN mock-up. Total 21 baskets 1/10 scale of PLUS7 fuel assembly which is a representative fuel assembly type of APR-1400 including cartridge heaters were installed to simulate the decay heat of spent fuel. Copper heat pipes having outer diameter of 6 mm and containing water as working fluid were located at the center of each basket and they were connected to the condenser (heat sink). The initial operating pressure of the heat pipe was 0.2 bar corresponding the boiling temperature of 60 °C. Gap between canister and cask wall was also considered in design and the gap was filled with air (in general casks helium is charged for the high heat conductance). Condenser containing the heat sink medium of the UCAN plays a role of upper lid. The heat sink medium used in the experiments were air and water for the comparison of effectiveness of heat sink medium on the performance of the hybrid control rods. Six support plates and eight support rods were integrated to fix the baskets in the designed positions. The system was encapsulated by fitting the components in designed position. The encapsulation of the mock-up was confirmed by heat balance test.

Four thermocouples inside the canister measure the temperature evolutions inside the canister through the radial and axial directions. TC-H-01 and TC-H-02 were installed at the elevation of 300 mm from the bottom of canister and TC-L-01, 02 were located below 90 mm from the TC-H-01 and -02. The TC-H-01 recorded the temperature at wall of center basket. The TC-H-02 and TC-L-01, 02 measured the air temperature between the outer basket and second line of basket. Thus, the temperature evolution during experiment and temperature distributions at steady states could be recorded along radial and axial direction. A K-type thermocouple was installed inside the condenser and measured the heat sink temperature variation. Two K-type thermocouples were deposited on the walls of cask and condenser and the measured temperature data would be used in the calculation of heat transfer rate through the external wall and structural stored energy.

Test matrix of the experiment to confirm the effectiveness of UCAN design is presented in Table 4-2. The total heat applied to the heaters was 90 W (0.22 kW/m) showing equal linear power density with reference cask of KORAD. The power density level of the experiment is maintained about 15 % of full scale cask due to material problem of the mock-up (acrylic). Constant heat was generated by the cartridge heaters and the temperature variations and distributions were observed to confirm the effect of hybrid control rod and heat sink design on temperature behavior of spent fuel dry storage cask. The heat loads showing similar temperature distributions with the hybrid control rod installed- and heat sink installed-cask design for the purpose of quantitative evaluation of efficiency of the UCAN design.

Table 4-1. Scales of general metal cask and UCAN mock-up

Components	Dimensions [mm]	
	Metal cask (KORAD)	UCAN mock-up
Cask body	Φ2126 x 5285	Φ210 x 530
Basket assembly	241 x 241 x 4550	20 x 20 x 450
Canister	Φ1686 x 4880	Φ170 x 480
Hybrid control rod	-	Φ6 x 500
Q/basket (kW)	1.0	0.1
Q'/basket (kW/m)	0.22	0.22

Table 4-2. Test matrix for observation of impact of UCAN design on cask safety

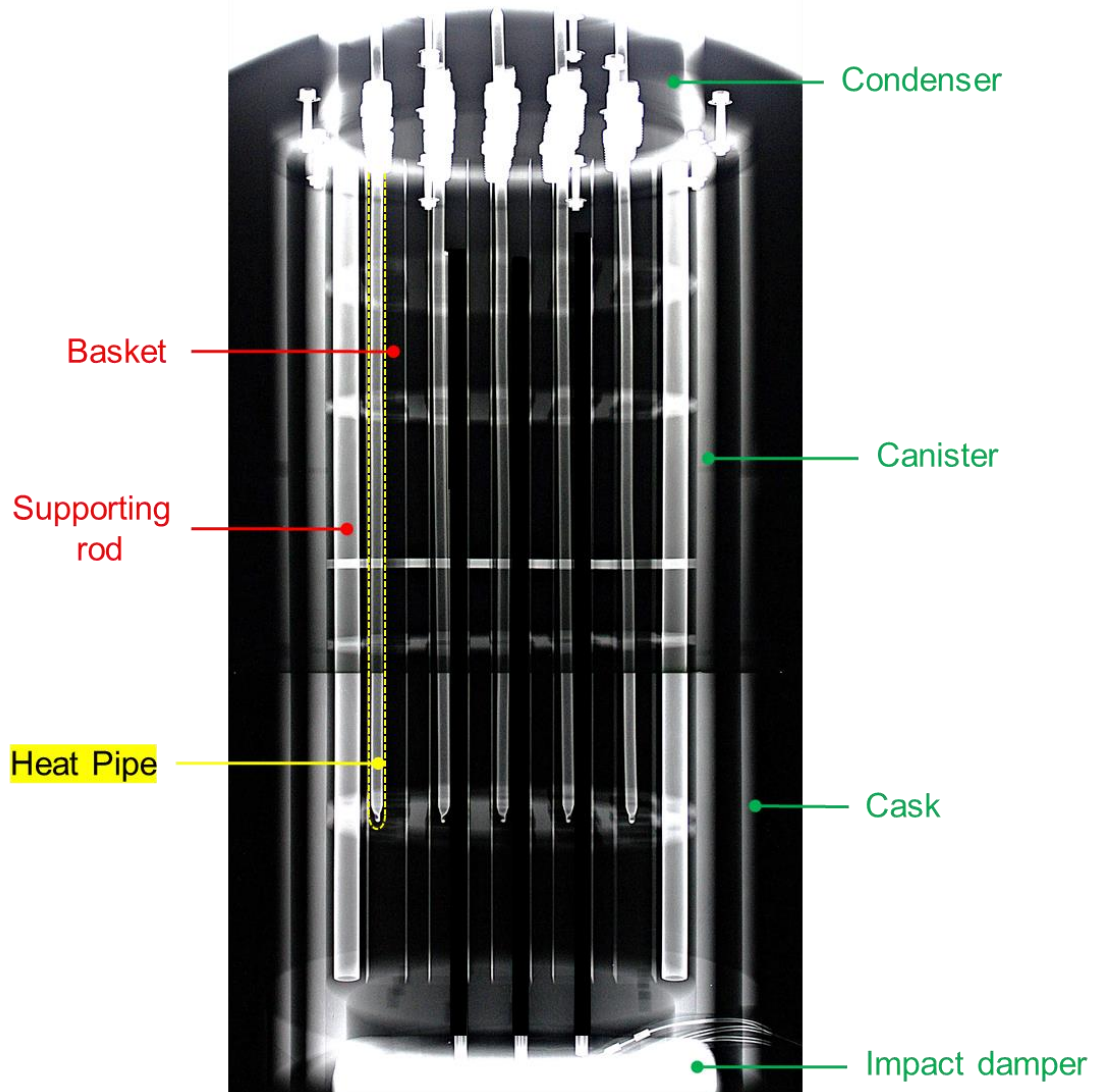| Parameters	Types of spent fuel dry storage casks		
	General cask	UCAN mock-up #1	UCAN mock-up #2
Heat pipe	None	21	21
Heat sink at condenser	Air	Water	Air
Heat input (W)	55 – 90	90	75 – 90
Operating conditions	Normal (Vertical)		

Fig. 4-2. X-ray image of UCAN mock-up including components

4.3 Results and Discussion

For the purpose of confirming the effectiveness of the UCAN design, heating experiments were carried out. Applying total heat of 90 W which corresponds to the linear density of full-scale metal transportation/storage cask, temperature evolutions during the experiments were measured according to cask designs. Three designs were studied to observe the effect of the hybrid control rod and heat sink design on thermal margin of cask. The UCAN designs equipped with the hybrid control rod and heat sink charged with air or water, and general cask without the hybrid control rod and heat sink were the designs for experiments. The cask wall was exposed to the atmosphere and air inside the cask was sealed. To quantify the effectiveness of the UCAN design, heat input levels showing the similar temperature distributions at steady states with UCAN integrated with the hybrid control rod and water heat condenser were found by iterative experiments.

4.3.1 Effects of hybrid control rod and heat sink

The effect of the hybrid control rod on temperature evolutions at transient phase and temperature distributions at steady states were measured. The temperature data was compared with that of normal cask (decay heat removal by air convection and radiation at the walls without hybrid control rod). The temperature evolutions of normal cask and UCANs with air condenser under the decay heat density of 0.93 kW/m^3 were plotted in Figs. 4-3 and 4-5.

Air temperatures at condenser and inside the canister were 80 °C and 95 – 105 °C (112 °C for basket wall) for normal cask. Similar wall temperature evolutions at cask and condenser were observed because the decay heat removal is achieved by radiation and convection through radial direction of the normal cask. Variations of temperatures at each part of UCAN with air condenser were shown in Fig. 4-4. The temperature increase rate of UCAN with air condenser was similar with normal cask. Air temperature at condenser lid reached 100 °C at steady state. Temperatures of air inside canister were 88 – 105 °C. Condenser wall temperature was always higher than that of cask wall because the hybrid control rods transport the decay heat from the basket to the condenser section. The axial temperature gradient from the lowest elevation to condenser section (temperature difference between TC-L-01 to TC-H-01) was lower than normal cask owing to enhanced axial heat transfer rate through the hybrid control rods. Consequently, heat transfer the hybrid control rod reduces the canister temperature and increases condenser temperature guaranteeing the extended temperature margins of canister compared to normal cask. Hence, it is advantageous in terms of long-term integrities of spent fuels and structures. Water was selected as a heat sink medium since it has higher specific heat compared to air, in other words, the heat sink temperature would be below than air condenser. The higher temperature difference between canister and condenser could enhance the heat transfer rate of the hybrid control rods. Fig. 4-5 shows

the temperature variations of UCAN with water condenser. UCAN with water condenser showed the reduced temperature increase rate compared to normal cask and UCAN with air condenser as predicted in the design step. At steady state, the water temperature reaches 90 °C. The higher temperature of the condenser increases the radiation heat transfer at the wall of condenser. Inside temperatures of the canister were 75 – 80 °C, which are significantly lower temperatures in comparison with normal cask and UCAN with air condenser. The lower axial temperature gradient along the canister and water condenser was observed compared to other designs meaning that the higher heat spreading.

The thermal analyses were conducted based on the measured temperature data and below heat balance equation to quantify the effect of the hybrid control rod and condenser on thermal behavior of the cask.

$$\dot{Q}_{in} = \dot{Q}_{condenser} + \dot{Q}_{structure} + \dot{Q}_{radiationCask} + \dot{Q}_{radiationCondenser} \qquad (4\text{-}1)$$

$$\dot{Q}_{condenser} = m_{water} c_{p,water} \frac{(T_{t+\tau} - T_t)}{dt} \text{ or } m_{air} c_{p,air} \frac{(T_{t+\tau} - T_t)}{dt} \qquad (4\text{-}2)$$

$$\dot{Q}_{structure} = m_{acrylic} c_{p,acrylic} \frac{(T_{t+\tau} - T_t)}{dt} + m_{basket} c_{p,basket} \frac{(T_{t+\tau} - T_t)}{dt} \qquad (4\text{-}3)$$

$$\dot{Q}_{radiationCask} = \sigma \varepsilon A_{cask} \left(T_{cask,wall}^4 - T_{env}^4 \right) \qquad (4\text{-}4)$$

$$\dot{Q}_{radiationCondenser} = \sigma \varepsilon A_{condenser} \left(T_{cond,wall}^4 - T_{env}^4 \right) \qquad (4\text{-}5)$$

In the analyses, heat input was assumed to be converted to stored energy of structures such as basket, canister, cask, and condenser with radiation heats from cask wall and condenser wall to environment.

The analyzed heat transfer rates (air: radiation heat transfer from cask wall to environment, stored energy in structures, and heat pipe or condenser: radiation heat transfer from condenser wall to environment) according to cask designs were plotted in Figs. 4-6 to 4-8.

Stored energy of structures was dominant at the initial phase of operation for UCAN with air condenser and normal cask. In case of normal cask, the heat generated from the basket was removed by radiations through condenser (20 %) and cask wall (70 %) with conversion to 10 % of stored energy in structures. The ratio between radiations through condenser and cask wall was coincident with surface area ratio of them. While the radiation heat transfer at the condenser was increased to 30 % because the hybrid control rods transferred the heat from canister to condenser axially. UCAN with water condenser showed equal radiation heat transfer rates at condenser section and cask wall because the heat sink temperature at steady state was higher than other designs by axial heat transfer through the hybrid control rods.

4.3.2 Thermal margins

The power densities achieving the similar temperature distributions at steady states were found by iterative experiments for the quantitative analysis of effect of cask design on the thermal margin and spent fuel storage capability. UCAN equipped with water condenser showed the highest power density (0.93 kW/m^3) to achieve average temperature of 80 °C inside the canister. The power density of UCAN with water condenser was 1.29 and 1.63 times of the air condenser and normal cask (0.72 kW/m^3 and 0.56 KW/m^3). However, the axial temperature gradients of the UCAN with air condenser and normal cask were higher than UCAN with water condenser. The general cask showed the highest basket temperature compared to the UCAN designs. The higher axial temperature gradient demonstrates lower effective thermal conductivity along the axial direction (inefficient heat transfer through axial direction). The normalized axial temperature gradients were 1.13 and 2.33 for air condenser and normal cask with standard of 1.0 of UCAN with water condenser as shown in Table 4-3. The reduction of the temperature gradient along the axial direction of the fuel assemblies could reduce the thermal strain applying on the spent fuels. Thus, the UCAN equipped with water condenser can enhance the storage capacity and thermal margin with reduction of thermal strain. The application of the hybrid control rod to spent fuel dry storage cask will secure the integrity of the spent fuel in terms of issues related to the thermal strain and temperature-induced material embrittlement.

Table 4-3. Power densities of similar temperature distributions at steady states and its status

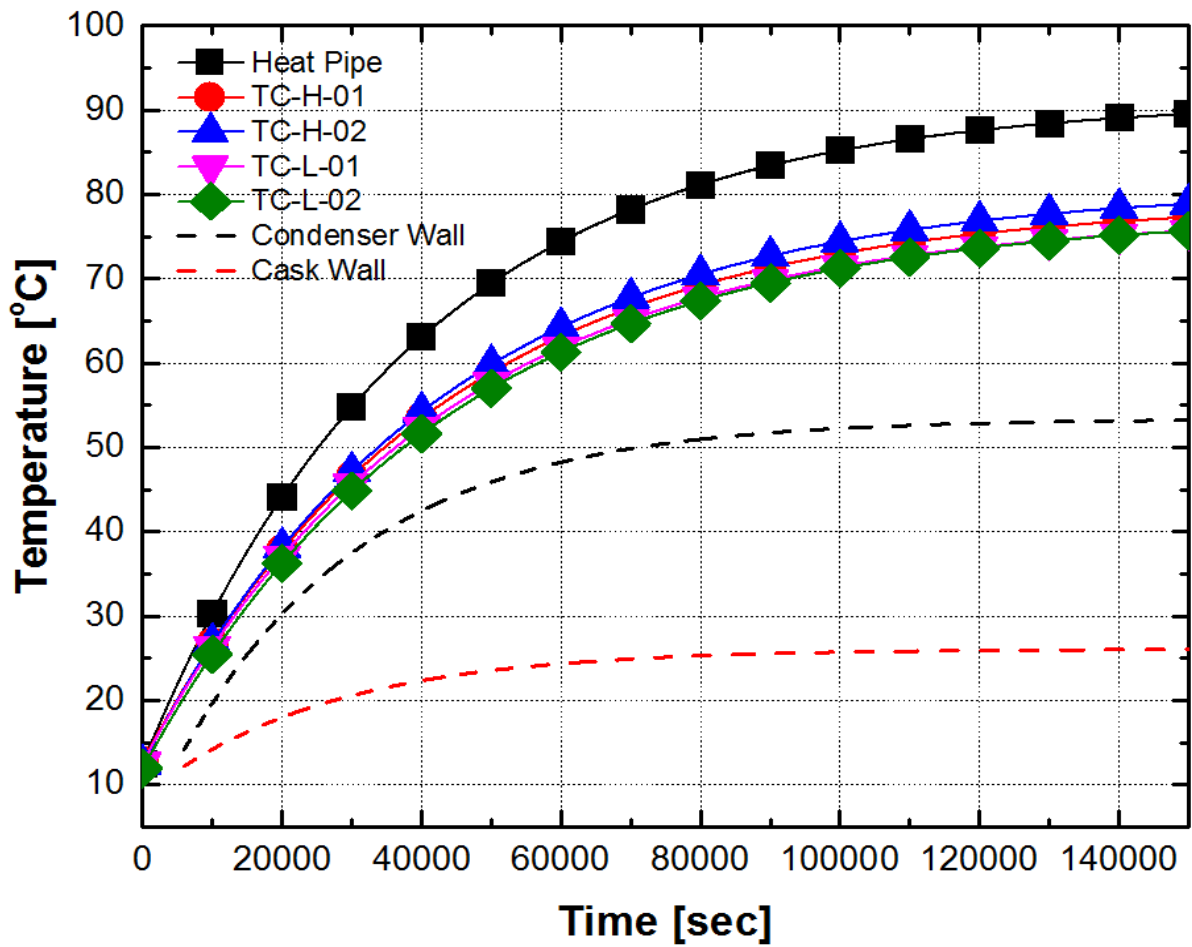| Designs	Power density (kW/m^3)	Normalized axial temperature gradient
UCAN with water condenser	0.93	1.0
UCAN with air condenser	0.72	1.13
Normal cask	0.56	2.33

Fig. 4-3. Temperature evolution of UCAN mock-up with water heat sink (Q'''=0.93 kW/m^3)
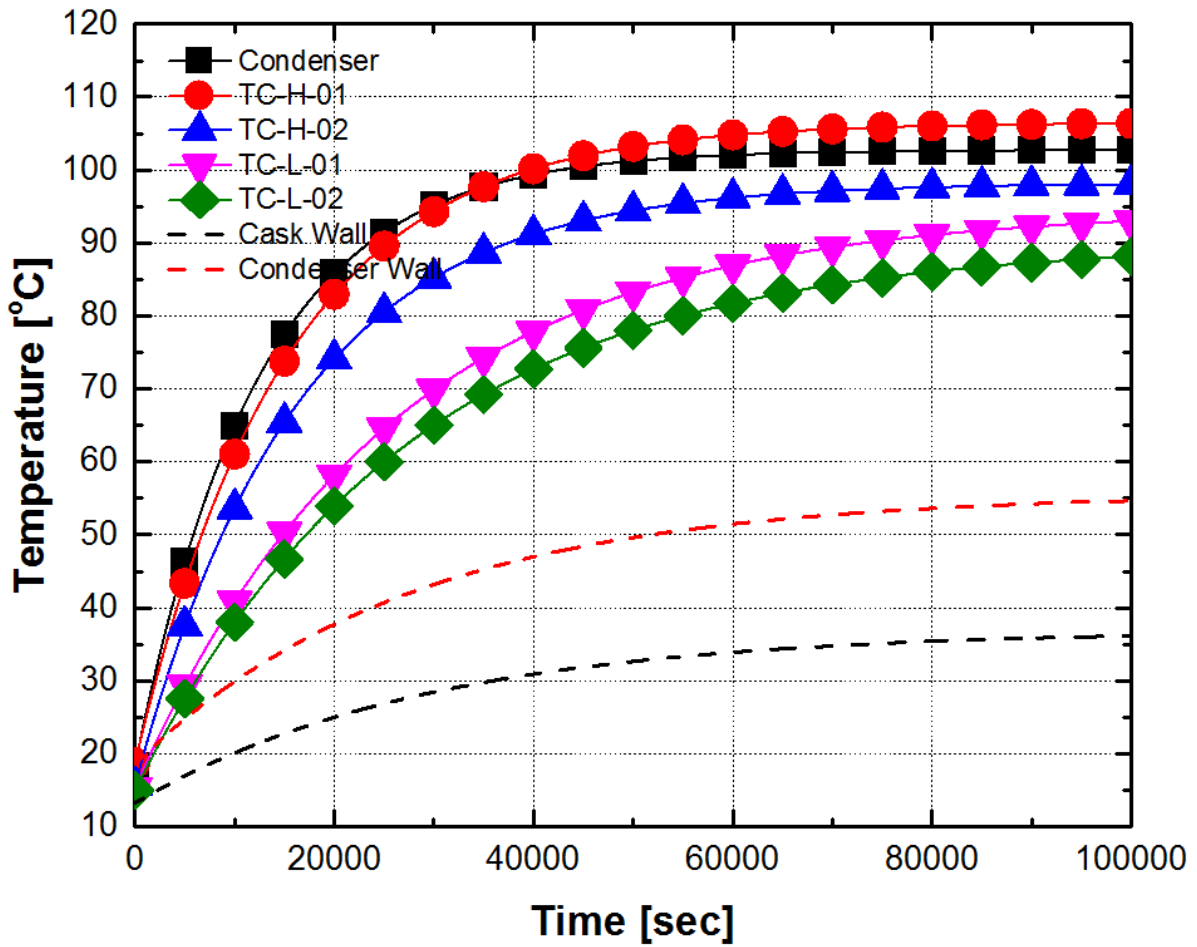
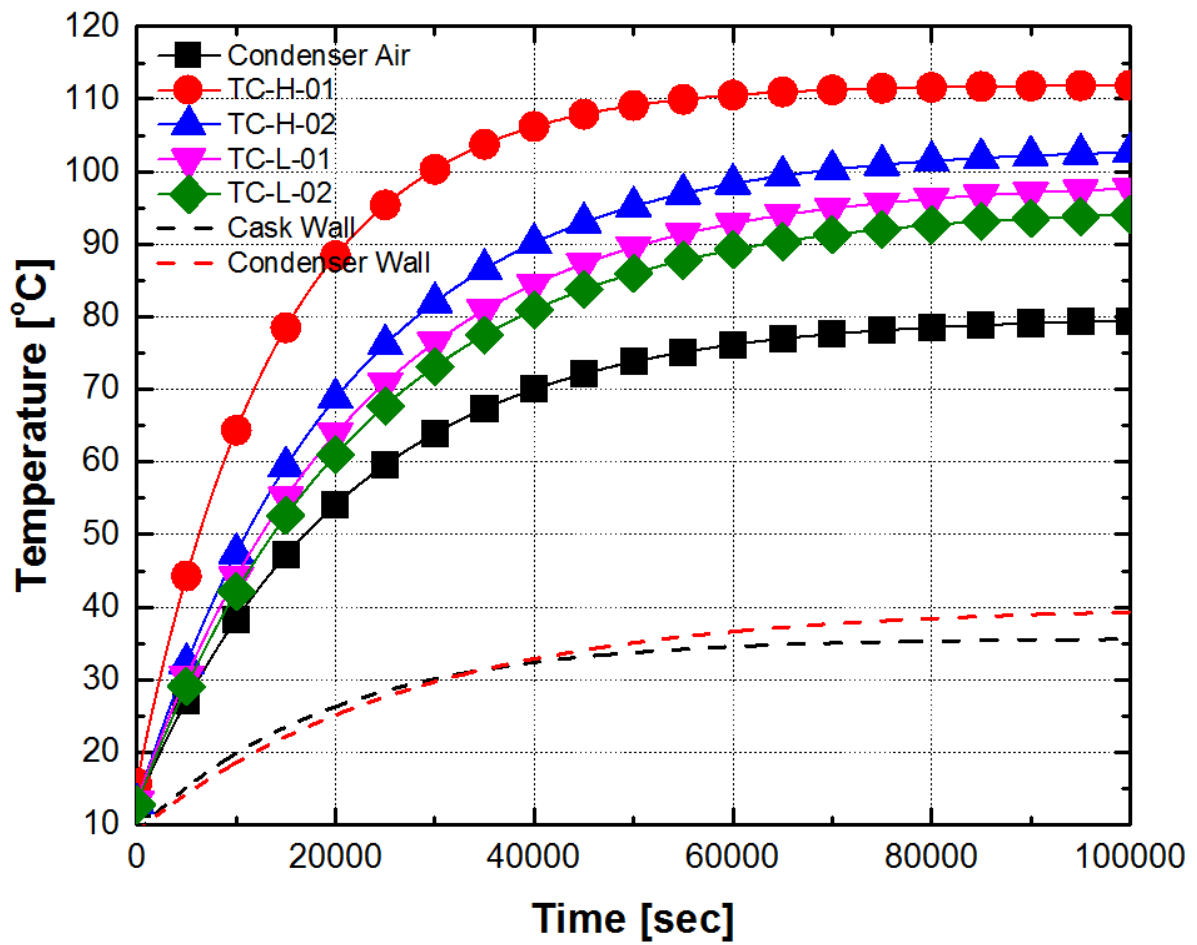Fig. 4-4. Temperature evolution of UCAN mock-up with air heat sink (Q'''=0.93 kW/m^3)

Fig. 4-5. Temperature evolution of general cask mock-up (Q'''=0.93 kW/m^3)
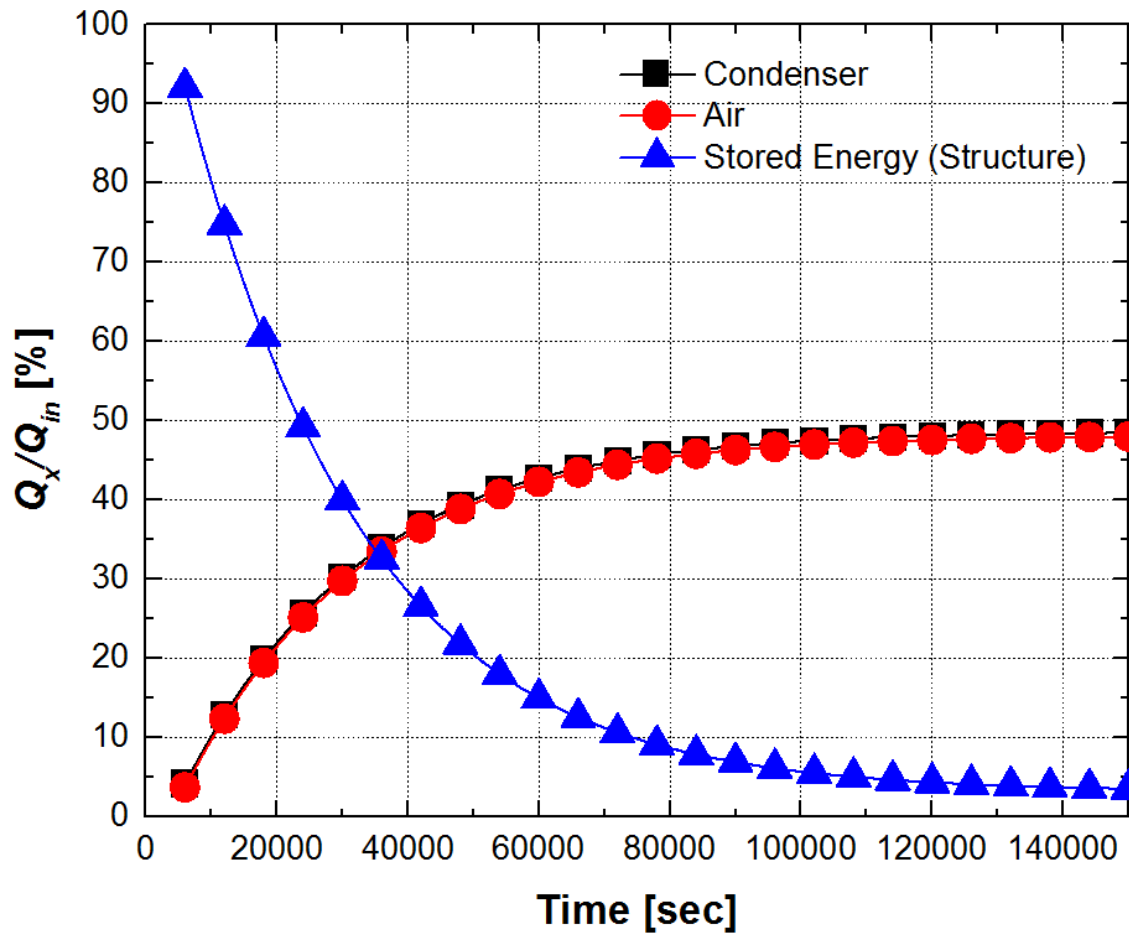
Fig. 4-6 Variation of heat transfer rates of UCAN mock-up with water heat sink (Q'''=0.93 kW/m³)
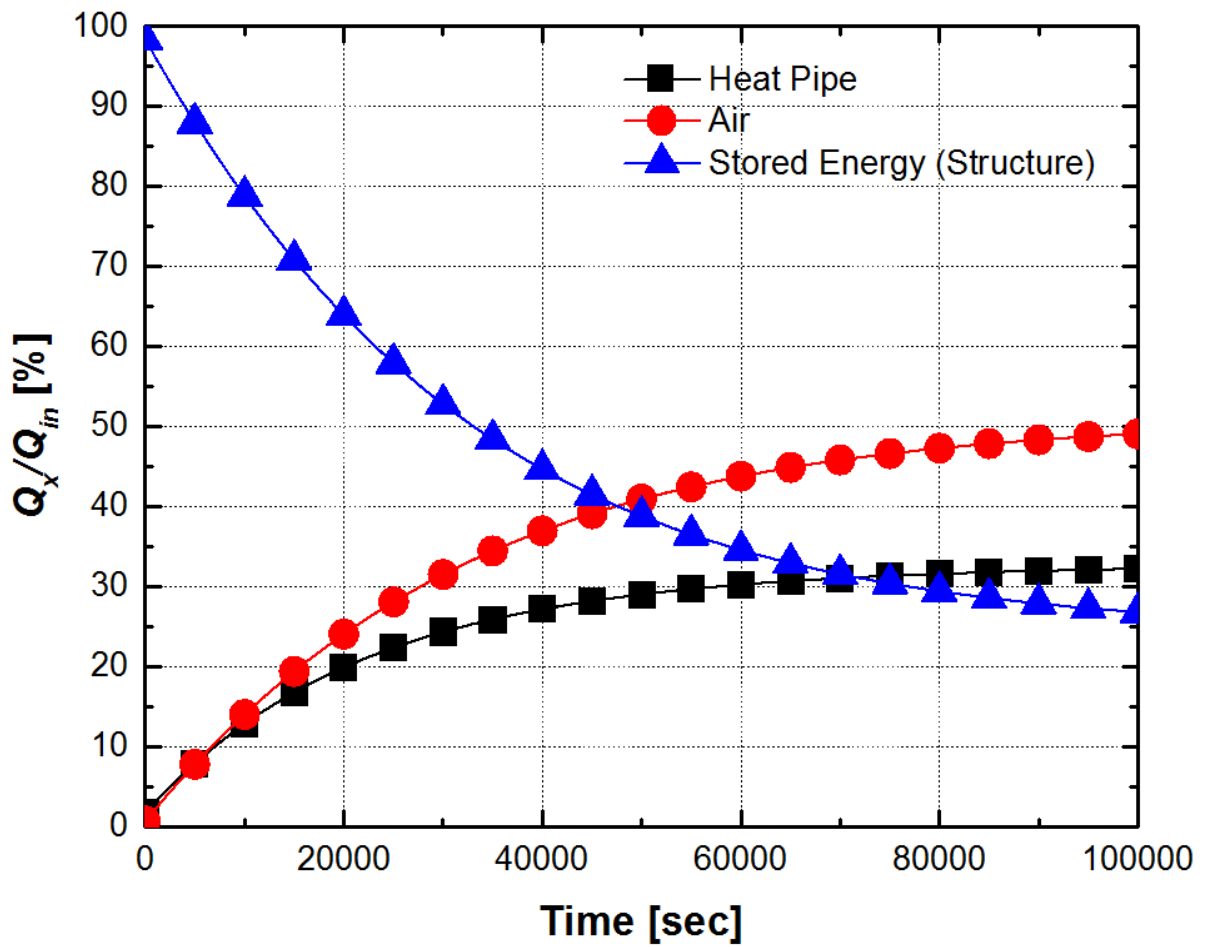
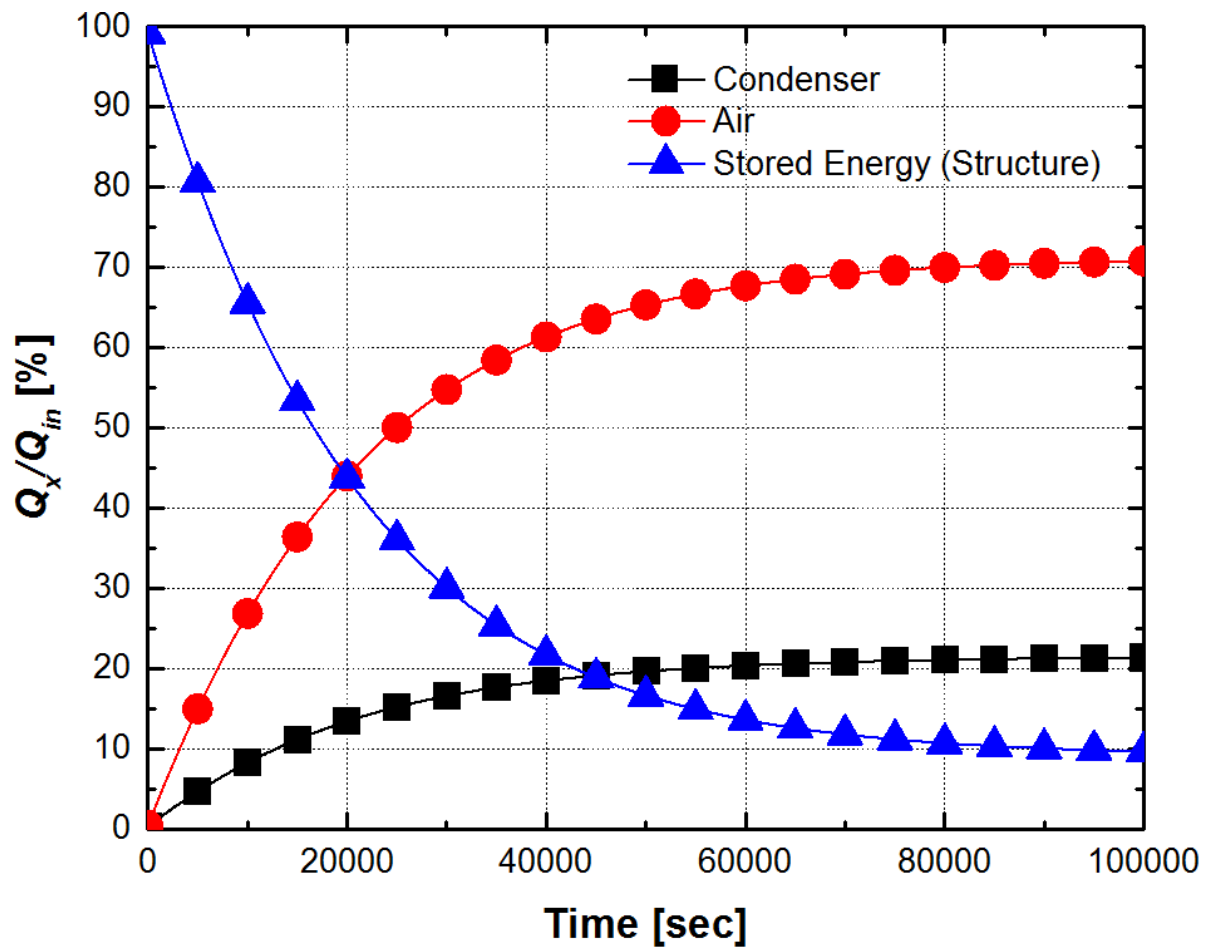Fig. 4-7 Variation of heat transfer rates of UCAN mock-up with air heat sink (Q'''=0.93 kW/m^3)

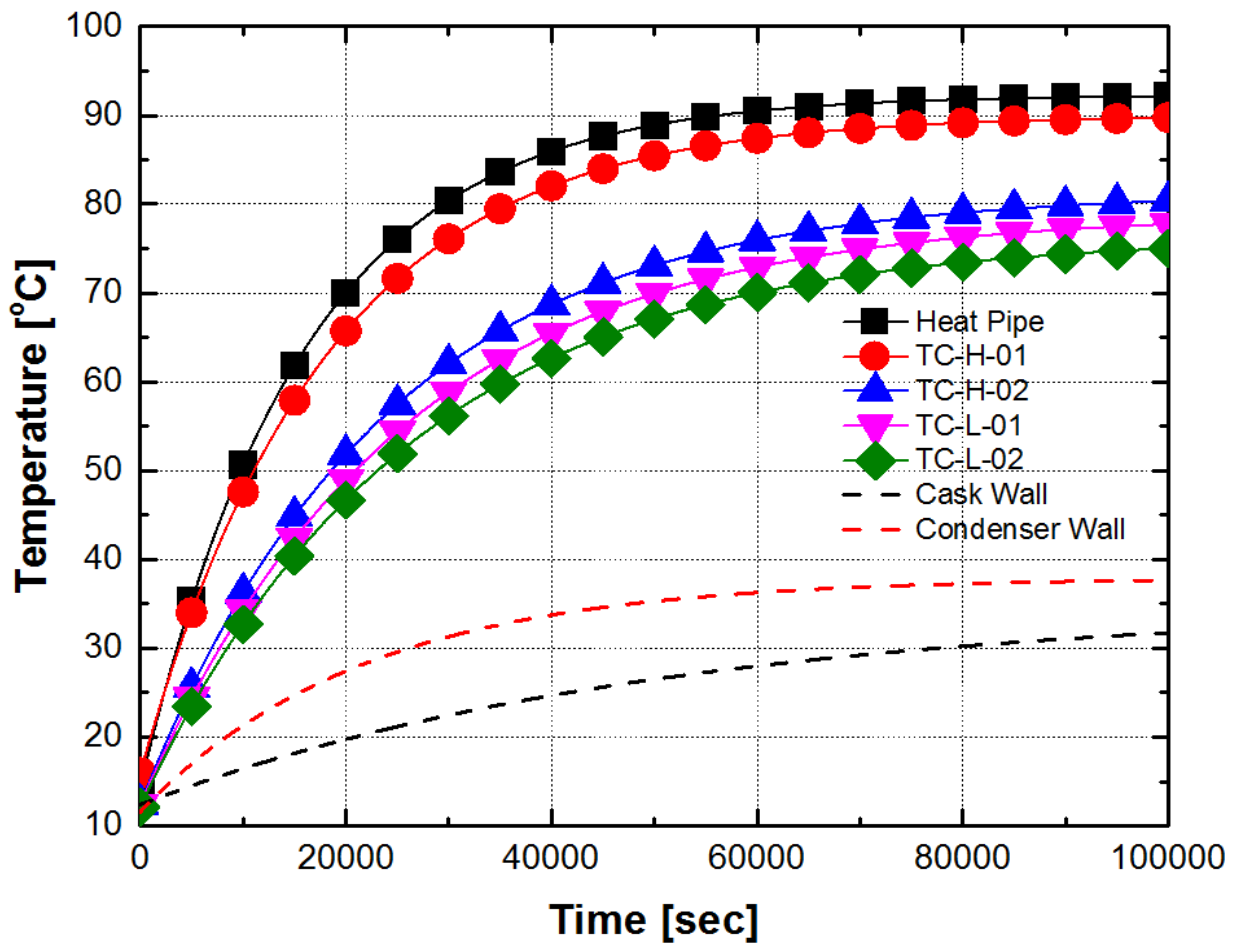Fig. 4-8 Variation of heat transfer rates of general cask mock-up (Q'''=0.93 kW/m^3)

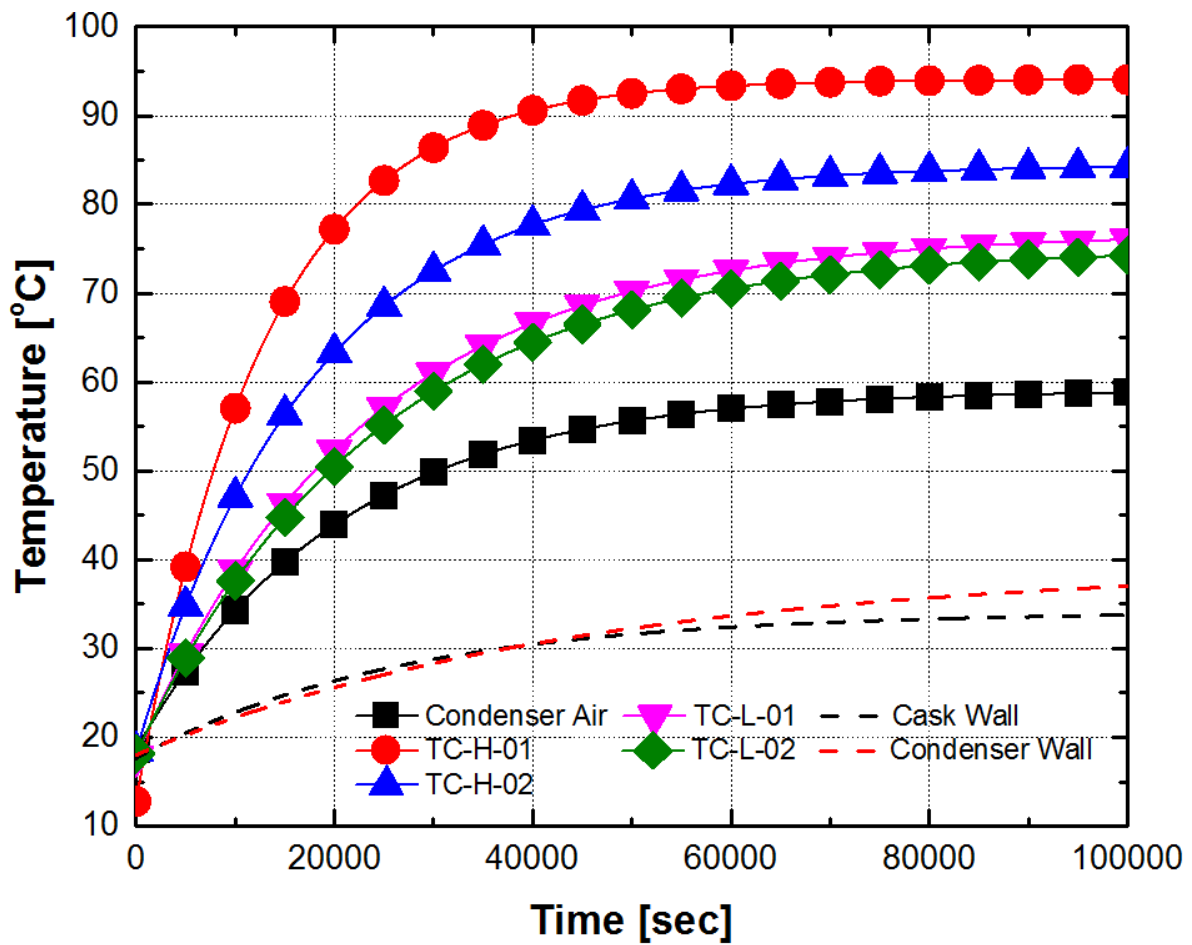Fig. 4-9 Temperature evolution of UCAN mock-up with air heat sink (Q'''=0.72 kW/m^3)

Fig. 4-10 Temperature evolution of general cask mock-up (Q'''=0.53 kW/m^3)

Chapter 5. CONCLUSIONS AND RECOMMENDATIONS

5.1 Conclusions

5.1.1 Thermal performances of pressurized hybrid control rod

Hybrid control rod which is a new type of thermosyphon containing neutron absorber was designed including dimensions, compositions, and operating strategies as a decay heat removal device for passive in-core cooling system.

Thermal performances of the hybrid control rod according to pressurization strategies, fill ratio of working fluid, and initial pressures were measured by experiments. Self-pressurization strategy was selected as an operating strategy of the hybrid control rod due to advantage of passive operation. The evaporation and condensation heat transfer characteristics of the self-pressurized hybrid control rod were analyzed by comparison with predictions of existing correlations. Imura's correlation was selected as evaporation heat transfer model of the hybrid control rod due to good agreement with experimental data. For the condensation model, new correlation considering the effects of non-condensable gas and entrainment on heat transfer was suggested. The flooding-based maximum heat removal rate of the hybrid control rod was derived by reflecting the difference of cross-sectional areas across evaporator and adiabatic sections. The proposed models related to the condensation heat transfer and operation limit were validated with additional experiments controlling the type of non-condensable gas and cross-sectional area of the evaporator section.

Based on the experimental data and models, guideline for the hybrid control rod design was proposed. The design of the hybrid control rods according to operating conditions and target heat removal rate is expected to be possible by referring the proposed guideline.

5.1.2 Prospect of PINCs on nuclear safety

Application study of PINCs on spent fuel dry storage cask was conducted. UCAN integrated with the hybrid control rod and condenser lid was designed.

UCAN mock-up having 1/10 scale of metal cask developed by KORAD was manufactured. The effects of heat pipes and heat sink media of condenser were observed by experimental works with mock-up. The UCAN design showed better performance than general metal cask in terms of temperature margin of structures with recommendation of use of heat sink having high specific heat.

The heat transfer efficiencies of heat pipe during transportation and postulated accident conditions were degraded due to reduction of driving force of working fluid convection, however, equipment of the heat pipe and condenser enhanced the thermal margin of spent fuel dry storage cask.

5.2 Recommendations

Hybrid control rods and passive in-core cooling system are fully passive device which do not require any signals or power sources to be operated. Components having possibility of the failure are eliminated and components which have been proven are utilized in the organization of the system. Therefore, application of the hybrid control rods will be advantageous in terms of enhanced nuclear safety regarding the design basis accidents, especially station blackout which condition of unable use of active safety systems and present passive safety systems. The passive in-core cooling system based on the pressurized hybrid control rods can be easily applied to various nuclear facilities managing the heat of fission. In addition, designs of the hybrid control rod and PINCs can be optimized according to the target facilities having different operating conditions.

References

1. Passive safety systems and natural circulation in water cooled nuclear power plants. IAEA, Vienna, *IAEA-TECDOC-1624,* **2009**

2. Bae, B.U.; Kim, S.; Park, Y.S.; Kang, K.H.; Ahn, T.H.; & Yun, B.J.; Evaluation of mechanistic wall condensation models for horizontal heat exchanger in PAFS (Passive Auxiliary Feedwater System). *Annals of Nuclear Energy*, **2017**, 107, 53-61.

3. Du, W.F.; Zhuo, S.; Yang, L.; & Zhao, R.C.; Numerical simulation and parameter sensitivity analysis of coupled heat transfer by PCCS containment wall. *Applied Thermal Engineering*, **2017**, 113, 867-877.

4. Payot, F.; Reinecke, E.A.; Morfin, F.; Sabroux, J.C.; Meynet, N.; Bentaib, A.; March, P.; Zeyen, R.; Understanding of the operation behavior of a passive autocatalytic recombiner (PAR) for hydrogen mitigation in realistic containment conditions during a severe light water nuclear reactor (LWR) accident. *Nuclear Engineering and Design*, **2012**, 248, 178-196.

5. Nam, G.; Park, J.; & Kim, S.; Conceptual design of passive containment cooling system for APR-1400 using multipod heat pipe. *Nuclear Technology*, **2015**, 189, 278-293.

6. Mochizuki, M.; Nguyen, T.; Mashiko, K.; Saito, Y.; Singh, R.; Nguyen, T.; & Wuttijumnong, V.; Prevention possibility of nuclear power reactor meltdown by use of heat pipes for passive cooling of spent fuel. *Frontiers in Heat Pipes*, **2013**, 4, 01300.

7. Sviridenko, I. I.; Heat exchangers based on low temperature heat pipes for autonomous emergency WWER cooldown systems. *Applied Thermal Engineering*, **2008**, 28, 327-334.

8. Gou, P.F.; Saratoga.; Fennern, L.E.; Jose, S.; Sawyer, C.D.; Gatos, L.; Nuclear reactor heat pipe, *United States Patent*, **1997**.

9. Hejzlar, P.; Todreas, N.E.; & Driscoll, M.J.; Passive decay heat removal in advanced LWR concepts. *Nuclear Engineering and Design*, **1993**, 139, 59-81.

10. Dunkel, T.L.; Emergency heat removal system for a nuclear reactor. *United States Patent*, **1976**.

11. Peterson, G.P.; & Compagna, G.L.; Review of cryogenic heat pipes in spacecraft applications. *Journal of Spacecraft*, **1987**, 24, 99-100.

12. Hu, G.; Zhao, S.; Sun, Z.; & Yao, C.; A heat pipe cooled modular reactor concept for manned lunar base application, *Proceedings of 2013 21st Int Conference on Nuclear Engineering*, **2013**, 2.

13. Jeong, Y.S.; Kim, K.M.; Kim, I.G.; & Bang, I.C.; Hybrid heat pipe based passive in-core cooling system for advanced nuclear power plant. *Applied Thermal Engineering*, **2015**, 90, 609-618.

14. Kim, K.M.; & Bang, I.C.; Comparison of flooding limit and thermal performance of annular and concentric thermosyphons at different fill ratios. *Applied Thermal Engineering*, **2016**, 99, 179-188.

15. Jeong, Y.S.; & Bang, I.C.; Hybrid heat pipe based passive cooling device for spent nuclear fuel dry storage cask. *Applied Thermal Engineering*, **2016**, 96, 277-285.

16. Reay, D.A.; & Kew, P.A.; Heat Pipes (fifth edition), Butterworth-Heinemann, Oxford **2006**.

17. Imura, H.; Kusuda, H.; & Ogata, J.; Heat transfer in two-phase closed- type thermosyphons. *Heat Transfer-Japanese Resource*, **1979**, 8, 41-53.

18. Shiraish, M.; Kikuchi, K.; & Yamanishi, T.; Investigation of heat transfer characteristics of a two-phase closed thermosyphon. *Heat Recovery Systems*, **1981**, 1, 287-297.

19. Kaminaga, F.; Okamoto, Y.; & Suzuki, T.; Study on boiling heat transfer correlation in a two-phase closed thermosyphon. *Proceedings of the Eighth International Heat Pipe Conference*, **1992**, 317-322.

20. Rohsenow, W.; A method of correlating heat transfer data for surface boiling of liquids. *Transaction of the ASME 74*, **1952**, 969-976.

21. Kutateladze, S.S.; Heat transfer and hydrodynamic resistance, Energoatomizdat Publishing House, Moscow, Russia, **1990**.

22. Labuntsov, D.A.; Heat transfer problems with nucleate boiling of liquids. *Thermal Engineering*, **1972**, 19, 21-28.

23. Kruzhilin, G.N.; Free-convection transfer of heat from a horizontal plate and boiling liquid. *Doklady Akademii Nauk SSSR*, **1947**, 58, 1657-1660.

24. Grob, U.; Pool boiling heat transfer inside a two-phase thermosyphon-correlation of experimental data. *Proceedings of the Ninth International Heat Transfer Conference*, **1992**, 170-175.

25. Chowdhury, F.M.; Kaminaga, F.; Goto, K.; & Matsumura, K.; Boiling heat transfer in a small diameter tube below atmospheric pressure on a natural circulation condition. *Journal of Japan Association for Heat Pipe*, **1997**, 16, 14-16.

26. Xin, M.D.; Chen, G.; & Chen, Y.G.; Flow and heat transfer in two-phase closed thermosyphon. *Proceedings of the Sixth International Heat Pipe Conference*, **1987**, 419-423.

27. Fujita, Y.; Nucleate boiling heat transfer and critical heat flux in narrow space between rectangular surface. *International Journal of Heat and Mass Transfer*, **1988**, 31, 229-239.

28. El-Genk, M.S.; & Saber, H.H.; Heat transfer correlations for liquid film in the evaporator of enclosed, gravity assisted thermosyphons. *Journal of Heat Transfer*, **1998**, 120, 477-484.

29. Noie, S.H.; Heat transfer characteristics of a two-phase closed thermosyphon. *Applied Thermal Engineering*, **2005**, 25, 495-506.

30. Hashimoto, H.; & Kaminaga, F.; Heat transfer characteristics in a condenser of closed two-phase thermosyphon: effect of entrainment on heat transfer deterioration. *Heat Transfer-Asian Research*, **2002**, 31, 212-225.

31. Jouhara, H.; & Robinson, A.J.; Experimental investigation of small diameter two-phase closed thermosyphons charged with water, FC-84, FC-77 and FC-3283. *Applied Thermal Engineering*, **2010**, 30, 201-211.

32. Gross, U.; Reflux condensation heat transfer inside a closed thermosyphon. *International Journal of Heat and Mass Transfer*, **1992**, 35, 279-294.

33. Andros, F.E.; Heat transfer characteristics of the two-phase closed thermosyphon (wickless heat pipe) including direct flow observations. Ph.D. Thesis, Arizona State University, **1980**.

34. Japikse, D.; Advances in thermosyphon technology. *Advances in Heat Transfer*, **1973**, 9, 1-111.

35. Stoyanov, N.M.; Effect of the angle of inclination of a closed evaporative thermosyphon on heat transfer. *Teploenergetika*, **1968**, 15, 74-76.

36. ESDU, Heat Pipes-Performance of Two-phase Closed Thermosyphons. Engineering Sciences Data Unit 81038, London, **1981**.

37. Larkin, B.S.; An experimental study of the temperature profiles and heat transfer coefficients in a heat pipe for a heat exchanger. *Proceeding of 4th International Heat Pipe Conference*, **1981**, 177-191.

38. Rosler, S.; Takuma, M.; Groll, M.; & Maezawa, S.; Heat transfer limitation in a vertical annular closed two-phase thermosyphon with small fill rates. *Heat Recovery System and CHP*, **1987**, 7, 319-327.

39. Vijra, N.; & Singh, T.P.; An experimental study of thermal performance of concentric annular heat pipe. *American International Journal of Research in Science, Technology, Engineering, and Mathematics*, **2015**, 9, 176-182.

40. Lin, T.F.; Lin, W.T.; Tsay, Y.L.; & Wu, J.C.; Experimental investigation of geyser boiling in an annular two-phase closed thermosyphon. *International Journal of Heat and Mass Transfer*, **1995**, 38, 295-307.

41. Boo, J.H.; & Park, S.Y.; An experimental study on the thermal performance of a concentric annular heat pipe. *Journal of Mechanical Science and Technology*, **2005**, 19, 1036-1043.

42. Faghri, A.; Chen, M.M.; & Morgan, M.; Heat transfer characteristics in two-phase closed conventional and concentric annular thermosyphons. *Journal of Heat Transfer*, **1989**, 111, 611-618.

43. Imura, H.; Sasaguchi, K.; & Kozai, H.; Critical heat flux in a closed two-phase thermosyphon. *International Journal of Heat and Mass Transfer*, **1983**, 26, 1181-1188.

44. Tien, C.L.; & Chung, K.S.; Entrainment limits in heat pipes. *AIAA Journal*, **1979**, 17, 643-646.

45. Nouri-Borujerdi, A.; & Layeghi, M.; A Numerical analysis of vapor flow in concentric annular heat pipes. *Transaction of ASME*, **2004**, 126, 442-488.

46. Yoshida, M.; Imura, H.; & Ippohshi, S.; Flow and heat transfer in a two-phase double-tube thermosyphon. *Transaction of the Japan Society of Mechanical Engineers*, **1991**, 57, 1428-1433.

47. Ismail, O.S.; & Adewoye, G.T.; Analysis and modeling of laminar in pipes using numerical approach. *Journal of Software Engineering and Application*, **2012**, 5, 653-658.

48. Faghri, A.; & Thomas, S.; Performance characteristics of a concentric annular heat pipe: Part I-Experimental prediction and analysis of the capillary limit. *Journal of Heat Transfer*, **1989**, 111, 844-850.

49. Faghri, A.; Performance characteristics of a concentric annular heat pipe: Part II-Vapor flow analysis, *Journal of Heat Transfer*, **1989**, 111, 851-857.

50. Florencio, S.S.; Ignacio, C.M.; Ariel, E.M.C.; Pedro, Q.D.; & Miguel, T.V.; Study of an annular two-phase thermosyphon used as isothermal source in thermometry. *Journal of Mechanical Engineering*, **2015**, 61, 273-282.

51. Seki, N.; Fukusako, S.; & Koguchi, K.; Single-phase heat transfer characteristics of concentric-tube thermosyphon. *Warme-und Stoffubertragung*, **1980**, 14, 189-199.

52. Nouri-Borujerdi, A.; & Layeghi, M.; A review of concentric annular heat pipes. *Heat Transfer Engineering*, **2005**, 26, 45-58.

53. Joung, W.; Kim, Y.G.; & Lee, J.; Transient characteristics of a loop heat pipe-based hydraulic temperature control technique. *International Journal of Heat and Mass Transfer*, **2016**, 103, 125-132.

54. Joung, W.; Gam, K.S.; & Kim, Y.G.; Realization of tin freezing point using a loop heat pipe-based hydraulic temperature control technique. *Metrologia*, **2015**, 52, 694-707.

55. Joung, W.; Gam, K.S.; Kim, Y.G.; & Yang, I.; Hydraulic operating temperature control of a loop heat pipe, *International Journal of Heat and Mass Transfer*, **2015**, 86, 796-808.

56. Kim, K.M.; & Bang, I.C.; Heat transfer characteristics and operation limit of pressurized hybrid heat pipe for small modular reactors. *Applied Thermal Engineering*, **2017**, 112, 560-571.

57. Kline, S.J.; & McClintock, F.A.; Describing uncertainties in single sample experiments. *Mechanical Engineering*, **1953**, 75, 3-8.

58. Niro, A.; & Beretta, G.P.; Boiling regimes in a closed two-phase thermosyphon. *International Journal of Heat and Mass Transfer*, **1990**, 33, 2099-2110.

59. Noie, S.H.; Sarmasti Emami, M.R.; & Khoshnoodi, M.; Effect of inclination angle and filling ratio on thermal performance of a two-phase closed thermosyphon under normal operating conditions. *Heat Transfer Engineering*, **2007**, 28, 365-371.

60. Mirshahi, H.; & Rahimi, M.; Experimental study on the effect of heat loads, fill ratio and extra volume on performance of a partial-vacuumed thermosyphon. *Iranian Journal of Chemical Engineering*, **2009**, 6, 15-26.

61. Sudo, Y.; Analytical study of critical heat flux under countercurrent flow limitation in vertical channels. *Transaction of JSME*, **1994**, 60, 4222-4228.

62. Bharathan, D.; & Wallis, G.B.; Air-water countercurrent annular flow. *International Journal of Multiphase Flow*, **1983**, 9, 349-366.

63. Monde, M.; Analytical study of critical heat flux in two-phase thermosyphon: Relationship between maximum falling liquid rate and critical heat flux. *Journal of Heat Transfer*, **1996**, 118, 422-428.

64. Imura, H.; Kusuda, H.; & Funatsu, S.; Flooding velocity in a counter-current annular two-phase flow. *Chemical Engineering and Science*, **1977**, 32, 79.

65. Ritcher, H.; Flooding in tubes and annuli. *International Journal of Multiphase Flow*, **1981**, 7, 647-568.

66. Moissis, R.; The transition from slug to homogeneous two-phase flow. *Journal of Heat Transfer*, **1963**, 85, 366-370.

67. Tippets, F.E.; Analysis of the critical heat flux condition in high pressure boiling water flows. *Transaction of ASME*, **1964**, 86, 23-38.

68. Anshus, B.E.; On the asymptotic solution to the falling film stability problem. *Industrial & Engineering Chemistry Fundamentals*, **1972**, 11, 502-508.

69. Pierson, F.W.; & Whitaker, S.; Some theoretical and experimental observations of the wave structure of falling liquid films, *Industrial & Engineering Chemistry Fundamentals*, **1977**, 16, 401-408.

70. Cho, Y.J.; Kim, Seok.; Bae, B.U.; Park, Y.; Kang, K.H.; & Yun, B.J.; Assessment of condensation heat transfer model to evaluate performance of the passive auxiliary feedwater system. *Nuclear Engineering and Technology*, **2013**, 45, 759-766.

71. Seo, K.; & Kim, T.H.; Feasibility study of condensation heat exchanger with helical tubes for a passive auxiliary feedwater system. *International Journal of Applied Engineering Research*, **2017**, 12, 940-944.

72. Chen, J.C.; Correlation for boiling heat transfer to saturated fluids in convective flow. *Industrial & Engineering Chemistry Process Design and Development*, **1966**, 5, 322-329.

73. Churchill, S.W.; & Chu, H.H.S.; Correlating equations for laminar and turbulent free convection from a vertical plate. *International Journal of Heat and Mass Transfer*, **1975**, 18, 1323-1329.

74. Colburn, A.P.; & Hougen, O.A.; Design of cooler condensers for mixtures of vapors with noncondensing gases. *Industrial and Engineering Chemistry*, **1934**, 26, 1178-1182.

75. Wallis, G.B.; One-Dimensional Two-Phase Flow. New York: McGraw-Hill, **1969**.

76. Bankoff, S.G.; Tankin, R.S.; Yuen, M.C.; & Hsieh, C.L.; Countercurrent flow of air/water and steam/water through a horizontal perforated plate. *International Journal of Heat and Mass Transfer*, **1981**, 24, 1381-1385.

77. Nusselt, W.; Dieoberflachenkondensation des wasserdampfes. *Zeitschrift des Vereines Deutscher Ingenieure*, **1916**, 60, 541-575.

78. Monde, M.; Mitutake, Y.; Kubo, S.; & Saga, H.; Critical heat flux during natural convective boiling on uniformly heated inner tubes in vertical annular tubes submerged in saturated liquid. *Warme- und Stoffubertragung*, **1994**, 29, 271-276.

79. Taylor, G.I.; Generation of ripples by wind blowing over a viscous fluid. *The Scientific Papers of Sir G.I. Taylor*, **1963**, 3, 244-254.

80. Bertodano, M.A.L.; Jan, C.S.; Beus, S.G.; Annular flow entrainment rate experiment in a small vertical pipe. *Nuclear Engineering and Design*, **1997**, 178, 61-70.

81. Kataoka, I.; Ishii, M.; Nakayama, A.; Entrainment and deposition rates of droplets in annular two-phase flow. *International Journal of Heat and Mass Transfer*, **2000**, 43, 1573-1589.

82. Lee, J.C.; Choi, W.S.; Bang, K.S.; Seo, K.S.; & Yoo, S.Y.; Thermal-fluid flow analysis and demonstration test of a spent fuel storage system. *Nuclear Engineering and Design*, **2009**, 239, 551-558.

83. Shin, D.; Jeong, U.; Jeun, G.; & Kim S.J.; CFD analysis of natural convection flow characteristics of various gases in the spent fuel dry storage system. *The KSFM Journal of Fluid Machinery*, **2016**, 19, 19-28.

84. Bang, K.S.; Yu, S.H.; Lee, S.H.; Lee, J.C.; & Seo K.S.; Experimental investigation of heat removal performance of a concrete storage cask. *Annals of Nuclear Energy*, **2015**, 85, 679-686.

85. Kim, H.; Kwon, O.J.; Kang, G.U.; & Lee, D.G.; Comparisons of prediction methods for peak cladding temperature and effective thermal conductivity in spent fuel assemblies of transportation/storage casks. *Annals of Nuclear Energy*, **2014**, 71, 427-435.

86. Kim, H.; Lee, D.G.; Kang, G.U.; Cho, C.H.; & Kwon, O.J.; Analysis of heat transfer on spent fuel dry cask during short-term operations. *Journal of Computational Fluids Engineering*, **2016**, 21, 54-61.

87. Kang, G.U.; Kim, H.J.; & Cho, C.H.; Analysis on flow fields in airflow path of concrete dry storage cask using FLUENT code. *Journal of Computational Fluids Engineering*, **2016**, 21, 47-53.

88. Lee, S.J.; Thermal analysis of dry cask storage of used nuclear fuel using FATE^{TM} code, Tchnical Bulletin, Fauske & Associates. LLC, **2015**.

89. Frano, R.L.; Pugliese, G.; & Forasassi, G.; Thermal analysis of a spent fuel cask in different transport conditions. *Energy*, **2011**, 36, 2285-2293.

서로 성장해나가는 모습을 보게되어 더욱 보람을 느낀다. 그리고 우리 연구실 황소 일꾼 영신아. 그동안 많이 부족했던 날 도와주고 믿어줘서 고맙다. 앞으로도 좋은 선배역할 든든히 해주리라 믿는다. 스타일 좋고 감각적인 효는 나의 재미없는 유머에도 맞장구 쳐주고 부탁하는 일들 잘해줘서 고맙다. 지금은 사회에 진출한 유경이. 정말 진심으로 축하하고 승승장구하길 바란다. 내가 가장 잔소리도 많이 한 규민아. 잔소리해서 미안하지만 너의 잠재성은 최고인 것 같아 그런거니 이해 해주길 바란다. 몸 좋은 신흥 일꾼 민호. 때로는 안스럽기도 하지만 든든하게 묵묵히 자리를 지켜줘서 정말 고맙다. 유쾌한 우리 수민이. 선배로서 이야기 많이 들어주지 못해서 미안하고 얼른 씩씩한 수민이가 되어 같이 술 한잔 할 수 있길 기대한다. 나의 마지막 대학원 후배 한얼이. 갈수록 다크 서클이 커지는 것 같지만 잘 따라줘서 고맙다. 학부생 지용이는 우리 연구실 많이 좋아해줘서 고맙고 선배들을 뛰어넘는 연구자가 되길 바란다. 그리고 항상 힘든 부탁을 들어주시고 학위과정을 무사히 마칠 수 있도록 실험장치를 만들어 주신 네오시스 이종수 사장님. 감사드리고 밥 많이 사주세요.

　저를 이 자리에 있게끔 강하게 키워주신 아버지, 힘들 때마다 북돋아 주시고 다독여주시며 믿어주신 어머니. 정말 많이 감사드리고 사랑합니다. 지금까지 효자 노릇 못한 것 같아 죄송하지만 앞으로 은혜를 갚아 나갈 수 있도록 노력하겠습니다. 저의 학위 과정 동안 안부, 응원, 축하의 말을 해주신 모든 친척분들께도 감사드립니다. 마지막으로, 정말 헌신적으로 챙겨주고 이해해주고 함께해 준 그분께 진심을 다해 고맙다는 말을 글로나마 전하면서 저의 학위논문 마지막 장을 마칩니다.